AN ABSTRACT OF THE THESIS OF

PAUL ROY JONES III for the degree of DOCTOR OF PHILOSOPHY

in GEOPHYSICS presented on August 9, 1978

Title: SEISMIC RAY TRACE TECHNIQUES APPLIED TO THE DETERMINATION OF CRUSTAL STRUCTURES ACROSS THE PERU CONTINENTAL MARGIN AND NAZCA PLATE AT 9° S. LATITUDE

Abstract approved: Redacted for Privacy

Seismic refraction, reflection and gravity data obtained across the Peru continental margin and Nazca Plate at 9° S. permit a detailed determination of crustal structure. Complex structures normal to the profile require the development of a ray trace technique to analyze first and later arrivals for eleven overlapping refraction lines. Other data integrated into the seismic model include velocities and depths from well data, near surface sediment structures from reflection profiles and velocities obtained from nearby common depth point reflection lines. Crustal and subcrustal densities and structures were further constrained by gravity modeling to produce a detailed physical model of a convergent margin.

The western portion of the continental shelf basement consists of a faulted outer continental shelf high of

Paleozoic or older rocks. It is divided into a deeper western section of velocity 5.0 km/sec and a shallower, denser eastern section of velocity 5.65 to 5.9 km/sec. The combined structure forms a basin of depth 2.5 to 3.0 km which contains Tertiary sediments of velocity 1.6 to 3.0 km/sec. In this area, near-surface sedimentary structure suggests truncated sinusoidal features caused by exposure to onshore-offshore bottom currents.

The 3 km thick, 4.55 to 5.15 km/sec basement of the eastern shelf shoals shoreward. Together, this basement and the eastern section of the outer continental shelf high form a synclinal basin overlain by Tertiary sediments which have a maximum thickness of 1.8 km and a velocity range of 1.7 to 2.55 km/sec. The gravity model shows a large block of 3.0 g/cm$^3$ lower crustal material emplaced within the upper crustal region beneath the eastern portion of the continental shelf.

Refraction data indicates a continental slope basement of velocity 5.0 km/sec overlying a slope core material with an interface velocity of 5.6 km/sec. The sedimentary layers of the slope consist of an uppermost layer of slumped sediment with an assumed velocity of 1.7 to 2 km/sec which overlies an acoustic basement of 2.25 to 3.6 km/sec.

The high velocities (and densities) of the slope basement suggest the presence of oceanic crustal material overlain by indurated oceanic and continental sediments. This slope melange may have formed during the initiation of subduction from imbricate thrusting of upper layers of oceanic crust. Once created, the melange forms a trap and forces the subduction of most of the sediments that enter the trench.

A ridge-like structure within the trench advances the seismic arrival times of deeper refractions and supports the suggestion that it is thrust-faulted oceanic crust which has been uplifted relative to the trench floor. The model of the descending Nazca Plate consists of a 4 km thick upper layer of velocity 5.55 km/sec and a thinner (2.5 km) but faster 7.5 km/sec lower layer which overlies a Moho of velocity 8.2 km/sec. The gravity model indicates that the plate has a dip of 5° beneath the continental slope and shelf. West of the trench, the lower crustal layers shallow, which may represent upward flexure of the oceanic plate due to compressive forces resulting from the subduction process.

The upper crustal layers of the 120 km long oceanic plate portion consist of a thin 1.7 km/sec sedimentary layer overlying a 5.0 to 5.2 km/sec upper layer. An underlying 5.6 to 5.7 km/sec lower layer becomes more shallow to the east within 60 km of the trench while a deeper 6.0 to 6.3 km/sec layer thickens to the east. The lower crustal model consists of a 7.4 to 7.5 km/sec high velocity layer which varies in thickness from 2.5 km to 4.0 km. The 8.2 km/sec Moho interface varies not more than ±0.5 km from a modeled depth of 10.5 km.

# Seismic Ray Trace Techniques Applied to the Determination of Crustal Structures Across the Peru Continental Margin and Nazca Plate at 9° S. Latitude

by

Paul Roy Jones III

A THESIS

submitted to

Oregon State University

in partial fulfillment of
the requirements for the
degree of

Doctor of Philosophy

Completed August 9, 1978

Commencement June 1979

APPROVED:

Redacted for Privacy

Associate Professor of Geophysics
in charge of major

Redacted for Privacy

Dean of the School of Oceanography

Redacted for Privacy

Dean of Graduate School

Date thesis is presented August 9, 1978

Typed by Deanna L. Cramer for Paul Roy Jones III

## ACKNOWLEDGEMENTS

This research was supervised by Dr. Stephen H. Johnson and I am grateful for his time and suggestions in supporting this study. In addition, I would like to thank Dr. Richard Couch for his expert knowledge on the development of gravity models. Conversions with fellow graduate students Joh Hanson, Judy Keser and Keith Wrolstad were helpful and appreciated. Finally, I would like to thank my parents for their patience and moral support during my academic career.

This research was conducted for the Nazca Plate Project and was supported through the National Science Foundation, International Decade of Ocean Exploration (Grant OCE76-05903-A02).

TABLE OF CONTENTS

Table of Contents -- continued

Page

## LIST OF FIGURES

List of Figures -- continued

# SEISMIC RAY TRACE TECHNIQUES APPLIED TO THE DETERMINATION OF CRUSTAL STRUCTURES ACROSS THE PERU CONTINENTAL MARGIN AND NAZCA PLATE AT 9° S. LATITUDE

## INTRODUCTION

The theory of plate tectonics is becoming well established through the worldwide study of the earth's crustal plates. As a part of the Nazca Plate Project funded by the National Science Foundation through the International Decade of Oceanic Exploration, Oregon State University (OSU) and the Hawaii Institute of Geophysics (HIG) obtained data to study in detail the processes of plate interaction which occurs between the Nazca oceanic plate and neighboring lithospheric plates. A significant portion of the data obtained lies along the eastern edge of the plate where it descends beneath the South American plate. This region is an important example of oceanic-continental plate convergence and along this boundary may lie evidence for the tectonic events which formed it.

Examples of active continental margins surround the Pacific Ocean basin, one of which is associated with the Peru-Chile Trench. This thesis is concerned with the analysis of a large set of mostly geophysical data obtained across the Peru margin at 9°S. The purpose of the study is to examine one area in great detail, determine the structure and to postulate hypotheses for its formation.

Previous research on the Peruvian continental margin concentrated on the broad geologic and tectonic features associated with this area and only recently has it been investigated in detail with marine geological and geophysical methods. The study of earthquakes that occur as the Nazca oceanic plate underthrusts the South American continental plate is important for determining contemporary tectonics in the region.

A study of earthquake hypocenters by Benioff (1954) established the presence of a dipping seismically active region (now known as a Benioff Zone) along the western margin of South America. The map by Barazangi and Dorman (1969) showed that the entire Peru-Chile Trench is seismically active. Later it was shown that seismicity displays a regionally segmented character (Kelleher, 1972; Kelleher et al., 1973; Swift and Carr, 1974; and Stauder, 1975) reflecting a change in the nature of subduction occurring along the corresponding segments of the convergent boundary. A first motion study by Abe (1972) on a shallow focus earthquake beneath the continental slope 10°44' S. indicates low-angle thrust faulting related to compressional stress within the descending plate.

Earlier surface work involved detailed bathymetric mapping of the Peru-Chile Trench (Zeigler et al., 1957; Fisher and Raitt, 1962). The first reported marine seismic refraction lines from Expedition Downwind (Scripps

Institute of Oceanography) for the Peru-Chile Trench and the Nazca Ridge (15°S.) were by Fisher (1958). Later, Fisher and Raitt (1962) and Hayes (1966) described these refraction lines and developed crustal cross sections near Callao, Peru (12°S.) which traversed the Peru-Chile Trench and the adjacent Andes. Scholl et al. (1968, 1970) obtained numerous airgun profiles across the Peru-Chile Trench and investigated the tectonics of the interaction of the oceanic-continental plates and the effect they might have on the trench sediments. The magnetic anomaly interpretations of Herron (1972) and Handschumacher (1976) help to reconstruct the Cenozoic spreading history of the southeastern Pacific.

The very large gravity anomalies associated with the Peru-Chile Trench were reported by Wuenschel (1952) from pendulum measurements made in 1947 aboard the submarine USS Conger. The surface ship gravity measurements presented by Hayes (1966) added significant detail and later Whitsett (1976) further mapped the area off southern Peru and modeled crustal and subcrustal cross sections of the coast and continental margin at 14°S. and 16.5°S.

Since its initiation in 1971, the Nazca Plate Project has produced detailed studies of the geology and geophysics of the Peru-Chile continental margin, trench and Nazca Plate (Kulm et al., 1973; Rosato, 1974; Prince et al., 1974; Hussong et al., 1975; Masias, 1976; Prince and Kulm, 1975; Kulm et al., 1975; Hussong et al., 1976; Kulm et al., 1976, Coulbourn and Moberly, 1976; Schweller, 1976; Kulm et al., 1977; Prince and Schweller, 1978; and others).

Imbricate thrusting in the Peru-Chile Trench and continental slope has been suggested from geological and geophysical studies. Kulm et al. (1973) and Prince and Kulm (1975) used single channel airgun profiles and piston cores to investigate a tholeiitic basalt ridge and suggested that the ridge was formed by compressional forces in the Peru Trench area. Based on multi-channel seismic reflection data, Kulm et al. (1975) presented further evidence of imbricate thrusting in the Peru continental slope. Additional work by Prince et al. (1974) and Prince and Schweller (1978) studied possible recent reverse faulting within the Peru-Chile Trench and between fault blocks of the oceanic floor just seaward of the trench. Hussong et al. (1975) suggested compressional faulting in the Nazca Plate 250 km from the trench. Structural cross sections of the basins of Peruvian and northern Chilean continental margins shown by Masias (1976) and Coulbourn and Moberly (1976) resemble those of arc-trench gaps. Here, the uppermost reflectors are undeformed turbidites while deeper reflectors are generally inclined landward with dips and deformation increasing with depth.

The crustal velocities and structures of the Peru continental margin, trench and part of the Nazca Plate displayed by Hussong _et al_. (1976) suggest that the rapidly moving Nazca oceanic crust (10 cm/yr; Minster _et al_., 1974) is thin and dense relative to other ocean basins. Structure and velocity distributions in the lower toe of the continental slope suggest uplifted imbricate thrust sheets containing oceanic sediments and rock. It was also found that slope velocities and structures change laterally and are interpreted as highly disrupted, downfaulted continental rocks. The basement rocks of the continental shelf are less faulted and covered with more than a kilometer of smoothly stratified sediments.

Acquired in March 1972 by OSU and HIG was a 360 km long seismic refraction and reflection, and gravity profile located across the continental shelf and slope, trench, and part of the Nazca Plate (Figure 1). The seismic refraction profile was designated Line 18-19 and this designation will be used for the seismic reflection and gravity profiles as well. Line 18-19 lies between 8°26'S., 79°06'W. and 9°52'S., 81°58'W. respectively. Other data gathered along the line include 3.5 kHz bathymetric profiles, a single channel reflection profile to the trench axis from near shore, and a multi-channel CDP reflection profile located 25 km to the north which was obtained under contract to Seiscom-Delta Corporation of Houston, Texas.

Hussong _et al_. (1976) reported a preliminary interpretation of HIG refraction data along Line 18-19. The

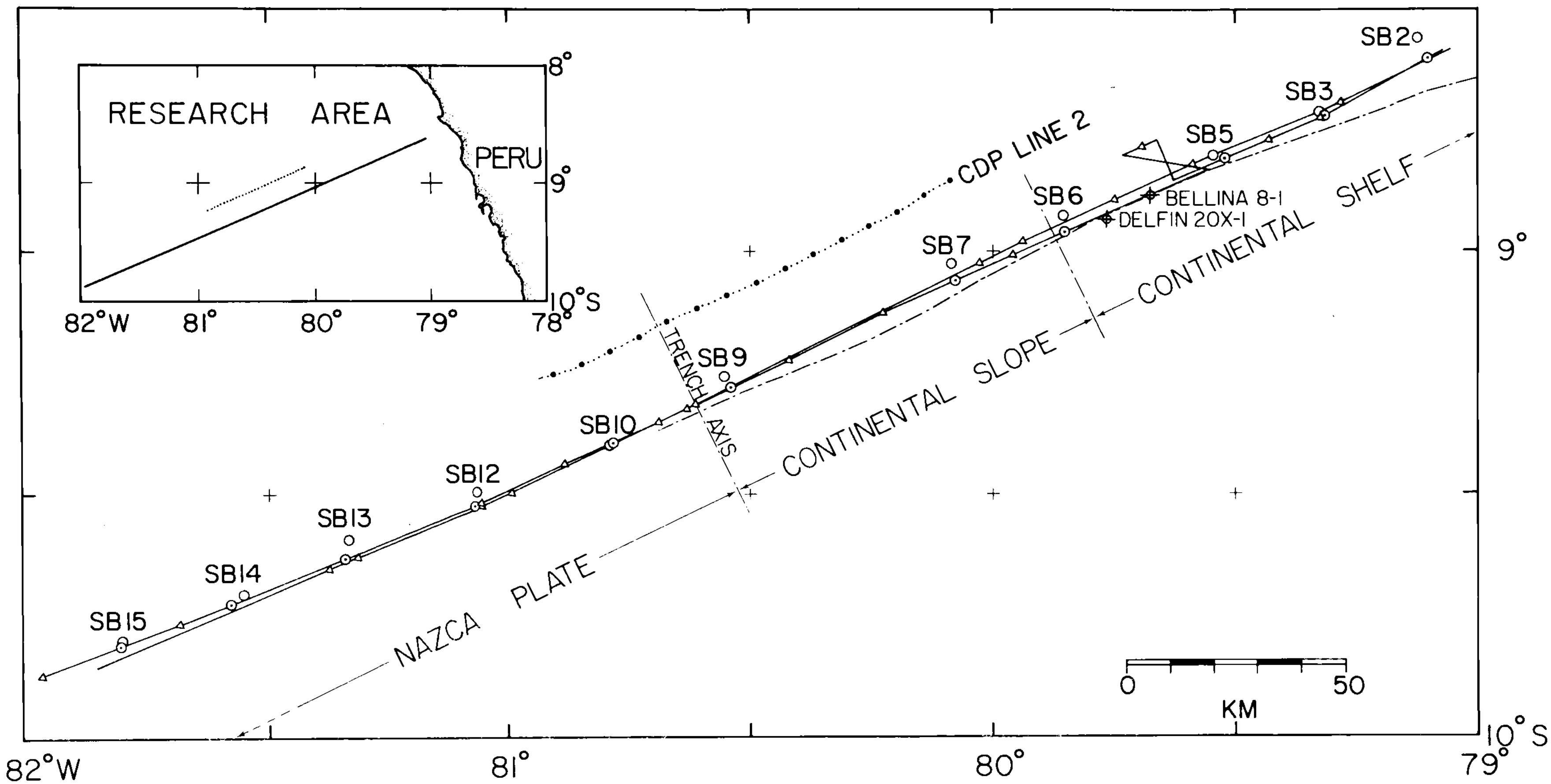


Figure 1. Location of seismic and gravity profiles at 9°S. Solid lines represent Line 18-19. The dashed and dotted lines are the 1974 OSU and CDP-2 tracklines. Triangles symbolize satellite navigation fixes; circles with dots and open circles are OSU sonobuoy deployment and HIG midship sonobuoy positions respectively. Crossed circles are exploratory well locations.

purpose of the present study is to determine a more detailed crustal and subcrustal cross section along Line 18-19 from seismic refraction and reflection data from both OSU and HIG data files and gravity data from HIG. The present study makes extensive use of secondary seismic arrivals in the refraction data, well log velocities and depths, near surface sediments structures and CDP velocity data to obtain an integrated model of the continental margin at 9°S.

# SEISMIC RAY TRACE METHODS

## Ray Tracing Methods

Conventional methods for the interpretation of refraction profiles work poorly in cases where subsurface structures change laterally along the profiles. A series of computer programs were developed for this study which compute and plot seismic reflection and refraction arrival times and visually display ray paths traced through a given and possibly complex model. This computer technique allows the interpreter to develop complex geological structure to match observed seismic refraction arrivals with those computed from a tentative model, to use velocity and depth information available from other data in order to compensate for near surface structures which affect the determination of velocities and depths to deep structures, and to model hypothetical cases in order to give a better understanding to the interpretation of seismic reflection and refraction data.

The computer ray tracing method can be used either as a forward modeling technique or in combination with conventional data inversion methods. The following is a review of ray tracing methods which have been described elsewhere.

Direct modeling techniques on a computer may be used to overcome the drudgery of trial and error interpretation encountered in indirect modeling and to improve the accuracy of the end result. The methods of Scott (1973) and Ocola (1972a, 1972b) are examples of raytracing used with inversion techniques for seismic refraction data. Both techniques are two-dimensional methods for determining layer boundaries represented by low-order polynomial functions of position where lateral homogeneity is required. The modeling of more complex geological structures requires a ray tracing method that allows for both vertical and lateral inhomogeneity. An inverse modeling technique called 'the delay-time-function method' (Morris, 1972) can determine lateral changes in both structure and velocity. The method assumes that the configuration of the boundary between the upper model layers and a basal refractor can be represented by a combination of polynomial functions and Fourier series. However, a complete determination of complex geological models is not possible because the method only allows for lateral velocity variations in the basal refractor.

The objective of ray tracing as a forward modeling technique is to produce a theoretical travel time plot which will coincide with an observed arrival plot. Foreward modeling requires an a priori model which is most easily developed through the use of standard data inversion techniques. The initial model thus generated is usually quite simple and must be refined through iteration by the interpreter before a final model is determined which agrees best with the available data. The two main advantages to a forward modeling technique are fewer restrictions on the model and the ability to use quantitative information not available from seismic refraction or reflection data.

The forward modeling technique of seismic ray tracing in laterally inhomogeneous media has been approached by several authors. The methods of Yacoub et al. (1968), Jacob (1970), Sorrels et al. (1971), and Shah (1973) use velocity models comprised of constant velocity geological units of arbitrary shape in either two or three dimensions. The methods of Yacoub et al. (1968) and Jacob (1970) are poorly suited for seismic refraction exploration because provision is not made for the critically refracted ray traveling along an interface (headwave). In a step towards further complexity, Gerbrande (1976) traces rays through models with two dimensional elements where velocity gradients are permitted. Velocity gradient modeling usually requires well control or very close shot spacing to warrant its use.

The ray tracing technique developed for the analysis of Line 18-19 seismic refraction and reflection data was used on a Data General NOVA minicomputer. Computational speed becomes very important when tracing ray paths in complex geological structures. For this reason, a method similar to Sorrells *et al*. (1971) and Shah (1973) was chosen because it is based on vector operations which are computationally faster than similar methods based on numerical integration (Jacob, 1970) or transcendental functions (Yacoub *et al*., 1968; Gerbrande, 1976).

## Derivation of Equations

Computer program RAYTRACE (Appendix I) is based upon the ray solution to the wave equation wherein the wave equation is transformed to the eikonal equations whose solutions are in terms of wave surfaces and ray paths (Officer, 1958, pp. 37-47). Through the use of ray paths, analysis techniques can be developed from the laws of geometrical optics provided the seismic wavelength is reasonably short in relation to the velocity gradients. The ray path method is adequate except for problems which involve diffraction effects including surface waves, interference of waves, and the amplitude of wave motion (Grant and West, 1965).

Despite the above problems, the laws of geometrical optics form the basis upon which most seismic reflection and refraction interpretation methods are based. The following derivation of equations for RAYTRACE is given with this in mind.

## Basic Ray Tracing Equations

In this section one starts with the basic vector equations of reflection and refraction at an interface and derives the general refraction equation in terms of unit vectors.

Consider the geometry in Figure 2. Let $\hat{n}_{j+1}$ specify the unit vector normal to the (j+1)th interface. The interface separates constant velocities $V_j$ from $V_{j+1}$ and may be at any orientation. A ray specified by the unit vector $\hat{p}_j$ is incident on the interface from the medium characterized by the velocity $V_j$. At the interface, both reflection and refraction may occur but refracted unit ray vectors orient according to Snell's law. Consider first the reflected unit ray vector $\hat{p}_j^r$ and its normal and tangential components to the interface.

Let the incident and reflected unit vectors be given as

$$\hat{p}_j = \vec{p}_j^{\,N} + \vec{p}_j^{\,T} \tag{1}$$

and

$$\hat{p}_j^r = \vec{p}_j^{\,rN} + \vec{p}_j^{\,rT} \tag{2}$$

where N = normal and T = tangential components of

$$\vec{p}_j^{\,N} = -\vec{p}_j^{\,rN} \; . \tag{3}$$

Because vectors $\hat{p}_j$, $\hat{p}_j^r$ and $\hat{n}_{j+1}$ are coplanar then

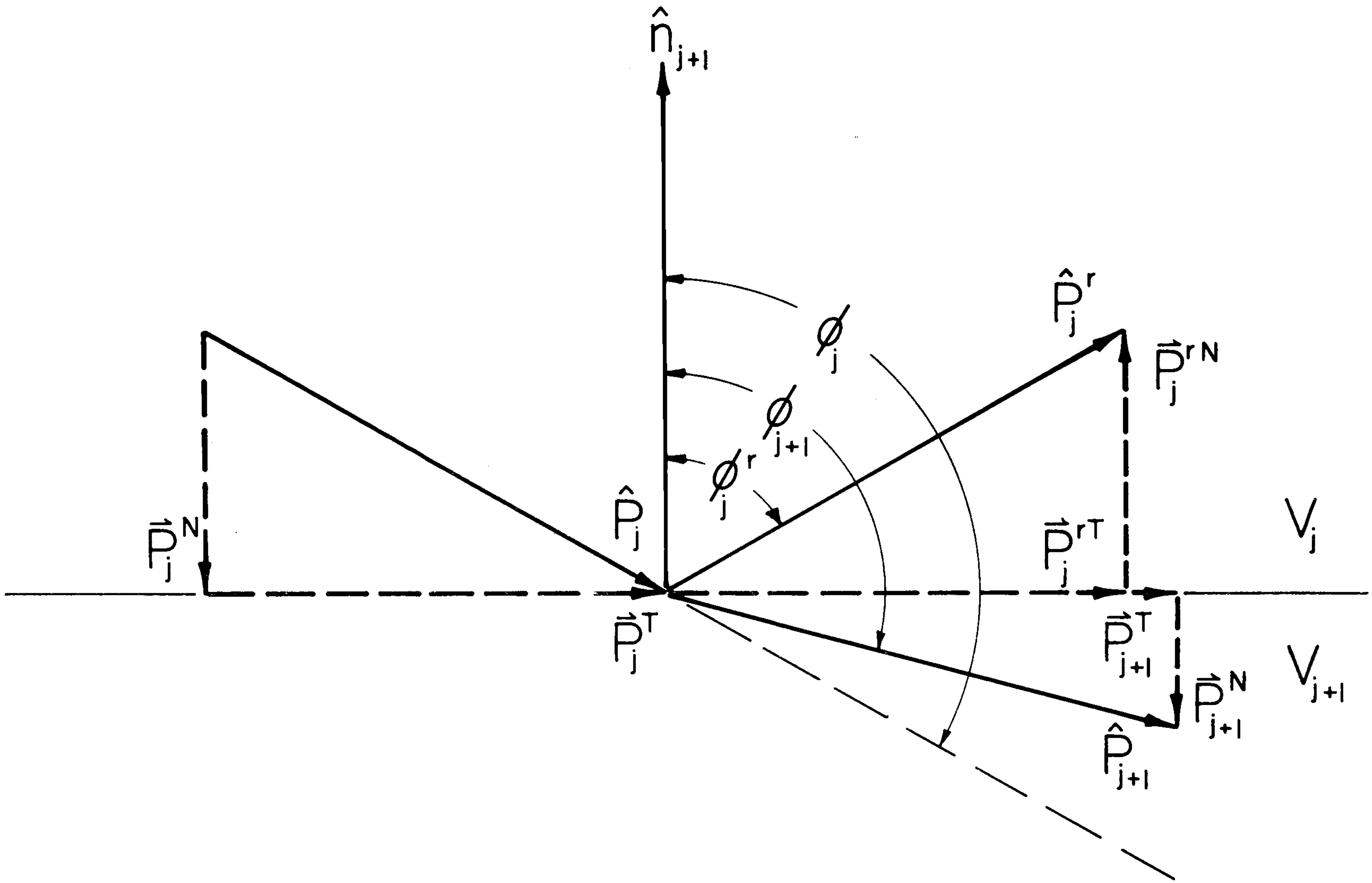


Figure 2. Geometry of reflection and refraction at a plane interface.

$$\vec{p}_j^{\,T} = \vec{p}_j^{\,rT} \quad . \tag{4}$$

From equations (3) and (4) in (2), one obtains

$$\hat{p}_j^{\,r} = -\vec{p}_j^{\,N} + \vec{p}_j^{\,T} \tag{5}$$

or by adding (1) to (5)

$$\hat{p}_j^{\,r} = \hat{p}_j - 2\vec{p}_j^{\,N} \quad . \tag{6}$$

Equation (6) may be written as

$$\vec{p}_j^{\,N} = (\hat{p}_j \cdot \hat{n}_{j+1})\hat{n}_{j+1} \tag{7}$$

or

$$\hat{p}_j^{\,r} = \hat{p}_j - 2(\hat{p}_j \cdot \hat{n}_{j+1})\hat{n}_{j+1} \quad . \tag{8}$$

Equation (8) represents a reflection vector in a medium with a velocity $V_j$. Therefore the reflection vector for a medium with velocity $V_{j+1}$ can be represented by,

$$\hat{p}_{j+1}^{\,r} = \hat{p}_{j+1} - 2(\hat{p}_j \cdot \hat{n}_{j+1})\hat{n}_{j+1} \quad . \tag{8a}$$

Now let $\hat{p}_{j+1}$ represent the refracted ray in medium j+1

$$\hat{p}_{j+1} = \vec{p}_{j+1}^{\,N} + \vec{p}_{j+1}^{\,T} \tag{9}$$

Snell's law states that

$$\frac{\sin\phi_j}{V_j} = \frac{\sin\phi_{j+1}}{V_{j+1}} \tag{10}$$

where $\phi_j$ is the angle of incidence and $\phi_{j+1}$ is the angle of refraction. Since

$$\sin\phi_j = \frac{\left|\vec{p}_j^{\,T}\right|}{\left|\hat{p}_j\right|} = \left|\vec{p}_j^{\,T}\right| \tag{11a}$$

and

$$\sin\phi_{j+1} = \frac{\left|\vec{p}_{j+1}^{\,T}\right|}{\left|\hat{p}_j\right|} = \left|\vec{p}_{j+1}^{\,T}\right| \tag{11b}$$

then

$$\left|\vec{p}_{j+1}^{\,T}\right| = \frac{V_{j+1}}{V_j}\left|\vec{p}_j^{\,T}\right| , \tag{11}$$

and since the directions of $\vec{p}_j^{\,T}$ and $\vec{p}_{j+1}^{\,T}$ are the same,

$$\vec{p}_{j+1}^{\,T} = \frac{V_{j+1}}{V_j}\vec{p}_j^{\,T} . \tag{12}$$

Now consider the relationship for the normal components of the incident and refracted rays. Given the equations

$$\cos\phi_{j+1} = \frac{\left|\vec{p}_{j+1}^{\,N}\right|}{\left|\hat{p}_j\right|} = \left|\vec{p}_{j+1}^{\,N}\right| \tag{13a}$$

$$\cos\phi_j = \frac{\left|\vec{p}_j^{\,N}\right|}{\left|\hat{p}_j\right|} = \left|\vec{p}_j^{\,N}\right| , \tag{13b}$$

whereby the expansion of (13a) results in

$$\left|\vec{p}_{j+1}^{\,N}\right| = [1 - \sin^2\phi_{j+1}]^{\frac{1}{2}} \tag{13c}$$

and

$$\left|\vec{p}^{N}_{j+1}\right| = \left[\frac{\sin^2\phi_{j+1}}{\sin^2\phi_j}\left(\frac{\sin^2\phi_j}{\sin^2\phi_{j+1}} - \sin^2\phi_j\right)\right]^{\frac{1}{2}} \tag{13d}$$

and finally through the use of Snell's law from (10) and a familiar trigonometric identity one obtains

$$\left|\vec{p}^{N}_{j+1}\right| = \pm\frac{V_{j+1}}{V_j}\left[(\cos^2\phi_j - 1) + \left(\frac{V_j}{V_{j+1}}\right)^2\right]^{\frac{1}{2}} . \tag{13e}$$

Substitution of (13b) into (13e) gives

$$\left|\vec{p}^{N}_{j+1}\right| = \pm\frac{V_{j+1}}{V_j}\left[\left|\vec{p}^{N}_{j}\right|^2 + \left(\frac{V_j}{V_{j+1}}\right)^2 - 1\right]^{\frac{1}{2}} \tag{13f}$$

and by rearrangement of (13f) we see that the normal components are not linearly related to each other as are the tangential components of the incident and refracted rays of equation (12)

$$\vec{p}^{N}_{j+1} = \pm\frac{V_{j+1}}{V_j}\left[\left|\vec{p}^{N}_{j}\right|^2 - \frac{V^2_{j+1} - V^2_j}{V^2_{j+1}}\right]^{\frac{1}{2}}\hat{n}_{j+1} . \tag{13}$$

Rearrangement of (1) gives

$$\vec{p}^{T}_{j} = \hat{p}_j - \vec{p}^{N}_{j} \tag{14}$$

and from (9) and (12) one forms

$$\hat{p}_{j+1} = \vec{p}^{N}_{j+1} + (\hat{p}_j - \vec{p}^{N}_{j})\,\frac{V_{j+1}}{V_j} \tag{15}$$

By substitution of (13) and (7) into (15), the refracted unit vector may be derived,

$$\hat{p}_{j+1} = \pm\frac{V_{j+1}}{V_j}\left[\left|\vec{p}_j^N\right|^2 - \frac{V_{j+1}^2 - V_j^2}{V_{j+1}^2}\right]^{\frac{1}{2}} \hat{n}_{j+1} + (\hat{p}_j - (\hat{p}_j \cdot \hat{n}_{j+1})\hat{n}_{j+1}) \frac{V_{j+1}}{V_j} \tag{16a}$$

and by rearrangement forms

$$\hat{p}_{j+1} = \frac{V_{j+1}}{V_j}\left\{\hat{p}_j - \left[\hat{p}_j \cdot \hat{n}_{j+1} \mp \left(\left|\vec{p}_j^N\right|^2 - \frac{V_{j+1}^2 - V_j^2}{V_{j+1}^2}\right)^{\frac{1}{2}}\right]\hat{n}_{j+1}\right\} \tag{16b}$$

which may be written as

$$\hat{p}_{j+1} = \frac{V_{j+1}}{V_j}\left\{\hat{p}_j - \left[\hat{p}_j \cdot \hat{n}_{j+1} \mp \left((\hat{p}_j \cdot \hat{n}_{j+1})^2 - \frac{V_{j+1}^2 - V_j^2}{V_{j+1}^2}\right)^{\frac{1}{2}}\right]n_{j+1}\right\} \cdot \tag{16}$$

The choice of sign in (16) is determined from the sign of the inner product, $\hat{p}_j \cdot \hat{n}_{j+1}$.

Ray Path-Length Equations

In this section one starts with the basic ray path-length equations and derives the general equations for computing the distance traveled by a ray through a multi-layered model. From the geometry of Figure 3 one can write

$$\vec{D} = h\hat{k} + \vec{M} \tag{17}$$

and

$$\hat{n} \cdot \vec{D} = h(\hat{n} \cdot \hat{k}) \tag{18}$$

where

$$\vec{D} = \left|\vec{D}\right|\hat{p} \ . \tag{19}$$

Since

$$\hat{n} \cdot \vec{D} = \left|\vec{D}\right|\hat{n} \cdot \hat{p} \tag{20a}$$

then

$$\left|\vec{D}\right| = \frac{h(\hat{n} \cdot \hat{k})}{\hat{n} \cdot \hat{p}} \ . \tag{20}$$

The travel time for this path is

$$T = \frac{h(\hat{n} \cdot \hat{k})}{V(\hat{n} \cdot \hat{p})} \ . \tag{21}$$

According to Figure 4 it is seen for j=1 that

$$\vec{D}_1 = h_2\hat{k} + \vec{M}_2 - \vec{D}_0 \tag{22a}$$

and

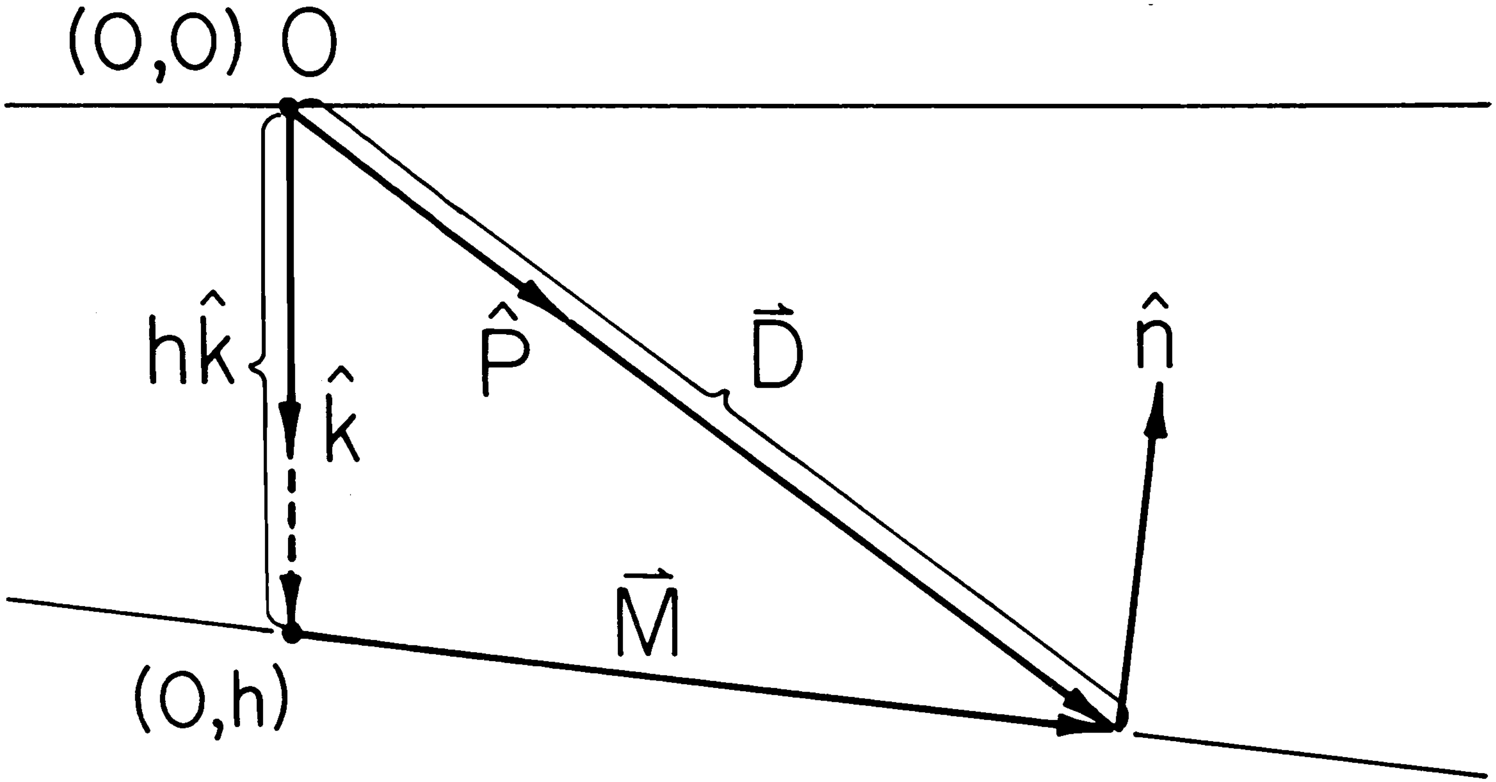


Figure 3. Geometry for the calculation of the length of the ray path between two plane interfaces.

$$\left|\vec{D}_1\right| = \frac{\hat{n}_2 \cdot (h_2\hat{k} - \vec{D}_0)}{\hat{n}_2 \cdot \hat{p}_1} \tag{22b}$$

Similarly for j = 2 one obtains

$$\left|\vec{D}_2\right| = \frac{\hat{n}_3 \cdot (h_3\hat{k} - (\vec{D}_0 + \vec{D}_1))}{\hat{n}_3 \cdot \hat{p}_2} \tag{22c}$$

By induction, the general formula for the ray path length in $j^{th}$ layer is

$$\left|\vec{D}_j\right| = \frac{\hat{n}_{j+1} \cdot (h_{j+1}\hat{k} - \sum_{\ell=0}^{j-1} \vec{D}_\ell)}{\hat{n}_{j+1} \cdot \hat{p}_j} \tag{22}$$

where $\vec{D}_0$, the initial path, is calculated separately. The time traveled is given by

$$T_j = \frac{\left|\vec{D}_j\right|}{V_j} \quad . \tag{23}$$

The total vector distance from origin to the (j+1)th interface is given by

$$\vec{S}_j = \sum_{\ell=0}^{j} \vec{D}_\ell \quad . \tag{24}$$

The total time for (24) is

$$\tau_j = \sum_{\ell=0}^{j} \frac{\left|\vec{D}_\ell\right|}{V_\ell} \quad . \tag{25}$$

Equations (24) and (25) are used whenever

$$\hat{n}_{j+1} \cdot \hat{p}_j \leq 0 \quad . \tag{26}$$

Rays satisfying equation (26) are called "downgoing" with respect to the (j+1)th interface. Consider a ray in Figure 4 originating from $\vec{Q}$ on the $\ell$th interface such that

$$\hat{n}_\ell \cdot \hat{p}_\ell \geq 0 \quad . \tag{27}$$

Rays satisfying equation (27) are called "upgoing" with respect to the $\ell$th interface.

Next consider the ray $\vec{D}^u_\ell$ which is an "upgoing" ray (see Figure 4). The ray is assumed to start at a point on the $\ell$th interface specified by radius vector $\vec{Q}$. One has

$$\vec{M}_\ell = (h_{\ell+1} - h_\ell)\hat{k} + \vec{M}_{\ell+1} + \vec{D}^u_\ell \tag{28a}$$

or

$$\vec{M}_{\ell+1} = \vec{Q} - h_{\ell+1}\hat{k} \tag{28b}$$

and

$$\vec{D}^u_\ell = h_\ell\hat{k} - \vec{Q} + \vec{M}_\ell \quad . \tag{28c}$$

Now if the inner product is taken with $\hat{n}_\ell$ one obtains

$$\hat{n}_\ell \cdot \hat{p}_\ell \left|\vec{D}^u_\ell\right| = \hat{n}_\ell \cdot (h_\ell\hat{k} - \vec{Q}) \tag{28d}$$

and therefore

$$\left|\vec{D}^u_\ell\right| = \frac{\hat{n}_\ell \cdot (h_\ell\hat{k} - \vec{Q})}{n_\ell \cdot p_\ell} \quad . \tag{28e}$$

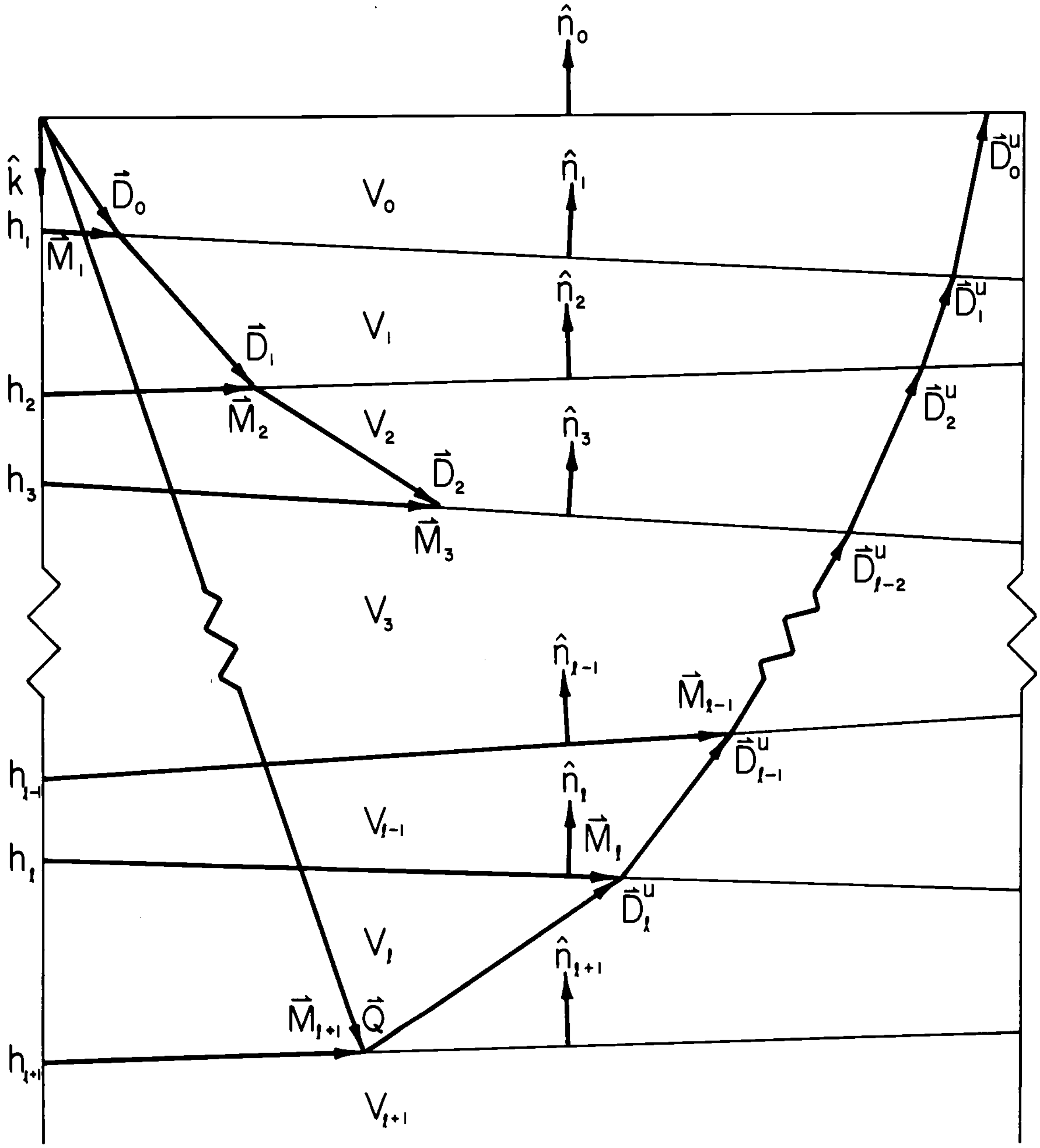


Figure 4. The geometry of refraction through several plane dipping layers.

Likewise one obtains

$$\vec{D}^u_{\ell-1} = \frac{\hat{n}_{\ell-1} \cdot (h_{\ell-1}\hat{k} - (\vec{Q} + \vec{D}^u_{\ell}))}{\hat{n}_{\ell-1} \cdot \hat{p}_{\ell-1}} \quad . \tag{28f}$$

The general formula for computing the "upgoing" path lengths is then

$$\left|\vec{D}^u_{\ell-j}\right| = \frac{\hat{n}_{\ell-j} \cdot (h_{\ell-j}\hat{k} - (\vec{Q} + \sum_{m=0}^{j-1} \vec{D}^u_{\ell-m}))}{\hat{n}_{\ell-j} \cdot \hat{p}_{\ell-j}} \tag{28}$$

where $j \geq 1$.

The travel time is given by

$$T^u_{\ell-j} = \frac{\left|\vec{D}^u_{\ell-j}\right|}{V_{\ell-j}} \tag{29}$$

<u>Critical Refraction</u>

In this section the equations necessary for the computation of travel times and distances associated with a critically refracted ray path are derived in vector notation.

The condition for critical refraction is

$$\sin\phi_\ell = \frac{V_\ell}{V_{\ell+1}} \tag{30}$$

where $\phi_\ell$ is the angle of incidence.

Equation (30) can be written as

$$(\hat{p}_\ell \cdot \hat{n}_{\ell+1})^2 = \frac{V_{\ell+1}^2 - V_\ell^2}{V_{\ell+1}^2} \quad . \tag{31}$$

The initial ray which will produce the incidence ray $\hat{p}_\ell$ must be found by numerical methods which are discussed in Appendix I. The unit vector in the direction of the ray after critical refraction is derived by substituting (31) into equation (16), so that

$$\hat{p}_{\ell+1} = \frac{V_{\ell+1}}{V_\ell} (\hat{p}_\ell - (\hat{p}_\ell \cdot \hat{n}_{\ell+1})\hat{n}_{\ell+1}) \quad . \tag{32}$$

The ray path of the critically refracted ray is given by

$$\vec{D}_{\ell+1} = r\hat{p}_{\ell+1} \tag{33}$$

where r is a scalar denoting the path length along the interface. The returning segment of the ray path is found through the use of equation (28) with $\vec{Q}$ defined as

$$\vec{Q} = \vec{S}_\ell + \vec{D}_{\ell+1} \tag{34}$$

where $\vec{S}_\ell$ is the radius vector from the origin to the point of critical refraction on the $\ell$th interface.

## Examples of Ray Trace Modeling

The construction of a velocity model by ray tracing, like any indirect interpretation method, requires a degree of skill and judgment which can only be acquired by experience. A number of interpretative aids were devised to simplify the procedure and these include visual plots of the ray paths through the model and theoretical travel time plots from a test model. Other options incorporated the choice to specify ray traces from one or more individual layers for any shot point location and a simple procedure to change the velocity or shape of the model.

Figures 5a to 5b illustrate these interpretation criteria. The geological model in Figure 5b represents a hypothetical case for a simple plane dipping layer of velocity 6 km/sec overlain by a 4 km/sec layer. Both layers are intersected by a 4.8 km/sec dike intrusion which has been displaced to the right across the plane dipping interface. Although surface shot points are located at both ends of this model, they could have been located anywhere on or within the model. Figure 5c represents the computer velocity model required by computer program RAYTRACE which requires the division of areas into quadralateral cells of constant velocity. The travel time plot in Figure 5a shows the compressional wave direct arrivals and the reflected and critically refracted arrivals from the plane dipping layer interface. Some of the reflected and refracted ray

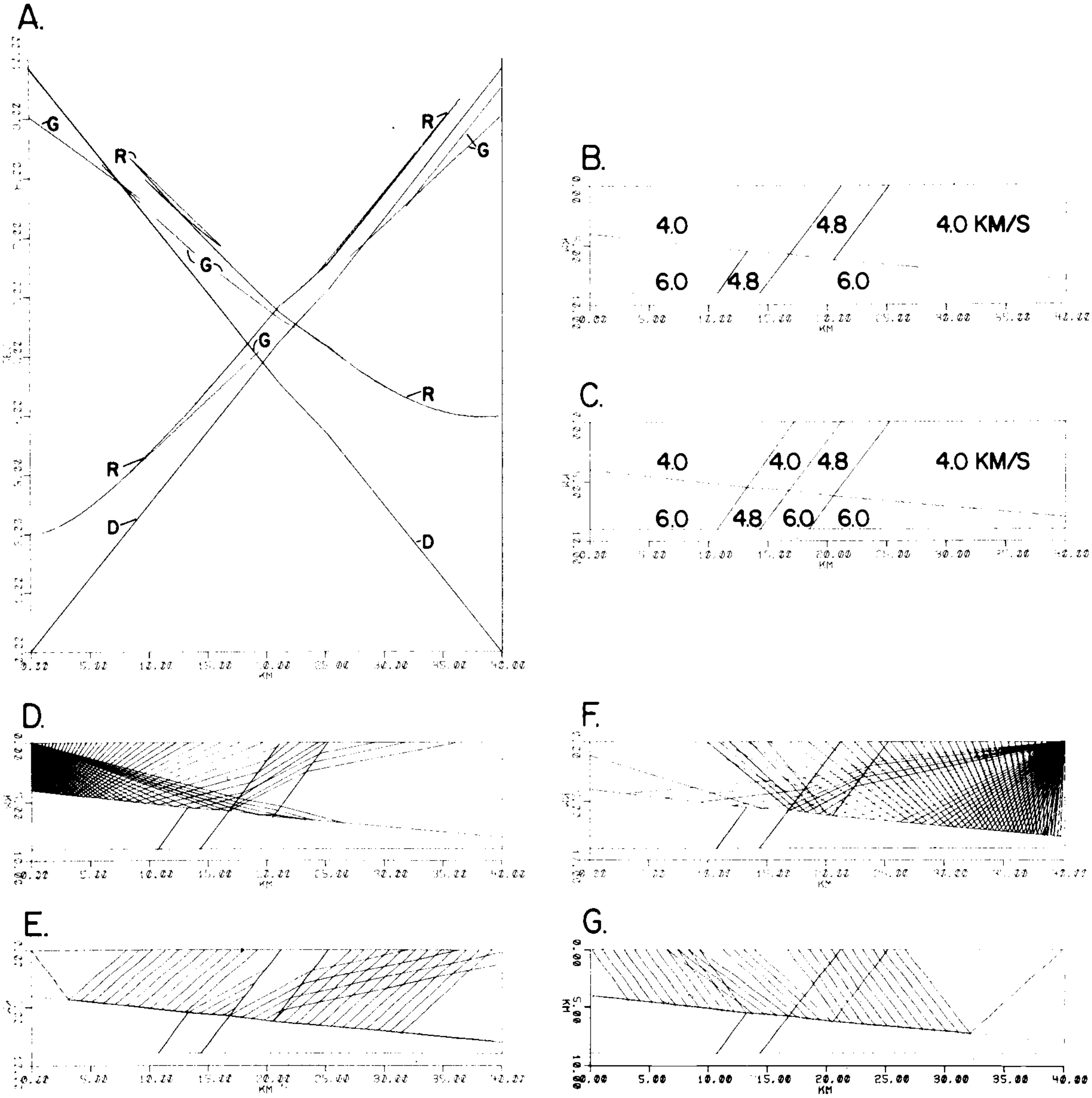


Figure 5. Model example for program RAYTRACE. Figure A represents the travel time curves where D = direct, R = reflected, and G = headwave refracted arrivals. Figure B represents the geological model and Figure C is the computer model. Figures D through G are examples of reflected and refracted ray paths.

paths are traced in Figures 5d to 5g. In the headwave refraction case in Figure 5e, the intrusion produces a shadow zone because in the center of the model rays going upward from the lower interface have exceeded the critical angle before entering the intrusion from the left, while those entering the intrusion from below are refracted to the right because of the velocity inversion. This visualization of the rays can be both instructive and useful in the iteration of the structure to produce agreement with the observed arrivals. A specific example of this is the estimation of horizontal offset distances of rays returning to the upper surface of a model from a headwave refractor. Once it is apparent that such an offset exists, an interpreter can modify a specific section of layer interface to match a time advancement or delay observed in a travel time curve by computation from the formula

$$\Delta z = \frac{V_n V_{n-1}}{2\sqrt{V_n^2 - V_{n-1}^2}} \Delta t$$

where $\Delta z$ is the interface displacement, $\Delta t$ is the arrival time difference, and $V_{n-1}$, $V_n$ are the velocities above and below the layer interface respectively (Pakiser and Black, 1957).

During the interpretation of seismic refraction data of Line 18-19, it was instructive to develop simple velocity-depth models and their respective travel time curves to serve as examples. Illustrated in Figures 6a through 6f are some of the travel time curves produced by ray tracing. The dimensions and velocities of these models represent variations of possible cases that might be observed on the continental shelf at 9°S. To simplify interpretation, the water layer has been removed. Figure 6a is a model of 4.5 km/sec half-space velocity overlain by a 2.5 km/sec layer and its corresponding travel time plot. Five variations applied to this model are illustrated in Figures 6b through 6f.

Figure 6b represents the simple case of a plane dipping layer and its corresponding travel time plot. The indication of a plane dipping layer is the later intercept time and higher updip apparent velocity as compared with the lower downdip apparent velocity of waves refracted from the same interface. Figure 6c demonstrates the effect of a dip change midway between shot points. Although there is a difference in intercept times, which suggests depth differences under each shot point, the major differences occurs in the change in apparent velocities midway between shot points. Both sets of refracted arrivals appear to bend upward rather than downward as would be expected for a multilayered case. It is important to stress the necessity for shooting in opposite directions.

Figures 6d through 6f deal with lateral variations in the half-space velocity. An important aspect is the change

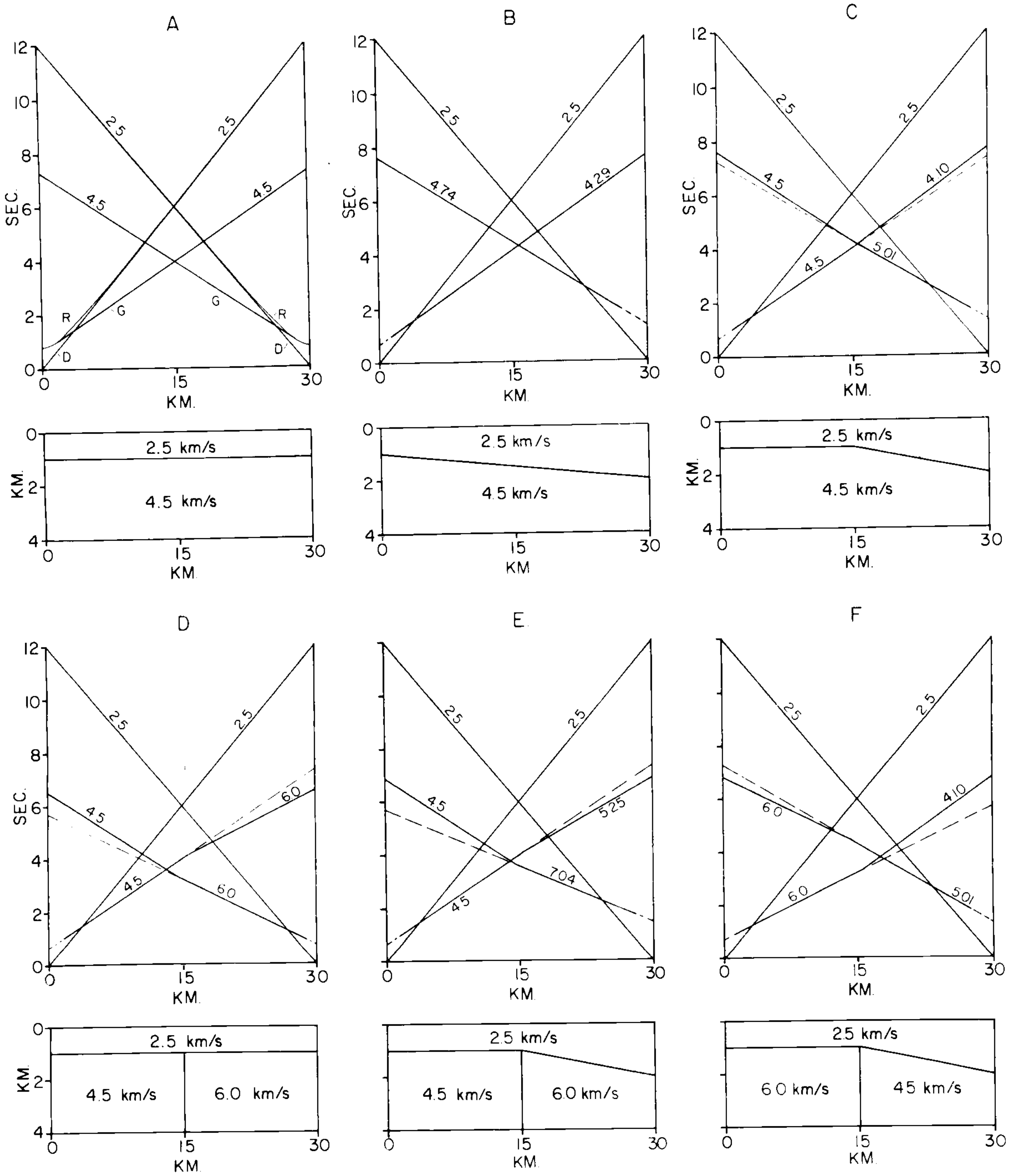


Figure 6. Examples of travel time curves produced by RAY-TRACE. Apparent velocities in km/sec are given for refracted arrivals.

in apparent velocity across each model which produces a set of refracted arrivals whose apparent velocity decreases with distance. This is a diagnostic feature in the analysis of seismic refraction records where lateral velocity variations exist. Finding lateral velocity variations in marine refraction data is often difficult due to incompletely reversed lines caused by sonobuoy drift and ship navigation error. For this reason it is common to determine an approximate solution for the structure by a delay-time method (Gardner, 1939; Pakiser and Black, 1957) before attempting lateral velocity determinations (Morris, 1972). The complication of combined structure and lateral velocity variations is demonstrated in Figures 6e and 6f.

# SEISMIC MODEL

## Refraction Line 18-19

The eleven-station seismic refraction profile shown in Figure 1 is an adaptation of the land seismic method of shooting overlapping refraction lines. Line 18-19 used more than 400 explosive charges over a profile length which exceeds 360 km. A description of the method and instruments used is given in the next section.

## Method and Instrumentation

The marine seismic refraction method for this experiment used single receivers and moving shot points. Standard military sonobuoys of the type AN/SSQ-41A were seismic detectors for Line 18-19. Each sonobuoy was modified to provide a longer lifetime for long seismic refraction profiles by substituting a dry cell battery pack for the seawater battery. Sonic information detected by 4 hydrophones deployed 18 meters below the surface was transmitted from the sonobuoy to the ship by a frequency modulated transmitter in the frequency band of 162 to 174 MHz. The sonic response of the sonobuoy increases at about 5 db/octave in the frequency range from 1 to 1000 Hz. The transmitted signal was received on a modified police band receiver, amplified, bandpass filtered and recorded at 50 mm/sec on an oscillographic camera. The recorded traces included high frequency, low frequency and unfiltered sonobuoy signals, clock channel and signal from the streamer which was used to detect the shot break.

The R/V Yaquina from Oregon State University and the R/V Kana Keoki from Hawaii Institute of Geophysics were the shooting ships for refraction Line 18-19. Both shooting ships used canned Nitromon as the chemical explosive with shot sizes varying from 1 to 200 pounds. Sonobuoys were deployed approximately every 30 km by the R/V Yaquina which acted as the lead ship. At the start of the line, the lead ship deployed a sonobuoy and began shooting to the west at three minute intervals. After a suitable interval, the R/V Kana Keoki, acting as the trailing ship 40 to 50 km behind, began to shoot and both ships alternated shots which were set off at three minute intervals. The combined refraction data from both ships produced reversed refraction lines because their tracklines were nearly identical (Figure 1). The maximum sonobuoy to ship distance was typically greater than 70 km and thus the profiles overlapped. This large distance was obtained by reception of the sonobuoy on the lead ship until the sonobuoy was about 30 km astern, at which time the sonobuoy was within telemetry range of the second ship which would then receive signals from the sonobuoy as the ship approached and passed it. The second ship continued to receive the sonobuoy until it was at least 30 km astern.

## Navigation

The position accuracy of marine seismic refraction profiles depends upon the errors in navigation of the shooting ship and the location of the sonobuoys (Sheriff, 1967). Unlike geophone strings used on land, sonobuoys are free to drift and thus require special techniques for accurate location. Both research vessels were navigated by satellite navigation fixes and by dead reckoning between fixes.

Radial distances from each shot point to the sonobuoy were computed from the corrected direct wave travel time and an assumed water velocity of 1.5 km/sec. An estimate of a sonobuoy location was determined by swinging arcs from alternating east and west shot points. The failure of the arcs to intersect gives an indication in the location error for both ships combined. The RMS error for sonobuoy location by both ships is approximately 110 meters in the distance range 10 to 25 km. The error was smaller for distances less than 10 km. At distances greater than 25 km it was necessary to extrapolate rather than observe a direct arrival time.

## Initial Data Reduction Methods

Arrival times were chosen on the basis of changes in amplitude, period and wave shape. Visual correlation of the traces with different band pass recordings on each seismogram also helped in determining first and secondary arrivals. Composite record sections were not constructed because it would have required hand-tracing over 1200 seismograms. Instead, a visual correlation of phases from seismogram to seismogram was performed by laying 4 to 5 sequential seismograms side by side. This permitted picking arrivals according to similarity of wave shape and the line-up of arrivals when hand-plotted on a preliminary time-distance plot. Corrections were made for depth of charge at time of detonation and to a surface datum. Computer generated time distance (T-X) plots of the fully corrected data were used in the model interpretations. In addition to the normal T-X plots, reduced T-X plots formed by subtracting the shot distance divided by 6.0 km/sec from each arrival time were used for sonobuoys 10 through 15.

Interpretations were made of the reversed and split spread profiles in terms of plane dipping layers by the methods of Adachi (1954) and Johnson (1976). These methods relate observed apparent velocities and intercept times to true velocities and layer thicknesses. Straight line fits to the observed arrival times was performed by eye except for sonobuoys 10 through 15 where the method of Steinhart and Meyer (1961) was used. This method fits least squares lines to the refracted arrivals of both profiles simultaneously while restraining the endpoints in order to satisfy reciprocity.

The purpose of the preliminary velocity and depth analysis is to develop an initial two-dimensional velocity model for ray tracing. The ray tracing technique then is used to improve the agreement between calculated and observed arrival times by making small changes to the structural model or to the velocities.

Confusion of P-wave with $S_V$-waves is a possible problem in seismogram analysis, especially in shallow water. A set of P-wave arrivals can be followed across a record section after they have been superseded by the next set of yet faster P-wave arrivals. $S_V$-waves in the low velocity sediments have been observed occasionally in shallow water but have not been reported in deep-water measurements (Ewing, 1963). According to Houtz _et al_. (1968) shear waves from the oceanic layer (Layer 3) are not recorded where thick sediment cover occurs and may be due to higher sediment velocities at the sediment-basement interface, where the conversion from P to $S_V$ waves occurs. The increase in the sediment-basement velocity ratio would decrease the shear wave amplitude. Data from Houtz _et al_. (1968) for the North Atlantic shows that shear waves are not observed when the sediment-basement velocity ratio is greater than 0.42. If Poisson's ratio is 0.25 in the basement layer then the shear wave velocity will range from 216 to 3.2 km/sec, corresponding to basement P-wave velocities of 4.5 to 5.5 km/sec. If the velocity of the sediment immediately above basement is 3.0 km/sec, then either no basement shear wave refraction can occur or they occur only at great distances from the shot point. Due to the high sediment-basement velocity ratios observed in the shallow-water profiles along Line 18-19, one concludes that no $S_V$-waves were confused with P-wave arrivals.

## Seismic Reflection Data

Both OSU and HIG obtained a number of single channel airgun reflection profiles along Line 18-19 in 1972. Figure 7 shows the OSU airgun profile for the continental shelf and part of the slope. The seismic sources were twin 40 cu. in. airguns and the streamer signal was band pass filtered in the range 30 to 160 Hz before display on a graphic recorder. A later airgun profile with a more expanded horizontal scale and better shelf and slope resolution was obtained from the R/V Yaquina in 1974 using twin 40 cu. in. airguns. Part of this profile is shown in Figures 8 and 9. A 3.5 kHz bathymetric profile obtained in 1972 also shows sub-bottom sediment resolution (Figure 10).

A 24-channel CDP digital seismic reflection line 100 km long crosses the Peru-Chile Trench at approximately 9°10'S. The profile line, called CDP-2, covers the continental slope and trench, parallels seismic refraction Line 18-19 and lies 25 km to the north (Figure 1). The data was acquired and processed by the Seiscom-Delta Corporation of Houston,

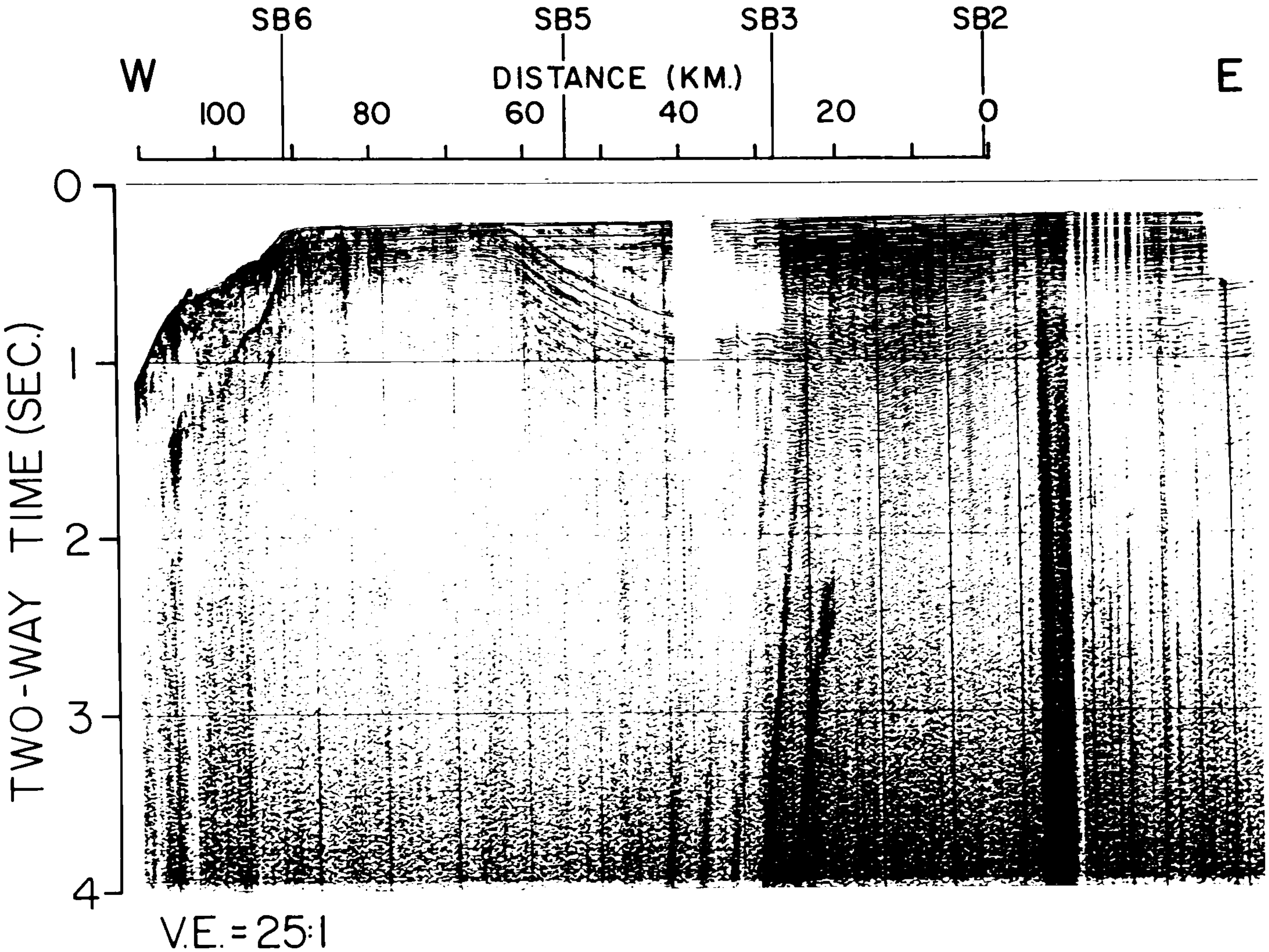


Figure 7. Single channel reflection profile across the continental shelf and upper slope at 9°S. (modified from Masias, 1976).

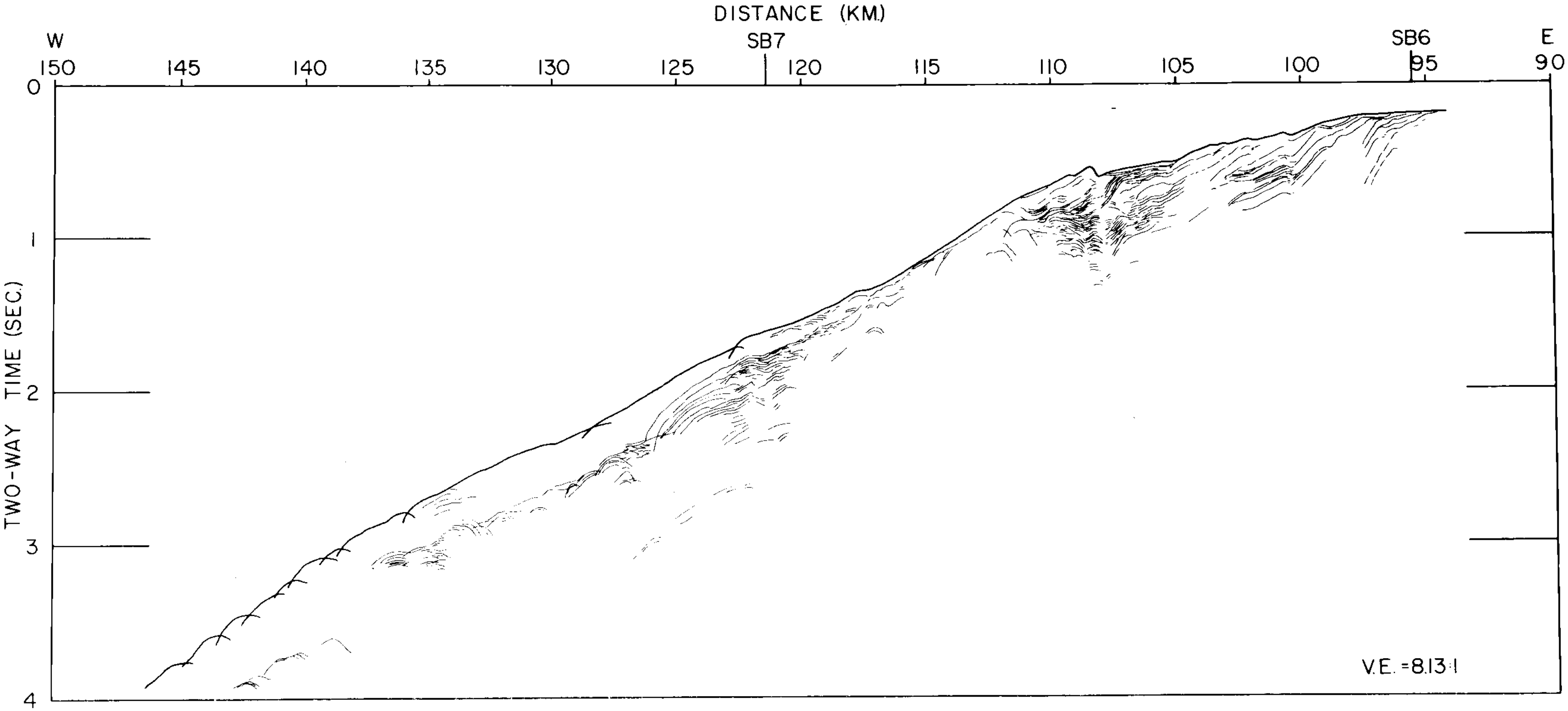


Figure 8. Line drawing interpretation of single channel reflection profile across the upper and middle continental slope at 9°S.

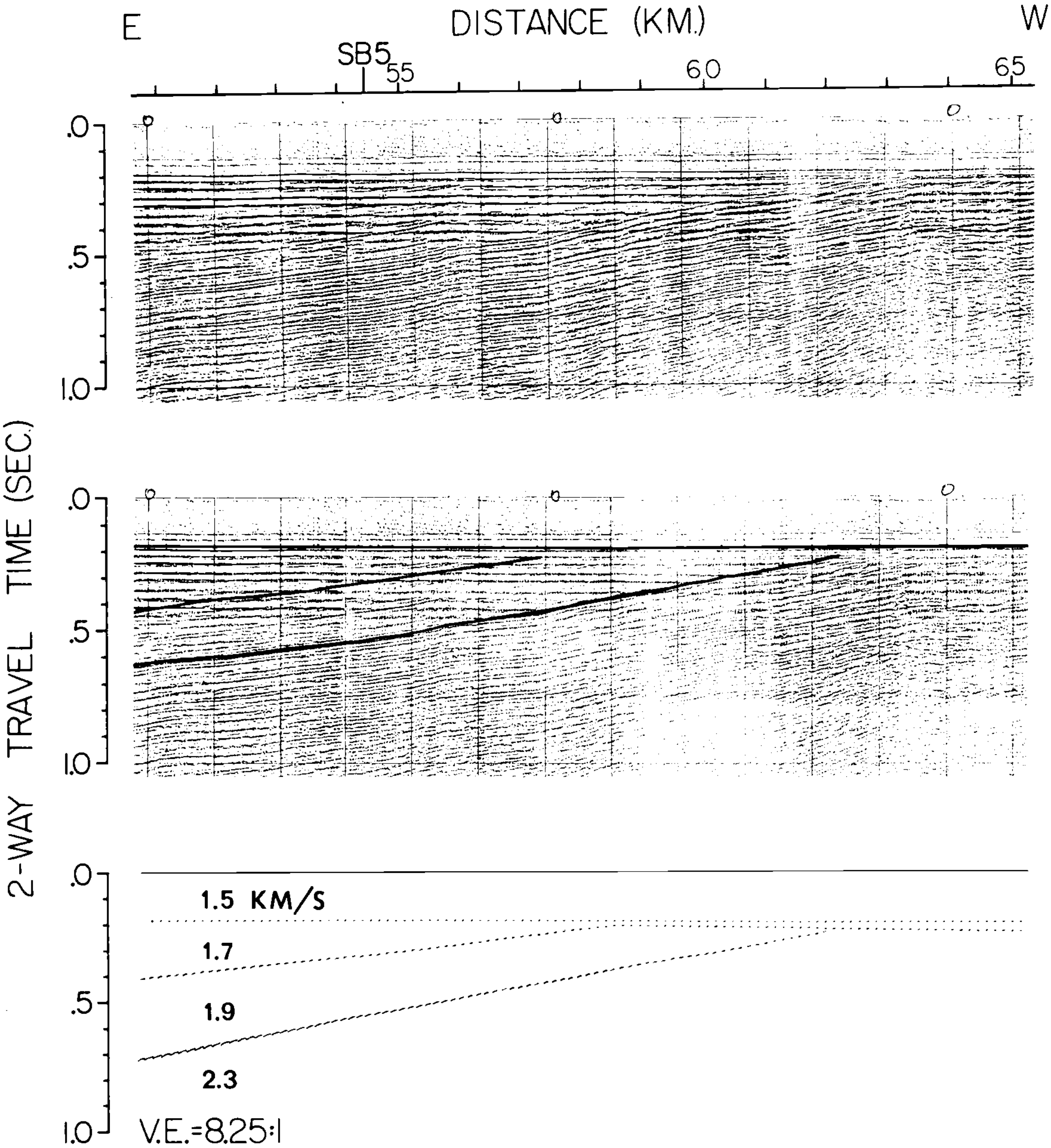


Figure 9. Single channel reflection profiles and model of near-surface sedimentary structure on the continental shelf near sonobuoy 5. Seismic profiles illustrate angular unconformities near 57 and 63 km. The lower diagram was simulated by program RAYGUN to match the seismic profile.

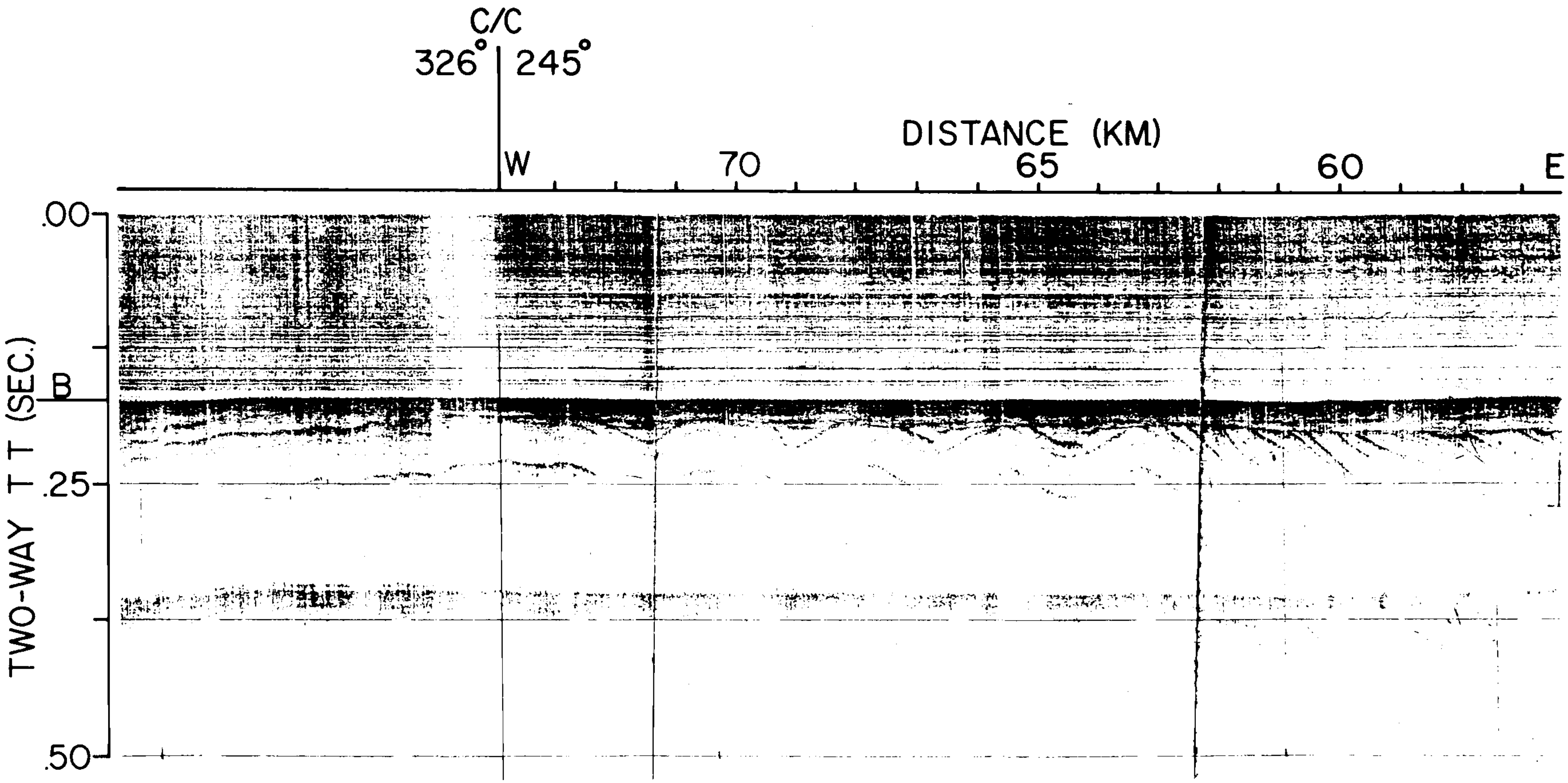


Figure 10. 3.5 kHz reflection profile of near-surface sedimentary structure on the outer continental shelf at 9°S.

Texas, under contract to OSU and HIG for the Nazca Plate Project under the I.D.O.E. Initially the data was processed to produce 1200% stacked time sections (for method see Mayne, 1962). Processing also included the computed average and interval velocities and the velocity spectra. The CDP data was later reprocessed by Exxon Production Research of Houston, Texas to produce a depth section (Figure 11).

The airgun profiles provided supplementary structural control for surface sediments not detected by seismic refraction methods. A velocity estimation from the CDP velocity analysis and from Johnson et al. (1975) was used to compute a velocity-depth model for the structures seen in the airgun profiles. Subprogram RAYGUN (see Appendix I) produces a time section from a velocity-depth model and a comparison is made to the original airgun profile as shown in Figure 9. Further depth modification can be made to the model until the synthetic and observed time sections match. In a similar manner, sedimentary structure of the upper continental slope and trench from reflection profiles was incorporated into the refraction velocity-depth models.

## Ray Trace Models

The ray trace technique was used to develop a velocity-depth model of the continental margin, trench, and Nazca Plate at 9°S. to match observed refraction data. In

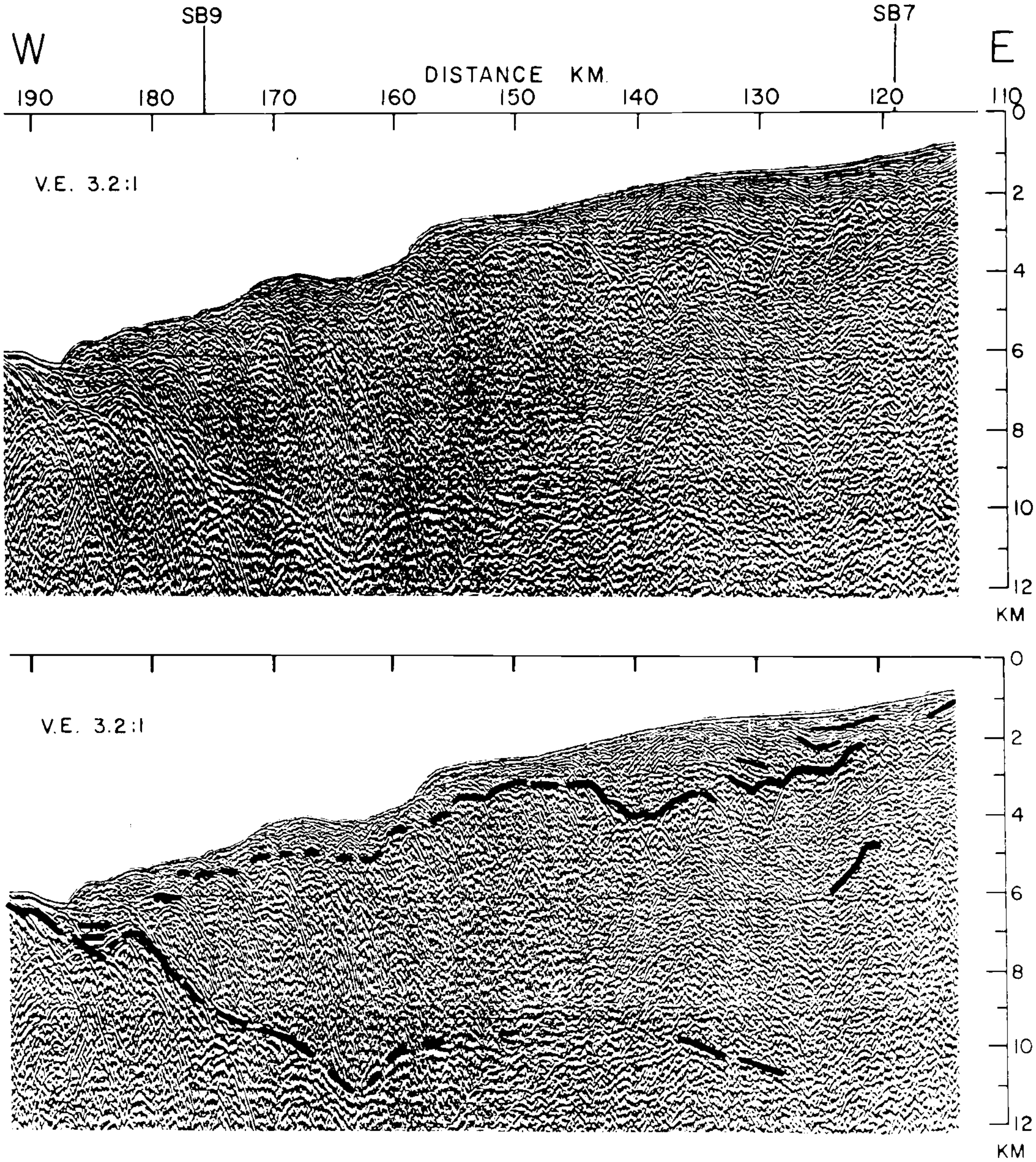


Figure 11. Non-migrated seismic depth section of CDP-2 (dotted line in Figure 1) across the continental slope and inner trench axis basin (modified from Kulm et al., 1977). Lower profile delineates prominent reflectors in seismic depth section.

addition, airgun profile records, velocity analysis of the CDP records and oil well velocity logs were incorporated in the model to supplement seismic refraction data especially where it was poor or sparse. The model of the continental margin is divided into four sections: continental shelf (Figures 12 and 13); continental slope (Figure 14); trench area (Figure 15); and Nazca Plate (Figure 16).

Ray trace travel time curves for P-waves are shown on each figure as solid lines for headwave refractions and dashed lines for layer reflections which are superimposed on observed arrivals. Located beneath each data plot is a ray trace velocity-depth model with 3:1 vertical exaggeration. Assumed velocities are given in parentheses. Seismic refraction interfaces are drawn as heavy solid lines while assumed interfaces or those derived from reflections only are represented with heavy dashed lines. The vertical heavy dashed lines represent lateral velocity changes. The water thickness was obtained from bathymetry in corrected meters.

On each figure R represents a single reflection arrival and G represents a refraction arrival. The subscripts 1,2, 3,... number the sub-bottom layers (the water layer is not counted) so that a reflection from the top layer 2 would be written $R_2$. The same numbering system applies to headwave refractions which travel along the upper interface of each layer.

Continental Shelf

Figures 12 and 13 show the seismic refraction data interpretation and ray trace model for the continental shelf. The shelf model has been divided into eastern (Figure 12) and western (Figure 13) sections. The interpretation of both sections suggest a sedimentary basin overlying a hard rock basement. Sub-structure was modeled as three sedimentary layers overlying a two-layer rock basement. The upper sediment layer has a velocity of 1.7 km/sec based on arrivals $G_1$ which were read from the seismograms before the onset of high amplitude bottom reflections. Refracted arrivals from a 1.9 km/sec layer are clearly seen in profiles extending to the west. The shape of the upper surface to the 1.9 km/sec layer is slightly curved on the basis of arrivals $G_2$ observed from sonobuoys 2 and 5. The 2.3 to 2.55 km/sec layer was modeled from arrivals $G_3$ detected at short ranges from sonobuoys 2, 3 and 5. At greater distances the attenuation of seismic energy by the sediments (Hamilton, 1974) probably accounts for the small number of $G_3$ arrivals observed. An angular unconformity observed at 63 km profile (Figure 9) was an additional constraint to the shape of the eastern sedimentary basin near sonobuoy 5. As shown in Figure 9, layer interfaces identified with the upper surfaces of the 1.7, 1.9 and 2.3 km/sec layers were modeled by subprogram RAYGUN (Appendix I) to produce a time section

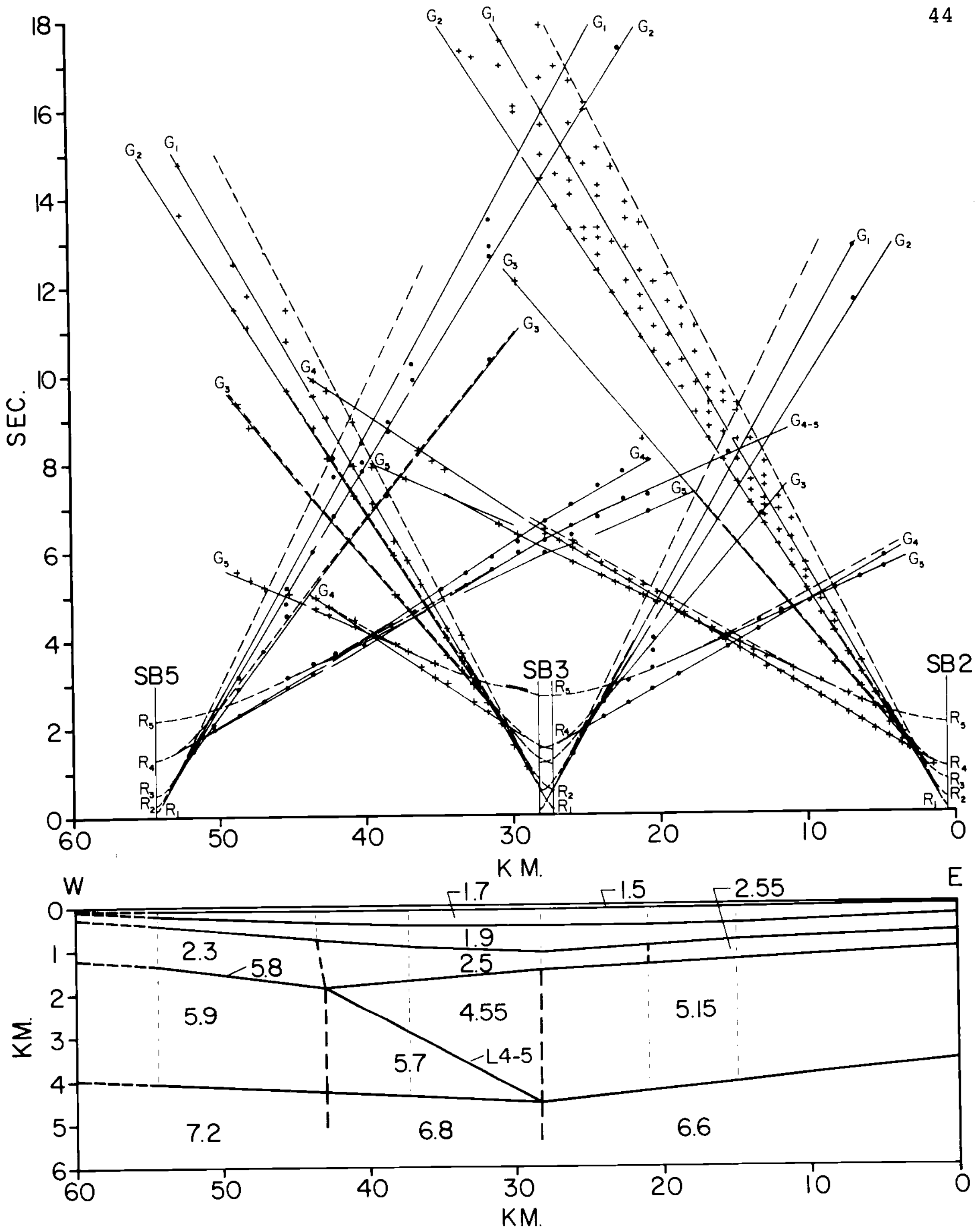


Figure 12. Seismic refraction data interpretation and ray trace model for the eastern continental shelf. R represents a single reflection arrival and G represents a refraction arrival. The subscripts 1,2,3,... number the sub-bottom layers. Velocities are in km/sec where assumed values are presented in parentheses. Vertical dashed lines are cell walls of computer model. Vertical exaggeration is 3:1.

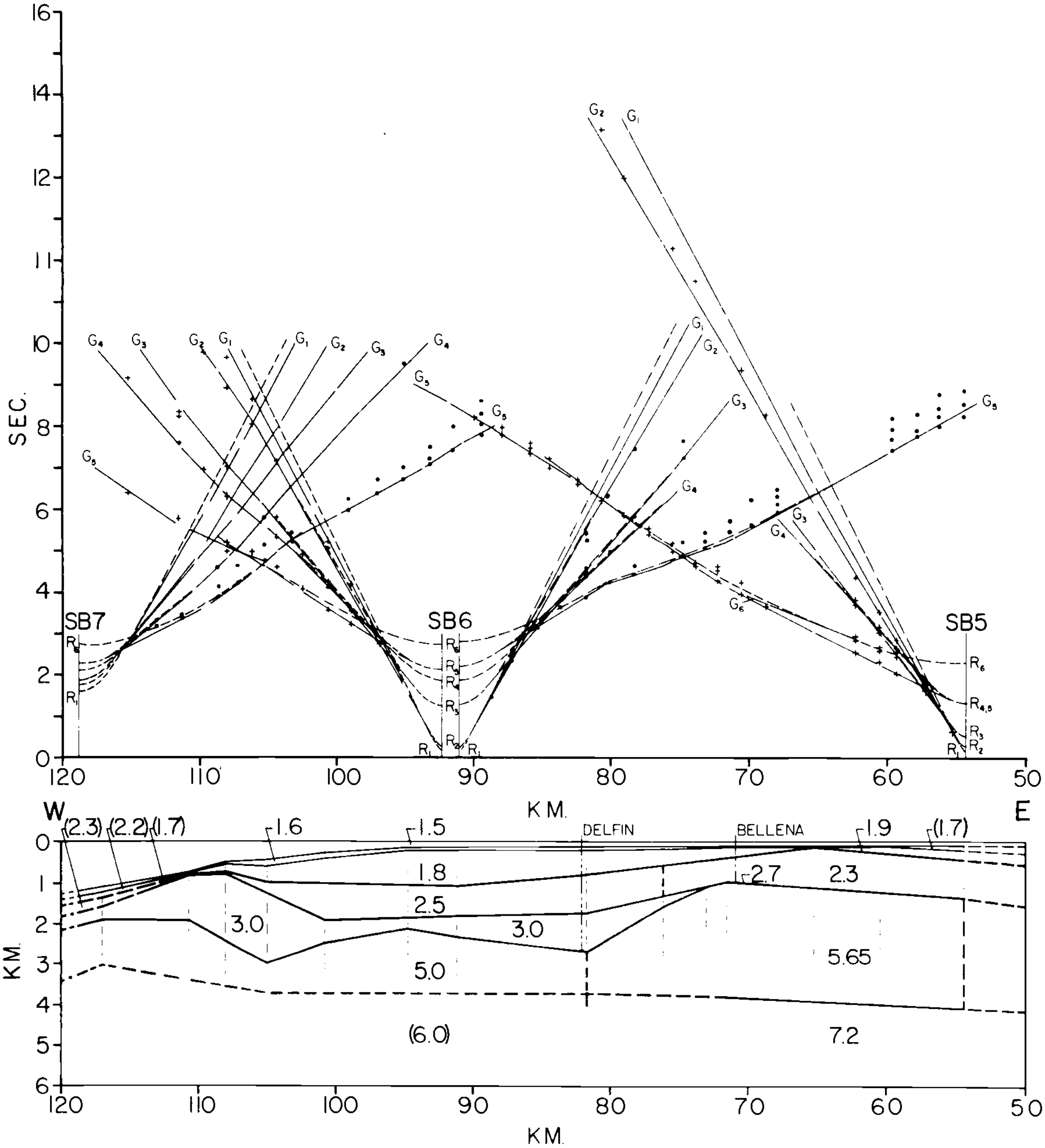


Figure 13. Seismic refraction data interpretation and ray trace model for the western continental shelf and upper slope. See Figure 12 for explanation of symbols. Delfin and Bellena are exploratory wells drilled to basement.

closely matching the observed airgun profile.

Layer 4 is divided into a faster western structure (5.7 to 5.9 km/sec) related to the outer continental shelf high, abutting a slower (4.55 to 5.15 km/sec) eastern structure. The velocity below both structures increases to the west from 6.6 to 7.2 km/sec ($G_5$ arrivals). The arrivals associated with layer L4-5 (Figure 12) are detected only in an eastern travel time branch ($G_{4-5}$) of sonobuoy 5. A large number of models were investigated by ray trace modeling and it was determined that the 5.7 km/sec wedge-shaped structure shown gave the best fit to the arrivals.

The model of the western section of the continental shelf (Figure 13) consists of a multilayered sedimentary basin overlying a two-layer rock basement. Exploratory oil wells Bellena 8-1 and Delfin 20X-1 provided velocity and depth to basement control for the western section.

Modeling of the sedimentary layers between sonobuoys 5 and 6 was limited mostly to arrivals detected at short ranges. Correct location of layer interfaces between these sonobuoys was achieved by correlation of sonic (velocity) logs of the two exploratory wells (proprietary information). Some near-surface indications of the 3.0 km/sec structure between 105 and 115 km can be seen on the tracing of the reflection profile shown in Figure 8.

The upper surface of the basement structure of the western section is based upon a well-defined set of first arrivals ($G_5$, 5.0 to 5.65 km/sec) seen in Figure 13. The depth to basement at exploratory well Bellena 8-1 was 0.98 km below sea level. Sonic logging at this well provided an average sediment velocity of 2.7 km/sec immediately overlying a quartz biotite gneiss basement with a velocity of 5.65 km/sec. The depth to basement at exploratory well Delfin 20X-1 was 2.65 km below sea level. Sonic logging indicated a basement velocity of 4.8 km/sec in a highly slickensided and fractured dark gray phyllite. With this information, the sediment-basement interface was modeled using first arrivals detected by sonobuoys 5, 6 and 7. An improved fit to the observed arrivals was achieved when a basement velocity of 5.0 km/sec was used west of the Delfin well.

A western extension of the 7.2 km/sec interface observed east of sonobuoy 5 was modeled for reflected arrivals. Due to a limited number of arrivals caused by several explosive misfires, the presence of the 7.2 km/sec interface west of sonobuoy 5 was not well established. Modeling indicated that this interface (using an assumed velocity of 6 km/sec) does not exist farther to the west.

## Continental Slope

Figure 14 shows the seismic refraction data interpretation and ray trace model for the continental slope. Two reversed refraction profiles, each 30 km long, were

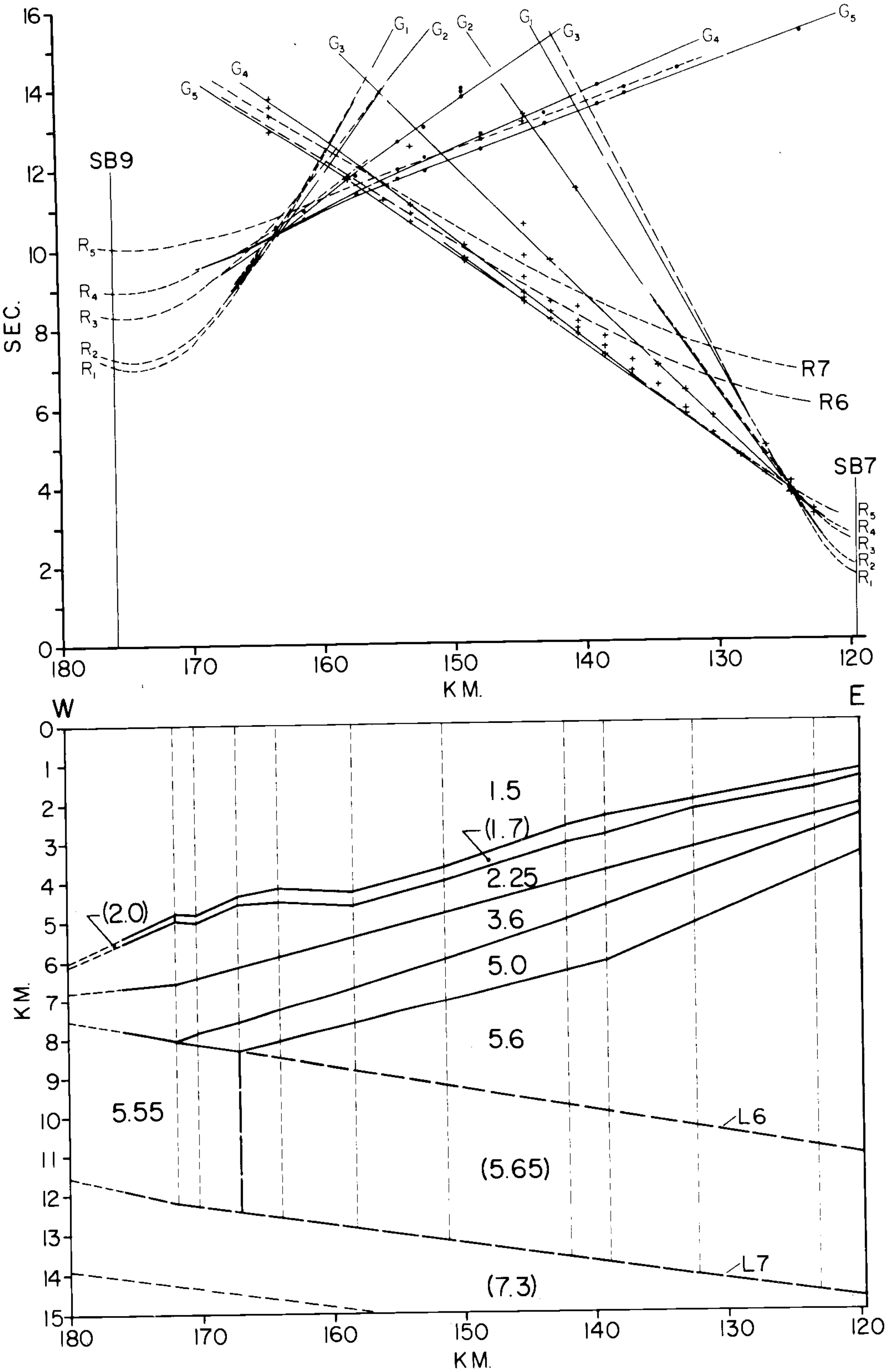


Figure 14. Seismic refraction data interpretation and ray trace model for the middle and lower continental slope. See Figure 12 for explanation of symbols. The layers L6 and L7 are assumed.

originally intended for this area. Instead, a 56 km long profile was obtained between sonobuoys 7 and 9 because the middle sonobuoy (number 8, now shown) malfunctioned during the shooting. A combination of the longer profile, frequent explosive charge misfires and severe topography made interpretation of the data difficult.

The 1.7 km/sec layer in Figure 14 was not observed in the refraction data ($G_1$) but a sedimentary layer overlying an acoustic basement was observed for this area in the 1974 airgun profile (Figure 8). The distance from sea floor to acoustic basement was modeled by computer program RAYGUN (Appendix I) and the results were incorporated in the ray trace model of the continental slope. A poorly observed 2.25 km/sec layer (interval velocity verified from CDP data) was used to model the velocity medium ($G_2$ arrivals) between the acoustic basement and a 3.6 km/sec refracting horizon. Between 130 and 145 km in Figure 14 are a series of arrivals located between those arriving for the 3.6 km/sec ($G_3$) and 5.0 km/sec ($G_4$) refractors. The arrivals may correspond to a refracting layer located in the upper slope. This interface was not modeled because of insufficient data from the reverse line. Between sonobuoys 7 and 9, the majority of refracted first arrivals ($G_5$) are from a 5.6 km/sec basal refractor that appears to define the core of the continental slope.

Hyperbolas for reflections R6 and R7 (Figure 14) from the major upper layers of the descending Nazca Plate were modeled in the data. A velocity of 5.65 km/sec was assumed for the top layer in order to produce a reflecting surface at L6. The surface at L7 was extrapolated from a similar interface located in the Nazca Plate model (Figures 15 and 16). The Moho interface reflections were not modeled due to its extreme depth. The absence of reflected energy at hyperbolas R6 and R7 will be addressed in the discussion.

## Trench Area

Figure 15 shows the interpretation of the seismic refraction data and raytrace model for the Peru-Chile Trench and part of the Nazca Plate. The velocity-depth model divides into an eastern section (sonobuoys 9 and 10) related to the tectonics of the trench and a western section (sonobuoys 10 and 12) related to the Nazca Plate.

The eastern area in Figure 15 represents a model based upon an assumed and partially observed upper section (velocities 1.7 to 3.6 km/sec) overlying an observed crustal plate section (velocities 5.55 to 8.2 km/sec). The dimensions and shape of the sedimentary basin (1.7 to 1.9 km/sec layers) located within the trench are modeled from a 1972 airgun profile (Figure 20 of Prince, 1974) located at a trench crossing 5 km to the south of Line 18-19. Kulm *et al*. (1974) reported the trench fill in this area to be

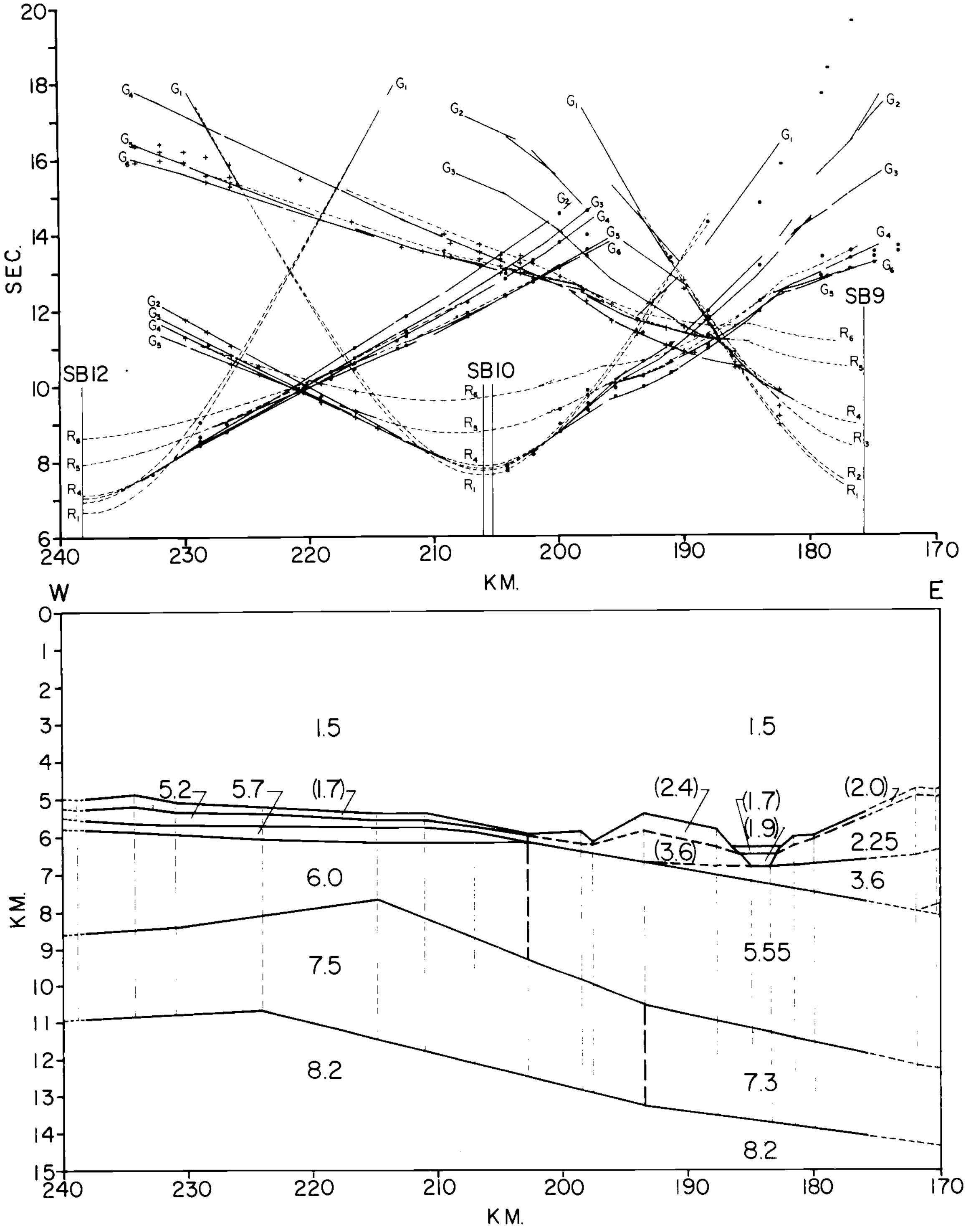


Figure 15. Seismic refraction data interpretation and ray trace model for the trench and part of the Nazca Plate. See Figure 12 for explanation of symbols.

composed of turbidites. Velocities of 1.7 to 1.9 km/sec from Hamilton et al. (1974) were used to model the turbidite fill. Due to several misfires of explosives at short distances, it was not possible to analyze the sonobuoy 9 data to the west for the velocity and structure above the 5.55 km/sec layer. A velocity of 2.0 km/sec assumed for the first layer and velocities 2.25 and 3.6 km/sec were extrapolated from values observed on the slope. The velocities associated with the ridge in the trench (centered around 192 km in Figure 15) are based on the CDP interval velocities calculated for this structure. The effect of the ridge structure on deeper layer arrivals is clearly seen on sonobuoys 9 and 10 in Figure 15 where arrival time advancements of up to 0.3 sec are produced. An overall deficiency of well defined arrivals for the 1.7 to 3.6 km/sec layers indicates a poorly defined upper structure for the descending plate and slope base.

Between sonobuoys 9 and 10, the majority of refracted first arrivals ($G_4$) are from the 5.55 km/sec upper surface of the descending Nazca Plate. The arrivals labeled $G_5$ are from a 7.3 km/sec interface located within the plate. Moho arrivals labeled $G_6$ are also detected in the eastern section.

The western section in Figure 15 represents the eastern Nazca Plate prior to subduction. As discussed earlier, refracted arrivals ($G_1$) of the upper sediment layer are usually not detected in deep ocean seismic refraction records. An assumed velocity of 1.7 km/sec was used to model the sediment layer and is assumed to extend from the sea floor to the first basement layer.

Although not reproduced here, reduced travel time plots were used to expand the time scale and separate arrival times observed for the western section in Figure 15. The ridge structure made it possible to ray trace the 5.2 and 5.7 km/sec layers into the trench area. The 5.55 km/sec layer in the trench is probably a composite of the 5.2, 5.7 and 6.0 km/sec layers observed between sonobuoy 10 and 12. The shallowing of the upper surfaces of the 7.5 km/sec layer and 8.2 km/sec Moho interface may be related to the tectonics of the descending plate.

## Nazca Plate Near the Trench

Figure 16 displays the data and model of the Nazca Plate near the trench. The velocity and structure of this 120 km-long crustal section is based on observed arrivals of sonobuoys 12, 13, 14, and 15.

The sub-bottom model in Figure 16 consists of 5 layers overlying an upper mantle of uniform velocity (8.2 km/sec). Using an assumed velocity of 1.7 km/sec, the thickness of the sediment layer(0.15 to 0.21 km) was computed by the method given earlier. The thickness agrees with a sediment isopac map of the Nazca Plate (HIG, 1977, unpublished map)

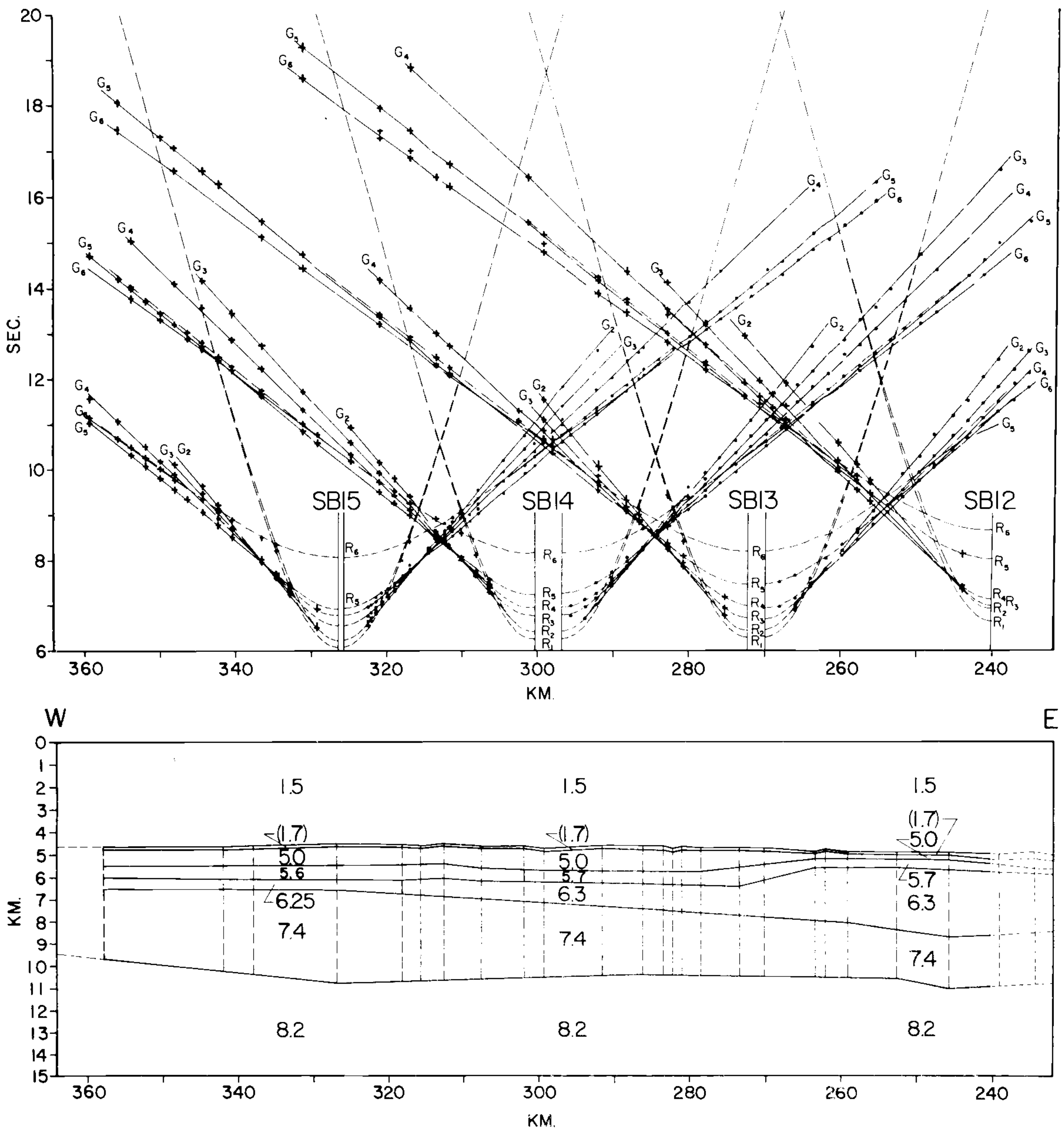


Figure 16. Seismic refraction data interpretation and ray trace model for the Nazca Plate. See Figure 12 for explanation of symbols.

and with DSDP SITE 320 where 155 m of sediment overlie a basalt basement (Yeats *et al.*, 1976).

Due to the small variation in apparent velocities and data scatter and also perhaps due to the homogeneous nature of the material, a much simpler model evolved on the plate than on the shelf and slope. A model with relatively constant layer velocities satisfied observed variations in the layer interfaces. The model in Figure 16 shows a uniform thickness in the 5.0 and 5.6 to 5.7 km/sec layers west of 275 km. Eastward of this location the 5.0 km/sec layer thins considerably and the 5.7 km/sec layer lies closer to the sea floor. The thickness of the 6.3 km/sec layer tapers from 3 km to 0.5 km from east to west. The opposite tapering occurs for the 7.4 km/sec layer (2.3 km to 3.5 km from east to west) so that the overall crustal thickness is relatively uniform (approximately 5.8 km, not including water layer). The depth of the Moho interface varies not more than ±0.5 km from 10.5 km for the 120 km long model.

# GRAVITY MODEL

## Gravity Measurements

The trackline map in Figure 1 shows the location of gravity measurements used for modeling the crustal section shown in Figure 17. Gravity measurements were obtained by surface ship gravity meters on board the R/V Yaquina (OSU) and R/V Kana Keoki (HIG), during the acquisition of seismic refraction Line 18-19. Due to more extensive coverage, the gravity record obtained by the R/V Kana Keoki was used in the crustal modeling. The land gravity data was obtained from the Defense Mapping Agency Aerospace Center in St. Louis, Mo.

The gravity data acquisition system aboard the R/V Kana Keoki included LaCoste and Romberg surface ship gravity meter S-33 which includes a stable platform and an analog recording system. Real-time on board signal processing used three 20 second analog filters and an analog filter with a 15 minute delay for the recorder producing a spatial sampling interval of 4.6 km for the ship's speed of 10 knots.

While in port at Callao, Peru, an absolute reference for the ship's gravity meter was obtained by using a portable land gravity meter to measure the difference between the acceleration of gravity at the ship's meter and at the

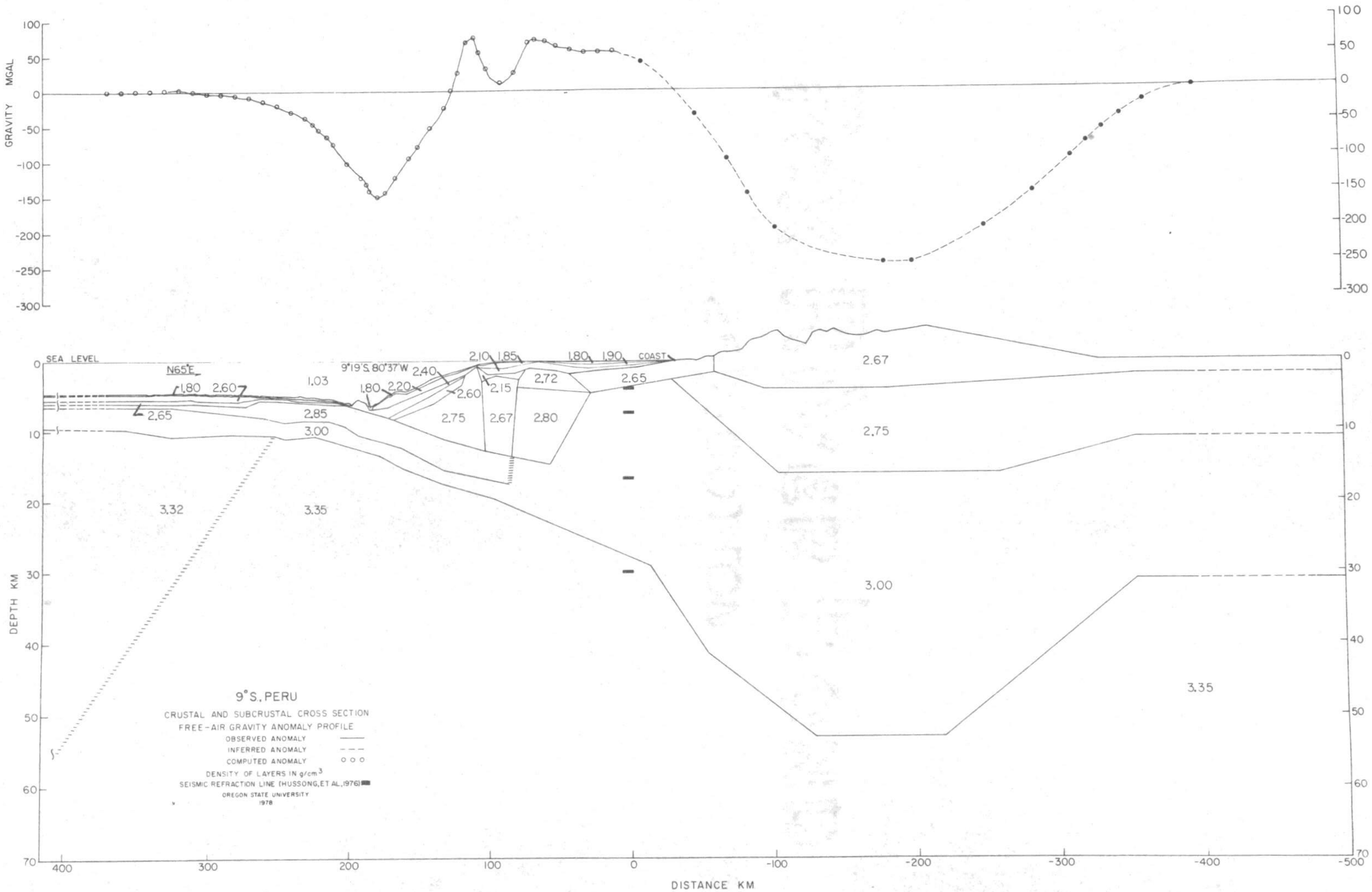


Figure 17. Crustal and subcrustal cross section along Line 18-19 at 9°S. The vertical exaggeration is 5:1.

nearby International Gravity Base Station (Woollard and Rose, 1963). The gravity value given by Woollard of 978.3127 gals (1 gal = 1 $cm/sec^2$) for IGBS WH1068 was adjusted to 978.2982 gals due to a 1967 modification of the accepted gravity value on a pier in the basement of the Commerce Building, Washington, D.C. that was reset from 980.1188 gals (to which Woollard's work is referenced) to 980.10429 gals.

Calculation of the free air anomaly from the observed gravity is given by the equation

$$g_f = g + 0.3086h - \gamma(\mathrm{mgal})$$

where $g_f$ is the free air anomaly and g is the observed or measured gravity value. The free air correction (0.3086h) corrects for changes in gravity due to elevation differences h between the observation point and the spheroid. For sea level measurements the free air correction is zero. Theoretical Gravity was computed using the 1967 Gravity Formula,

$$\gamma = 978031.85\ (1 + 0.005278895\sin^2\phi + 0.000023462\sin^4\phi)\ \mathrm{mgal}$$

where $\phi$ is the latitude of the measurement and $\gamma$ is expressed in milligals (mgal).

## Gravity Modeling

Crustal sections are computed following the line integral method of Talwani (Talwani et al., 1959) as adapted by Gemperle (1970, 1975). The method is based on an assumption that structures are two-dimensional and infinite in extent in each direction normal to a given profile. Line 18-19 is normal to structures which parallel the margin so that the two-dimensional requirement is satisfied. Only the vertical component of gravity is computed from the gravity model.

The crustal and subcrustal model in Figure 17 extends to a depth of 70 km and, to avoid edge effects, extends a large distance to each side of the central area which contains the structure of interest. Subtraction of the gravitational attraction of a standard mass column corresponding to zero free air gravity from the gravitational attraction computed for a point on the model yields the free air anomaly value for that point. The mass column gravity value of 9223.6 mgal for the model in Figure 17 is calculated from a mass column created by extending the mantle layer of the mass column given by Barday (1974) by an additional 20 km.

## Crustal and Subcrustal Gravity Model

Figure 18 repeats the velocity-depth model determined above by ray tracing. Illustrated in Figure 19 is a simplified version of the velocity-depth model in Figure 18 which

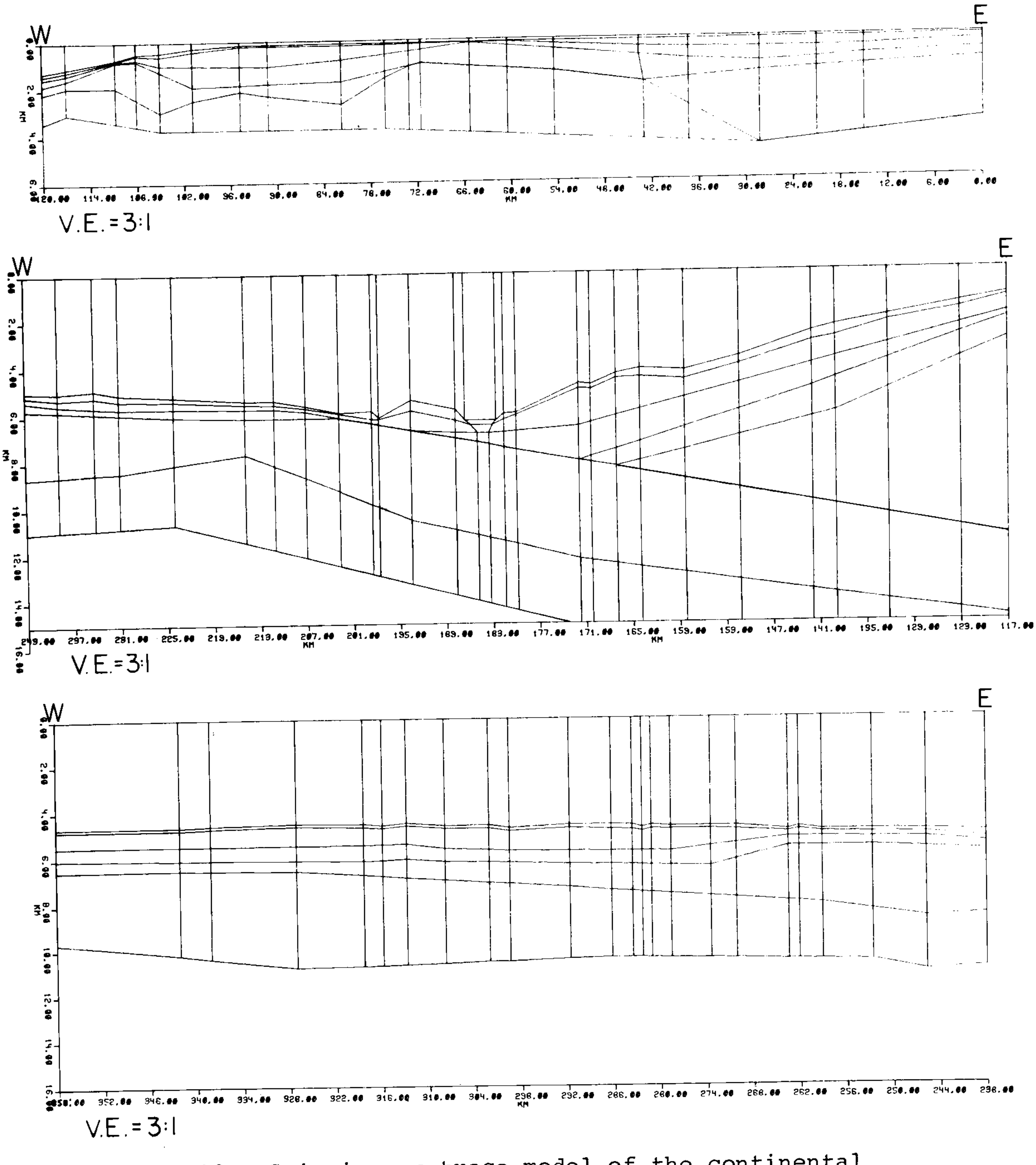


Figure 18. Seismic ray trace model of the continental shelf and slope, trench and Nazca Plate at 9°S.

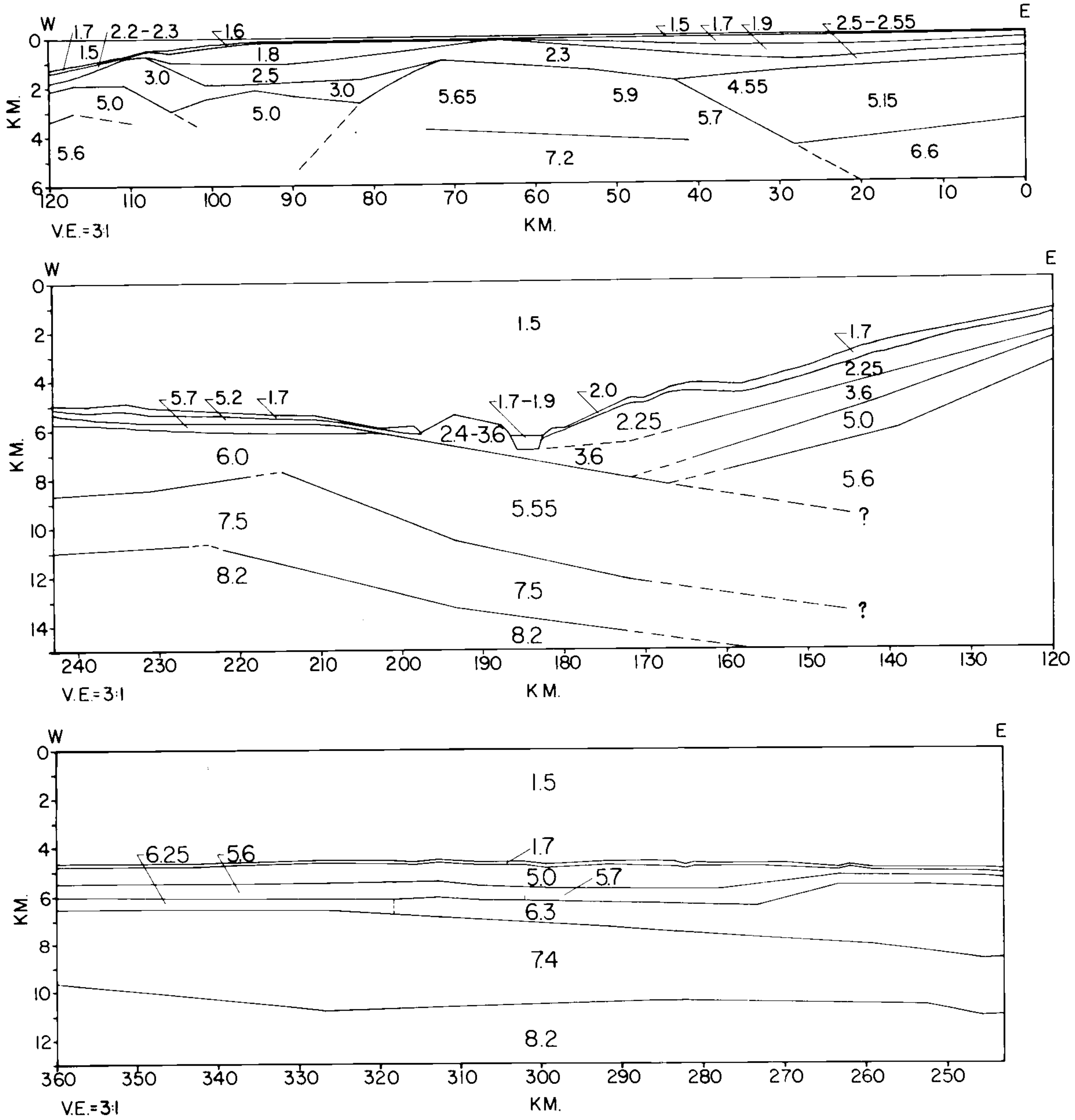


Figure 19. Interpretation of seismic ray trace model of continental shelf and slope, trench and Nazca Plate at 9°S. Undetected interfaces are symbolized by dashed lines.

includes the velocities used to estimate densities. For model distances west of 0 km the velocities in Figure 19 were used to constrain the initial density values obtained from the Ludwig, Nafe and Drake (1970) curve which relates seismic velocity to density. With few exceptions, the layer boundaries in Figure 17 were never moved during the gravity modeling. The exceptions to this layer boundary control are the Moho interface and the upper interface of the 7.5 km/sec layer east of 210 km and near surface layer boundaries between 115 and 120 km. The densities, on the other hand, were varied slightly from the initial values in order to fit the calculated model gravity to the observed gravity.

Land gravity control is based upon two coastal gravity values obtained from the Defense Mapping Agency and values obtained from a bouguer gravity anomaly map of South America (Technical Paper No. 73-2, DMAAC).

Except for the topography and some surface geology information, the layer boundaries of the gravity model are not constrained east of 0 km. The elevations were obtained from Air Force chart ONC N-25, 2nd edition (1973) which was contoured at 1000 foot intervals. Use of the exact elevation given for each chosen land gravity station eliminated any error (approximately 0.1 mgal/meter) that would arise from an elevation difference between the model cross section and the gravity station.

Seismic refraction Line 20-21 (Hussong _et al._, 1976) which is located 7 km north of Line 18-19 and parallel to the coast of Peru forms the initial boundary control for the subcrustal layers located near 10 km in Figure 17. Besides this line, there is no refraction control close to the crustal section along Line 18-19. For this reason densities and approximate layer thicknesses were obtained from crustal and subcrustal cross sections of southern Peru by Whitsett (1976). The depth to Moho under the Andes has been found to decrease from 70 km under the western Cordillera and western Altiplano region at 15°S. (James, 1971) to 45 km under the Cordillera Central at 1°N. (Case _et al._, 1973). Based on this information, the depth to Moho was modeled at 53 km. This is in general agreement with the maximum depth-to-Moho trends of Whitsett (1976) who modeled Moho depths of 67 km at 16.5°S. and 60 km at 14°S.

The model of the upper crustal region under the continental shelf combines seismic refraction, gravity and geological information. The eastern sedimentary basin of the continental shelf is represented by a three layer sequence of increasing density from 1.8 to 2.1 g/cm$^3$. The underlying block of 2.65 g/cm$^3$ was extended onshore where Cretaceous pillow lavas, cherts and pyroclastics are mapped on the Geological Map of the Western Cordillera of Northern Peru (Anonymous, 1973). The upward extension of the large block of 3.0 g/cm$^3$ lower crustal material to the bottom of the 2.65 g/cm$^3$ layer was necessary in order to obtain the positive gravity anomaly of 50 to 70 mgal observed in this area. The upper surface of the 3.0 g/cm$^3$ block lies 3.5 km higher than a similar interface detected by Line 20-21 (Hussong et al., 1976). Also, the Moho location in the model is 2 km above the depth located by Line 20-21 (Figure 17). The difference may be due to errors in the determination of the deeper layers of this line because the refracted arrivals did not reverse well (Hussong et al., 1976) or because of dip parallel to the margin.

The western edge of the anomaly at 75 km in Figure 17 represents the western limit of the outer continental high modeled from the seismic refraction data (Figure 19). The outer continental shelf high is modeled with an upper block of 2.72 g/cm$^3$ and a lower block of 2.8 g/cm$^3$ that extends to the subducted plate boundary. Located between a 2.75 g/cm$^3$ block and the outer continental shelf high is a block with a density of 2.67 g/cm$^3$. Both seismic refraction and exploratory well data indicate the upper surface of this block to be faulted and probably down-dropped relative to the surrounding blocks. The surface velocity of 5.0 km/sec for this block (Figure 19) indicates a density range of 2.45 to 2.75 g/cm$^3$ (Ludwig et al., 1970). After extensive modeling, a density of 2.67 g/cm$^3$ was assigned to the total block to match the observed u-shaped anomaly in Figure 17.

Very few changes to the seismic refraction model of the continental slope (Figure 19) were necessary for modeling the observed gravity anomaly of this area. Modifications were made near 105 km of the seismic model in order to extend the upper boundary of the 2.75 g/cm$^3$ block closer to the surface. The modification helped to produce the 75 mgal peak observed at this location. At the slope base, the partially observed layer boundary locations from the seismic refraction modeling (Figure 14) were used to model the layers of the 1.8, 2.2, 2.4, and 2.6 g/cm$^3$ densities (Figure 19).

Near the trench, the descending Nazca Plate was seismically modeled as a two layer structure consisting of a 2.85 g/cm$^3$ (5.55 km/sec) layer overlying a thinner 3.0 g/cm$^3$ (7.5 km/sec) layer. Eastward of 230 km, it was necessary to shift slightly some of the plate interfaces. This is not significant since no seismic refraction control exists landward of the slope base. The gravity model suggests that the slope of the descending plate is about 5° down to a depth of 30 km.

West of 230 km no modifications to the seismic model were required to generate an acceptable gravity model. The density layering sequence of 1.8, 2.6, 2.65, 2.85, and 3.0 g/cm$^3$ represents the oceanic plate. A density of 3.35 g/cm$^3$ was used for the upper mantle. It was necessary to change the upper mantle density from 3.35 to 3.32 g/cm$^3$ to produce a zero mgal anomaly at western locations far removed from the trench. Without the density transition in the upper mantle it would have been necessary to invoke large lateral density changes in the lower crust.

# GEOLOGICAL INTERPRETATION OF MODELS

The purpose of this chapter is to suggest rock materials represented by the seismic velocities and model densities. Attempts will be made to assign these materials to geologic units known to exist in the area and to relate their structures to the tectonic environment of the Peru continental margin and trench area.

## Continental Shelf

Precambrian or early Paleozoic rocks are believed to form the core of the outer continental shelf high and partially form the basement of the continental shelf basins near refraction Line 18-19 (Masias, 1976). Early Paleozoic rocks are exposed in the Amotape mountains of northwestern Peru and in the coastal ranges of southern Peru (Kulm *et al.*, 1973). The early Paleozoic rocks of northwest Peru are comprised of schists and phyllites (Cobbing and Pitcher, 1972). Radiometric dating of a similar exposure of rocks in southern Peru along the trend of the Arequipa batholith indicate Precambrian ages of 679 ± 12 m.y. and 642 ± 16 m.y. (Steward *et al.*, 1974). Furthermore, Paleozoic rocks crop out on the offshore islands of Lobos de Tierra (6.5°S., 81.1°W.) and Lobos de Afuera (6.9°S., 80.8°W.) (Masias, 1976). Driller's logs from wells Bellena 8-1 and Delfin 20X-1 (Figure 1) report basement rocks composed of quartz biotite gneiss and dark gray phyllite respectively (proprietary information). These rock types agree with those of the early Paleozoic sequence found onshore in northern Peru.

Geological and geophysical evidence indicate that the outer continental shelf high was and perhaps still is a tectonically active structure. The drilling log at the Delfin well reported a fractured and highly slickensided basement rock which indicates fault movement between the 5.0 and 5.65 km/sec basement structures shown in Figure 13. From the well logs, Miocene sediments conformably overlie Oligocene sediments which nonconformably overlie the basement rocks. This suggests that the fault movement(s) occurred during or before the Oligocene epoch. The seismic refraction velocities and layer interfaces for the sediments of this area are based on well velocity correlations and on poorly observed arrival times and therefore relative subsidence of the central portion of the outer shelf sedimentary basin between 70 and 110 km as shown in Figure 13 is speculative.

The 2.67 g/cm$^3$ basement rock, located under the outer sedimentary basin of the continental shelf and required by the gravity model, is considerably less dense than the basement rocks located to the east and west (Figure 17). As mentioned earlier, the 2.72 to 2.80 g/cm$^3$ eastern basement is of continental origin and might represent the leading edge of the continental block prior to plate collision (Dietz and Holden, 1974). The source material for the 2.67 g/cm$^3$ block may have originated from a continental rise prism located at the base of the continental block (Dietz and Holden, 1974) which may have been subsequently trapped and pushed up against the continental block by the subducting plate. If this theory is true, the event may have occurred as long ago as 150 m.y. (middle Jurassic) when subduction along the Peru-Chile Trench initiated the major onset of volcanism and orogenic activity on the west coast of South America (Cobbing and Pitcher, 1972).

The sedimentary basin located landward of the outer continental shelf high (Figures 12 and 17) is part of the Salaverry Basin (Masias, 1976). The seismic reflection profiles presented by Masias (1976) suggest uplift of the seaward edge of the basin based on the landward (eastward) migration of the axis of deposition. The seismic refraction results of Line 18-19 for the sedimentary layers in the Salaverry Basin only weakly support the idea of a landward migration of the axis of deposition but they do suggest uplift of the seaward edge. The Delfin and Bellena well logs report a hiatus of greater than 200 million years between the basement and overlying sediments. A possible explanation is that the outer continental shelf high was nearer to the sea surface in the past and thus subjected to erosion (Shepard, 1973). Later subsidence followed by presently observed uplift may be added as an explanation of the results observed by Masias (1976). Contour currents moving parallel to the slope edge which prevent deposition could provide an alternate means of erosion.

The 3.5 kHz profile record illustrated in Figure 10 shows a series of sinusoidally shaped sedimentary structures located on the outer continental shelf. A course change during the traverse confirms that the structures parallel the coastline and that the peaks are truncated and unconformably overlain by more recent sediments. The sinusoidal structures have a peak to peak distance of 2 km and a peak to trough height of 10 meters. The true nature of the structures cannot be discovered without further data but they do suggest constructional features related to onshore-offshore bottom currents occurring during a time of lower sea level (Hunt _et al._, 1977).

Figure 17 shows the basement of the eastern portion of the continental shelf to be 2.65 g/cm$^3$ crustal material. Travis _et al._ (1976) show that sedimentary and volcanic rocks of Mesozoic age overlie Paleozoic strata in northern Peru and suggest that the Mesozoic rocks extend onto the continental shelf. Also, marine deposits of the late Cretaceous and Tertiary periods are confined to a narrow coastal belt onshore and are presumed to lie in basins landward of the outer continental shelf high located offshore. Hence, the 2.65 g/cm$^3$ (4.55 to 5.15 km/sec) basement material probably represents Mesozoic rocks while the overlying 1.9 to 2.1 g/cm$^3$ (1.7 to 2.55 km/sec) materials represent sediments of Tertiary age. The lateral velocity change from 5.15 to 4.55 km/sec in the Mesozoic basement may be due to faulting or juxtaposition of different material.

A prominent feature in Figure 17 is the large block of 3.0 g/cm$^3$ lower crustal material modeled in the upper crustal region under the 2.65 g/cm$^3$ basement. The location of the subcrustal block suggests rupture of the crust or intrusion at depth under the continental shelf. The section at Pisco (14°S.) modeled by Whitsett (1976) reveals a similar subcrustal block. Two alternative crustal structures suggested by Whitsett would apply equally well to the model in Figure 17. The first suggestion is to permit intrusion of the Moho into the lower portion of the 3.0 g/cm$^3$ block located under the coastline and thus reducing the density required of the lower crustal block while still producing the gravity anomaly observed along the eastern section of the continental shelf. The second suggestion places the 3.0 g/cm$^3$ block deeper under the continental shelf and thus allows the Moho between the trench and coast to dip less steeply. The overall effect raises the mantle material higher under the entire continental shelf and thus allows the 3.0 g/cm$^3$ block to reduce in size within the section. The latter suggestion would not be practical for the model in Figure 17 because it would require an anomalously low density for the 2.67 g/cm$^3$ crustal block centered at 90 km. It was felt that without deep refraction control it was best to keep the subcrustal model as simple as possible while meeting the requirements of the land gravity observations.

## Continental Slope

Kulm et al. (1977) propose that the continental slope region between 6° and 19.5°S. is forming by accretion. Characteristic features of accretion are long prominent benches on the lower continental slope, sedimentary basins on the shelf and upper slope, and thick trench deposits. A large bench along the lower continental slope at 170 km can be seen in Figure 19. Seely et al. (1974) suggests that these benches contain imbricate thrust sheets with reverse motion along planes which dip landward. The poor coverage of seismic refraction data for Line 18-19 in the region of the slope bench (Figure 14) did not permit a test of the imbricate thrust sheet model. The strong negative free air anomaly and great depths associated with the trench prevent the observation of gravity anomalies that might be associated with imbricate thrust sheets. The failure to model imbricate thrusting is due to a data limitation rather than an existence or nonexistence of the structures. Lithologies recovered from the lower continental slope region indicate incorporation of the descending plate sediments into the margin (Rosato, 1974; Kulm _et al_., 1974) and this may be connected with the imbricate thrust hypothesis.

From velocity analyses of CDP lines obtained at 9°S. and 12°S. (Kulm _et al_., 1975; Hussong _et al_., 1976), it appears that the major tectonic disruption of the slope basement interface occurs near the base of the slope. This observation agrees with the velocity-depth model for Line 18-19 (Figure 19) where no distinct arrivals were noted for a model with a layered slope base (Figure 14).

A well defined basement underlies the continental slope landward from the trench. The refraction data indicates a continental slope basement of velocity 5.0 km/sec overlying a slope core material with an interface velocity of 5.6 km/sec. Line CDP-1 across the continental slope at 12°S. confirms that a continuous slope basement interface of velocity 5 to 6 km/sec parallels the slope bottom (Hussong _et al_., 1976). CDP-2 located 25 km to the north of Line 18-19 (Figure 11) also confirms this observation where the velocity analysis of Kulm _et al_. (1975) indicates basement velocities of 5.0 to 5.3 km/sec. The wide angle refraction work of Geobel (1975) and Hussong _et al_. (1975) at 12°S. (sonobuoys 113 and 115) reveal that apparent velocities located deeper within the slope range from 6.3 to 6.8 km/sec. The true velocities may be lower because the data was obtained while shooting up slope and no corrections were made for dipping interfaces.

The seismic depth section in Figure 11 indicates a poorly-defined structure deep within the slope. This material is believed to be formed from accreted deposits derived from the offscraped sediments and upper crustal rocks of the descending Nazca Plate (Moore and Karig, 1976; Coulbourn and Moberly, 1977; Kulm et al., 1977). Therefore, the model of the continental slope basement based on seismic refraction data of Line 18-19 (Figure 19) represents only the upper surface of the melange of accreted deposits; the velocity within the melange is not well known. The gravity required a block of density 2.76 $g/cm^3$ to represent the slope melange. Considering the density of materials representing the crust of the Nazca Plate and accounting for sediment dewatering and compaction one must conclude that a large portion of the upper crustal rock material (2.6 to 2.85 $g/cm^3$) must be included with the sediments in the melange.

Tectonically connected with the accretionary process is the formation of sedimentary basins on the continental shelf and slope (Moore and Karig, 1976; Coulbourn and Moberly, 1977). In addition to the well-developed sedimentary basin on the continental shelf, line CDP-2 clearly shows a 2 km deep sedimentary basin on the upper slope between 120 and 144 km (Figure 11). The gravity data for

Line 18-19 does show a slight downward curvature in the free air anomaly measured along the upper slope (Figure 17), indicating a mass deficiency possibly associated with the basin. Gravity modeling of this anomaly indicates that small flexures in the slope basement and the descending plate can account for the observed anomaly. The refraction model (Figure 14) depicts a continuous, rather than isolated, sedimentary basin for the continental slope. Due to the longer distance between sonobuoys and fewer number of shot points, the model of the slope tends to integrate the overlying sedimentary velocities and structures and individual details are lost.

Several speculative interpretations can be made of the slope layers. The uppermost layer of 1.7 to 2.0 km/sec material (Figure 19) reveals very little structural layering in the seismic reflection profile in Figure 8. The material probably consists of slumped pelagic sediments mixed with terrigenous turbidites from the upper slope regions. The acoustic basement of 2.25 km/sec is real but the velocity is somewhat artificially derived (see model description for Figure 14). Together the 2.25 and 3.6 km/sec layers might represent consolidated sediments and indurated sediments related to the accretionary process (Hussong et al., 1975). The slope basement shown in Figure 11 is characterized by a highly diffracting interface suggestive of block faulting. The 5.0 km/sec interface on the slope in Figure 19 may be associated with the disrupted basement while the 5.6 km/sec interface marks a deeper and thus more uniform region within the accretionary prism (Hussong *et al.*, 1976).

The location of the Nazca Plate under the continental slope was not detected by the refraction data along line 18-19 (Figure 14). A possible explanation is that a velocity inversion occurs between the overlying slope material and the upper surface of the plate such that critical refraction cannot occur. A further search for deep reflections (R6 and R7 in Figure 14) from the plate interface also failed to indicate its presence. The CDP depth section (Figure 11) clearly shows a deep reflector associated with the upper surface of the descending plate. The numerous diffractions in this non-migrated depth section indicate that the upper surface of the Nazca Plate is highly faulted under the slope. Attenuation of seismic energy by crustal materials within the slope cannot account for the absence of distinct reflected energy observed in the seismograms for Line 18-19 because the 2600 cu.in. airgun source for the CDP-2 data is equivalent to 2.5 pounds of 60% dynamite (Kramer *et al.*, 1968) whereas 3 to 200 pound charges were used in the refraction work. The effect of a highly faulted surface on widely spaced explosive sources would be to scatter the reflecting energy such that reflections received at a point receiver (sonobuoy) are non-distinct.

The CDP method uses closely spaced shots (shot spacing was 30 meters for the record in Figure 11) and a 24 channel streamer 1.6 km long. The effectiveness of phase correlation in the CDP method for receiving scattered reflected energy can be easily seen.

## Trench Area and Nazca Plate

Kulm and Prince (1975) describe intensive deformation in the trench region that is perhaps due to the rapid rate of convergence of the Nazca and South American plates (10 cm/yr, Minster et al., 1974). Due to the structurally complex nature of the trench area, a simplified model evolved to generate the seismic refraction travel time curves for Figure 15. The following discussion explains the approximations made in modeling the trench area and how they may be interpreted.

Tensional stress along the line of flexure of the descending Nazca Plate has been cited as the cause of the normal faulting observed near the trench (Prince, 1974; Prince and Kulm, 1975; Schweller, 1976). The authors present seismic reflection records depicting sediment-buried block-faulted areas seaward of the Peru-Chile Trench which correlate with the 5.2 km/sec layer west at 205 km in Figure 19. The modeling of block faulting was not justified because the 2 km or greater shot point spacing cannot resolve the randomly sized blocks of 1 to 10 km in length and vertical offsets of 0.2 km or less. The small scatter in the observed arrival times (Figure 15) indicates the presence of the broken structure that is not well detected by the seismic refraction data.

A noteworthy feature of the Peru Trench is the prominent ridge-like structure located at 192 km in Figure 19. The reflection profiles of the Peru-Chile Trench area by Prince and Kulm (1975) show that the ridge separates the trench floor into an inner deeper basin and an outer shallower basin. Prince and Kulm (1975) and Kulm et al. (1973) suggest that the ridge represents a portion of faulted oceanic crust uplifted relative to the floor of the trench. Prince and Kulm (1975) proposed a five-stage imbricate thrust model whereby the ridge is related to the compressional stresses that develop as the two plates converge. They propose that the motion of normal block faulting is reversed when thrust faults develop along former extensional fault planes or along completely new fault planes. The first motion study by Abe (1972) on a shallow focus earthquake beneath the continental slope at 10°40'S. identify low angle thrust faulting related to compressional stresses within the descending plate. Based on the models presented by Prince and Kulm (1975), the upper interface of the 5.55 km/sec layer under the ridge (Figure 19) could be interpretated as the place of a thrust fault rather than the top of the Nazca Plate.

However, due to the complexity of the data, the 5.55 km/sec interface may be considered a simplification of the upper layers of the model west of 203 km. The velocity of the ridge at 192 km in Figure 19 is based on a similar feature observed in CDP-2 to the north where velocity analyses indicated a 2.4 to 3.6 km/sec ridge overlying a 5.2 km/sec interface. Since material recovered from the ridge indicates it is basalt (Kulm et al., 1973), a velocity of approximately 5 km/sec might be expected for it. The basalt of the ridge may be highly fractured and therefore have a lower interval velocity.

The layer interfaces that represent the descending plate are modeled as plane layers with very little change of dip and no faulting (Figure 19) which, in reality, would be an over simplification considering the structure of the upper surface (Prince and Kulm, 1975). In modeling the trench area, it was assumed that the major cause of travel time variations would be due to the topography and upper layer structures and not due to major structural changes in the deeper layers.

A shallowing of the lower crustal layers appears near 220 km in Figure 19 and a similar shallowing of less amplitude is modeled for the gravity model in Figure 17. The shallowing may represent upward flexure which is possibly related to a combination of plate bending and compressional forces due to crustal underthrusting. The surficial expression of normal block faulting (Prince and Kulm, 1975; Schweller, 1976) is probably directly related to the plate bending observed at depth. Thrust faulting, as observed by Hussong et al. (1975) at 12°S., was not observed in the crustal section along Line 18-19.

Large scale crustal thinning seaward of trenches is sometimes noted by a modest gravity high located near the thinned crust. Upward flexure of the oceanic plate as it bends to descend into the trench has been used to explain crustal thinning (Couch et al., 1970; Hanks, 1971; and Watts and Talwani, 1974). The observed gravity of Line 18-19 does not show a well defined gravity high seaward of the trench. In this region, from west to east, the crustal structure develops a thickening of the 2.85 g/cm$^3$ layer and a thinning of the 3.0 g/cm$^3$ layer while the upper mantle density changes from 3.32 to 3.35 g/cm$^3$. The net lateral changes in layer thickness and mantle density tend to compensate each other in the model with the result that no gravity high is seen either in the observed or modeled gravity. A lateral density change in the upper mantle near subduction zones has also been suggested by other researchers (Hales, 1969; Hussong et al., 1973, 1975). A slightly different version of the Pisco (14°S.) crustal and subcrustal cross section (first modeled by Whitsett, 1976) also required a lateral density change in the upper mantle when modeled with the mass column used in this study (R. Couch, personal communication, 1978).

The irregular layering of the Nazca Plate may be due to the Mendena fracture zone which intersects Line 18-19 between 260 km and 310 km in Figure 19. The changes in layer thickness in the crustal section may be related to an age difference of more than 15 million years (Herron, 1972) between the younger western and older eastern sections at this intersection.

# SUMMARY AND CONCLUSIONS

The ray trace method of seismic interpretation has application to interpretation of refraction and reflection data obtained from structurally complex areas. A vector method suitable for use on a minicomputer was applied to analysis of eleven overlapping refraction lines obtained normal to structural trends across the Peru margin at 9°S. The analysis combined primary and secondary seismic arrivals from refraction data, well log velocities and depths, near surface sediment structures, CDP velocity data and gravity data to obtain an integrated crustal and subcrustal cross section of the continental shelf and slope, trench and oceanic plate. Figure 20 summarizes the resulting geophysical and geological model which defines the structural elements of this convergent margin.

The basement of the continental shelf is structurally complex and can be divided into eastern and western portions. The western portion consists of a faulted outer continental shelf high of Paleozoic or older rocks. A deeper block to the west has a velocity of 5.0 km/sec and consists of fractured and slickensided phyllite in its upper surface. Basement velocities comparable to this were seen by Fisher and Raitt (1962) on the outer continental shelf 250 km to the south. A shallower but denser block abuts this block to the east and has a velocity of 5.65 to

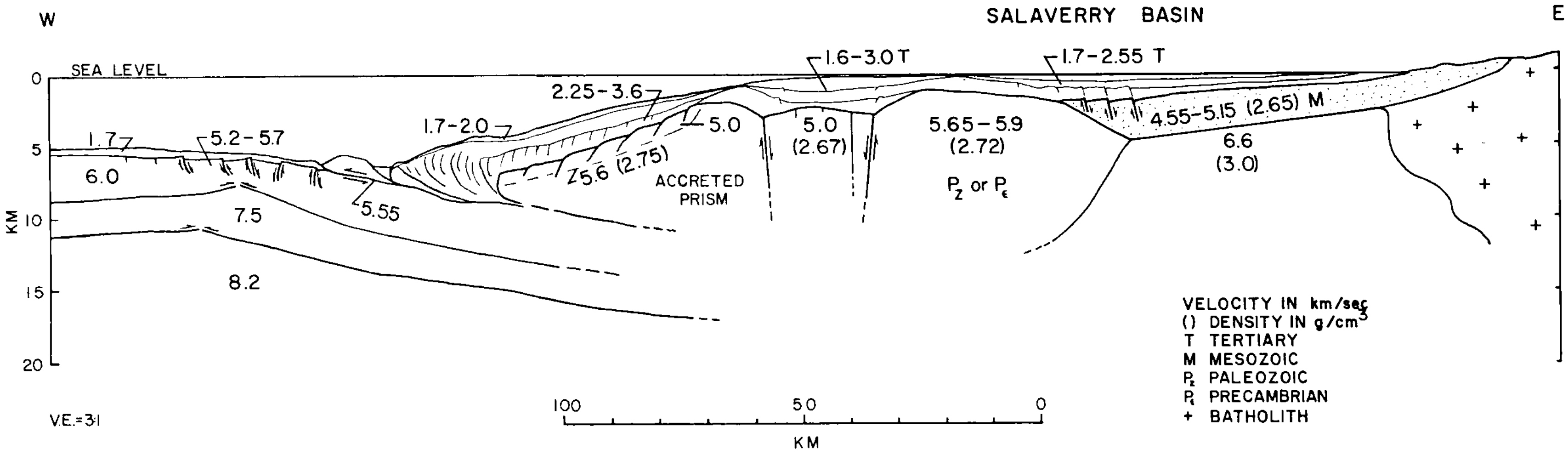


Figure 20. Geophysical and geological model of the continental margin and oceanic plate at 9°S.

5.90 km/sec. Quartz biotite gneiss has been obtained from the upper surface of this block which is believed to be the older of the two blocks. The combined structure forms a basin 2.5 to 3.0 km thick which contains Tertiary sediments with a velocity of 1.6 to 3.0 km/sec. A hiatus of at least 200 million years between basement and overlying sediments suggests that the area was subjected to erosion by bottom currents. Truncated sinusoidal sedimentary features observed in the near-surface may be related to onshore-offshore bottom currents and suggest that the outer continental shelf high was at one time nearer to the sea surface and thus subjected to bottom erosion.

Material 3 km thick with a velocity of 4.55 to 5.15 km/sec shallows to the east beneath sediments covering the eastern portion of the continental shelf. Similar velocities and thicknesses were seen by Hussong et al. (1976) 7 km north of Line 18-19. The eastern basement may consist of pillow lavas, cherts and pyroclastics of Mesozoic age which are confined to the narrow coastal belt onshore. Together, this basement and the eastern section of the outer continental shelf high form the synclinal Salaverry Basin which contains Tertiary sediments in its upper portion with a maximum thickness of 1.8 km and velocities which range from 1.7 to 2.55 km/sec. Underlying the Mesozoic basement is rock of unknown age which has a velocity of 6.6 km/sec and a density, based on gravity modeling, of 3.0 g/$cm^3$. The high density of the rock and its location on the eastern continental shelf suggests either crustal rupture and imbricate upthrust of oceanic crust or intrusion at depth under the continental shelf. A similar model was obtained by Whitsett (1976) at Pisco located 350 km to the south. The similarity suggests that the margins of these areas may have undergone similar deformation at depth.

A well-defined basement underlies the continental slope shoreward from the trench. The refraction data indicates a continental slope basement of velocity 5.0 km/sec overlying a slope core material with an interface velocity of 5.6 km/sec. The deeper material probably represents the upper surface of a melange of accreted deposits, however, the velocity within the melange is not well known. Other researchers (Fisher and Raitt, 1962; Hussong _et al._, 1975; and Hussong _et al._, 1976) report similar velocities for the upper basement of the continental slopes off the coast of Peru and Chile. Together the gravity model, which requires a density of 2.75 g/$cm^3$ to represent the melange, and the seismic velocities imply that the slope melange consists of a larger proportion of oceanic basalt and meta-basalt than oceanic sediments. This could result if the slope melange formed during the onset of subduction before large volumes of sediments would have been scraped off the descending plate. Once formed, the melange acts as a trap and forces the subduction of the majority of sediments that enter the trench.

Lack of close data points on the slope resulted in weakly determined sediment velocities and loss of structural details. The sedimentary layers overlying the slope basement consist of an uppermost layer of slumped sediments (1.7 to 2 km/sec) which reveal little structural layering of reflectors. These sediments overlie an acoustic basement of 2.25 to 3.6 km/sec (Figure 20). This basement probably represents a small volume of consolidated and indurated oceanic sediments which manage to accrete above the slope melange wedge in the past. Seismic ray trace models show that the slope base is devoid of well-defined layers. This is consistent with the prosed models of accretion by Prince and Kulm (1975) and Kulm _et al._ (1977).

A noteable example of the application of seismic ray trace methods occurs in the interpretation of significantly altered arrival times due to the presence of a ridge in the trench. The model of the ridge agrees with the suggestion of Prince and Kulm (1975) that the ridge represents a portion of thrust-faulted oceanic crust which has been uplifted relative to the trench floor. Beneath the trench the descending lithospheric plate is modeled by a 4 km thick upper layer of velocity 5.55 km/sec which overlies a thinner (2.5 km) but considerably higher velocity 7.5 km/

sec layer. The underlying Moho shows a velocity of 8.2 km/sec and dips at an angle of 5° under the continental margin.

A seismic model with relatively constant velocities satisfies observed variations in the layer interfaces for the Nazca Plate seaward from the trench. Upper crustal layers of the modeled plate consists of a thin 1.7 km/sec sedimentary layer overlying a 5.0 to 5.2 km/sec upper layer and a 5.6 to 5.7 km/sec lower layer which shoal to the east within 60 km of the trench while a deeper 6.0 to 6.3 km/sec layer thickens to the east. The lower crustal model consists of a 7.4 to 7.5 km/sec layer which varies in thickness from 2.5 to 4.0 km. This high velocity layer is a predominant feature of the Nazca Plate in this region (Hussong et al., 1976). The depth to an 8.2 km/sec Moho interface varies not more than ±0.5 km from 10.5 km for the 120 km long model of the Nazca Plate.

Refraction data indicates crustal thickening beneath the trench which is also noted along the Peru-Chile margin by others (Fisher and Raitt, 1962; Ocola and Meyer, 1973; Hussong et al., 1976). West of the trench, the higher velocity crustal layers shallow and this may represent upward flexure of the oceanic plate. In addition, development of normal faults can be observed in the upper crustal layer just seaward of the trench (Prince, 1974; Prince and Kulm, 1975; and Schweller, 1976). The combination of crustal thickening, upward flexure, normal faulting, and the ridge in the trench strongly suggest that compressional stresses are present where the plate enters the subduction zone (Figure 20).

# BIBLIOGRAPHY

Abe, K., 1972. Mechanisms and tectonic implications of the 1966 and 1970 Peru earthquakes. Phys. Earth and Planet. Inter. 5:367-379.

Adachi, R., 1954. On a proof of fundamental formula concerning refraction method of geophysical prospecting and some remarks. Kumamoto J. Sci., Ser. A. 2:18-23.

Barazangi, M., and J. Dorman, 1969. World seismicity maps compiled from ESSA Coast and Geodetic Service epicenter data, 1961-1967. Bull. Seismol. Soc. Amer. 59:369-388.

Barday, R., 1974. Structure of the Panama Basin from marine gravity data. Masters thesis. Oregon State University. Corvallis. 99 numb. leaves.

Benioff, H., 1954. Orogenesis and deep crustal structure - additional evidence from seismology. Geol. Soc. Amer. Bull. 65:385-400.

Case, J. E., L. G. Duran, A. Lopez, and W. R. Moore, 1971. Tectonic investigations in western Colombia and Eastern Panama. Geol. Soc. Amer. Bull. 82:2685-2712.

Cerveny, V. and R. Ravindra, 1971. Theory of Seismic Head Waves. University of Toronto Press, Toronto. 312 p.

Cobbing, E. J., and W. S. Pitcher, 1972. Plate tectonics and the Peruvian Andes. Nature Phys. Sci. 240:51-53.

Couch, R. W., J. C. Rose, and G. P. Woollard, 1970. Nazca Plate Project Proposal. Joint project Hawaii Institute of Geophysics, Oregon State University, and Pacific Oceanographic Laboratory (NOAA). International Decade of Ocean Exploration. 94 p.

Colbourn, W. T., and R. Moberly, 1977. Structural evidence of the evolution of fore-arc Basins off South America. Can. Jour. Earth Sci. 14:102-116.

Dietz, R. S., and J. C. Holden, 1974. Collapsing continental rises: actualistic concept of geosynclines - a review. (in) Modern and Ancient Geosynclinal Sedimentation, R. H. Dott, Jr. and R. H. Shaver, eds. Soc. Econ. Paleo. and Min. Spec. Publ. No. 19. Tulsa, Oklahoma.

Ewing, J. I., 1963. The Sea, Vol. III. M. N. Hill (ed.). Wiley-Interscience, New York. p. 14.

Fisher, R. L., 1958. Downwind investigation of the Nazca Ridge p. 20-23 in Fisher, R. L. (ed.), Preliminary report on expedition Downwind, IGY General Report Ser., IGY World Data Center A, Washington 2, 58 p.

Fisher, R. L., and R. W. Raitt, 1962. Deep-Sea Research 9:423-443.

Gardner, L. W., 1939. An areal plan of mapping subsurface structure by refraction shooting. Geophysics. 4:247-259.

Gemperle, M., 1970. Two dimensional gravity cross section computer program TALWANI. Geophysical data reduction technical report, School of Oceanography, Oregon State University, Corvallis.

__________, 1975. Two dimensional gravity cross section computer program - source blocks and field points generalized, GRAV2DLD. Supplement to Geophysical data reduction technical report, School of Oceanography, Oregon State University, Corvallis.

Goebel, V., 1974. Modeling of the Peru-Chile trench from wide angle reflection profiles. Masters thesis. Oregon State University. Corvallis. 73 numb. leaves.

Gebrande, H., 1976. A seismic-ray tracing method for two-dimensional inhomogeneous media. Explosion Seismology in Central Europe. Springer-Verlag, New York. 429 p.

Grant, F. S. and G. F. West, 1965. Interpretation Theory in Applied Geophysics. McGraw-Hill Book Co., New York. 584 p.

Hales, A. L., 1969. Gravitational sliding and continental drift. Earth and Plan. Sci. Letters 6:31-34.

Hamilton, E. L., 1974. Geoacoustic models of the sea floor. (in) Physics of Sound in Marine Sediments. L. Hampton, ed. Plenum Press, New York. 567 p.

Hamilton, E. L., D. G. Moore, E. C. Buffington, P. L. Sherrer and J. R. Curray, 1974. Sediment velocities from sonobuoys: Bay of Bengal, Bering Sea, Japan Sea, and North Pacific. J. Geophys. Res. 79:2653-2668.

Handschumacher, D. W., 1976. Post-eocene plate tectonics of the eastern Pacific. The Geophysics of the Pacific Ocean Basin and Its Margin. G. Sutton, M. Manghnami and R. Moberly, (eds.). Geophys. Mono. 19, A.G.U., Washington, D.C., pp. 177-202.

Hanks, T. C., 1971. The Kuril-trench-Hokkaido rise system: Large shallow earthquakes and simple models of deformation. Geophys. J. Roy. Astron. Soc. 23:173-185.

Hayes, D. E., 1966. A geophysical investigation of the Peru-Chile trench. Mar. Geol. 4:309-351.

Herron, E. M., 1972. Sea-floor spreading and the Cenozoic history of the East-Central Pacific. Geol. Soc. Amer. Bull. 83:1671-1692.

Houtz, R., J. Ewing, and X. Lepichon, 1968. Velocity of deep-sea sediments from sonobuoy data. J. Geophys. Res. 73:2615-2641.

Hunt, R. E., D. J. P. Swift and H. Palmer, 1977. Constructional shelf topography Diamond Shoals, North Carolina. Geol. Soc. Amer. Bull. 88:299-311.

Hussong, D. M., P. Edwards, S. H. Johnson, J. F. Campbell, and M. E. Odegard, 1973. Crustal and upper mantle structure of the Nazca plate (abstract), Int. Assoc. Seismol. Phys. Earth's Interior, XVII, Lima Program, p. 221.

Hussong, D. M., P. B. Edwards, S. H. Johnson, J. F. Campbell, and G. H. Sutton, 1976. Crustal structure of the Peru-Chile Trench: 8°S. - 12°S. latitude. (in) The Geophysics of the Pacific Ocean Basin and Its Margin, G. H. Sutton, M. H. Manghnani, and R. Moberly, (eds.). Geophys. Mono. 19, A.G.U. Washington, D.C., pp. 71-86.

Hussong, D. M., L. K. Wipperman, and M. E. Odegard, 1975. Compressional faulting of the oceanic crust prior to subduction in the Peru-Chile Trench. Geology 3:601-604.

Jacob, K. H., 1970. Three-dimensional seismic ray tracing in a laterally heterogeneous spherical earth. J. Geophys. Res. 75:6675-6689.

James, D. E., 1971. Plate tectonic model for the evolution of the Central Andes. Geol. Soc. Amer. Bull. 82:3325-3346.

Johnson, S. H., 1976. Interpretation of split-spread refraction data in terms of plane dipping layers. Geophysics. 41:418-424.

Johnson, S. H., G. E. Ness, and K. R. Wrolstad, 1975. Shallow structures and seismic velocities of the southern Peru margin. (abstract). EOS Transactions, A.G.U. 56:443.

Kelleher, J. A., 1972. Rupture zones of large south American earthquakes and some predictions. J. Geophys. Res. 77:2087-2103.

Kelleher, J. A., L. Sykes and J. Oliver, 1973. Possible criteria for predicting earthquake locations and their application to major plate boundaries of the Pacific and the Carribean. J. Geophys. Res. 78:2547-2585.

Kramer, F. S., R. A. Peters, and W. C. Walter, eds., 1968. Seismic Energy Sources 1968 Handbook. United Geophysical Corporation, Pasadena, Ca.

Kulm, L. D., J. M. Resig, T. C. Moore, Jr., and V. J. Rosato, 1974. Transfer of Nazca Ridge pelagic sediments to the Peru continental margin. Geol. Soc. Amer. Bull. 85:769-780.

Kulm, L. D., W. J. Schweller, and A. Masias, 1977. A preliminary analysis of the subduction processes along the Andea continental margin, 6° to 45°S. (in) Island Arcs, Deep Sea Trenches and Back-Arc Basins. Maurice Ewing Series 1. A.G.U., Washington, D.C. pp. 285-301.

Kulm, L. D., K. F. Scheidegger, R. A. Prince, J. Dymond, T. C. Moore, Jr., and D. M. Hussong, 1973. Tholeiitic basalt ridge in the Peru Trench. Geology. 1:11-14.

Kulm, L. D., R. A. Prince, W. French, A. Masias, and S. Johnson, 1975. Evidence of imbricate thrusting in the Peru Trench and continental slope from multi-fold seismic reflection data. EOS Trans. A.G.U., 56:442-443.

Ludwig, W. J., J. E. Nate and C. L. Drake, 1970. Seismic refractions. (in) The Sea, Vol. 4, Part I. A. Maxwell (ed.), Wiley, New York. p. 53-84.

Masais, A., 1975. Morphology, shallow structure, and evolution of the Peruvian continental margin, 6° to 18°S. Masters thesis. Oregon State University. Corvallis. 77 numb. leaves.

Mayne, W. H., 1962. Common reflection point horizontal data stacking techniques. Geophys. 27:952-965.

Minster, J. B., T. T. Jordan, P. Molnar, and E. Haines, 1974. Numerical Modeling of instantaneous plate tectonics. Geophys. J. Roy. Astron. Soc. 36:541-576.

Moore, J. C., and D. E. Karig, 1976. Sedimentology, structural geology, and tectonics of the Shikoku subduction zone, southwestern Japan. Geol. Soc. Amer. Bull. 87: 1259-1268.

Morris, G. B., 1972. Delay time function method and its application to the Lake Superior refraction data. J. Geophys. Res. 77:297-314.

Ocola, L. C., 1972a. A nonlinear least-squares method for seismic refraction mapping - Part I: algorithm and procedure. Geophysics. 37:260-272.

__________, 1972b. A nonlinear least-squares method for seismic refraction mapping - Part II: model studies and performance of REFRAMAP method. Geophysics. 37: 273-287.

Ocola, L. C. and R. P. Meyer, 1973. Crustal structure from the Pacific basin to the Brazilian shield between 12° and 30° south latitude. Geol. Soc. Amer. Bull. 84: 3387-3404.

Officer, C. B., 1958. Introduction to the Theory of Sound Transmission. McGraw-Hill, New York. 284 pp.

Pakiser, L. C., and R. A. Black, 1957. Exploring for ancient channels with the refraction seismograph. Geophysics. 22:32-47.

Prince, R. A., 1974. Deformation in the Peru Trench, 6° to 10°S. Masters thesis. Oregon State University, Corvallis. 91 numb. leaves.

Prince, R. A., J. M. Resig, L. D. Kulm, and T. C. Moore, Jr., 1974. Uplifted turbidite basins on the seaward wall of the Peru Trench. Geology. 2:607-611.

Prince, R. A., and L. D. Kulm, 1975. Crustal rupture and the initiation of imbricate thrusting in the Peru-Chile Trench. Geol. Soc. Amer. Bull. 86:1639-1653.

Prince, R. A., and W. J. Schweller, 1978. Dates, rates and angles of faulting in the Peru-Chile Trench. Nature. 271:743-745.

Rosato, V. J., 1974. Peruvian deep-sea sediments: evidence for continental accretion. Masters thesis, Oregon State University, Corvallis. 93 numb. leaves.

Scholl, D. W., R. von Huene, and J. B. Ridlon, 1968. Spreading of the ocean floor: Undeformed sediments in the Peru-Chile Trench. Science. 159:869-871.

Scholl, D. W., M. N. Christensen, R. von Huene, and M. S. Marlow, 1970. Peru-Chile Trench sediments and sea-floor spreading. Geol. Soc. Amer. Bull. 81:1339-1360.

Schweller, W. J., 1976. Chile Trench: Extensional rupture of oceanic crust and the influence of tectonics on sediment distribution. Masters thesis, Oregon State University, Corvallis. 90 numb. leaves.

Scott, J. H., 1973. Seismic refraction modeling by computer. Geophysics. 38:271-284.

Seely, D. R., P. R. Vail, and G. G. Walton, 1974. Trench Slope Model. (in) The Geology of Continental Margins. M. Talwani and W. C. Pitman III (eds.). Springer-Verlag, New York. pp. 249-260.

Shepard, F. P., 1973. Submarine Geology, 3rd ed., Harper and Row, New York. 517 p.

Shah, P. M., 1973. Ray tracing in three dimensions. Geophysics. 38:600-604.

Sorrells, G. G., J. B. Crowley, and K. F. Veith, 1971. Methods for computing ray paths in complex geological structures. Bull. Seism. Soc. Amer. 61:27-53.

Stauder, W., 1975. Subduction of the Nazca Plate under Peru as evidenced by focal mechanism and by seismicity. J. Geophys. Res. 80:1053-1064.

Steinhart, J. S. and R. P. Meyer, 1961. Minimum statistical uncertainty of the seismic refraction profile. Geophysics. 26:574-587.

Stewart, J. W., J. F. Evernden, and N. J. Snelling, 1974. Age determinations from Andean Peru: A reconnaissance survey. Geol. Soc. Amer. Bull. 85:1107-1116.

Swift, S. A. and M. J. Carr, 1974. The segmented nature of the Chilean seismic zone. Phys. Earth and Planet. Interiors. 9:183-191.

Talwani, M., J. L. Worzel and M. Landisman, 1959. Rapid gravity computations for two-dimensional bodies with application to the Mendocino submarine fracture zone. J. Geophys. Res. 64:49-59.

Travis, B. R., G. Gonzales, and A. Pardo, 1976. Hydrocarbon potential of Coastal basins of Peru. (in) Circum-Pacific Energy and Mineral Resources. M. T. Halbouty, J. C. Maher, and H. M. Lian (Eds.) Memoir 25. Amer. Assoc. of Petro. Geol., Tulsa, OK. 608 p.

Watts, A. B. and M. Talwani, 1975. Gravity effect of down-going lithosphere slabs beneath island arcs. Geol. Soc. Amer. Bull. 86:1-4.

Whitsett, R. M., 1976. Gravity measurements and their structural implications for the continental margin of southern Peru. Ph.D. thesis, Oregon State University, Corvallis. 82 numb. leaves.

Woollard, G. P. and J. C. Rose, 1963. International gravity measurements. George Banta Co., Menasha, Wisconsin. p. 121.

Wuenschel, P. C., 1952. Gravity measurements and their interpretation in South America between latitudes 15°-33° south. Ph.D. thesis, Columbia University, New York. 191 numb. leaves.

Yacoub, N. K., J. H. Scott, and F. A. McKeown, 1968. Computer technique for tracing seismic rays in two-dimensional geological models. U.S.G.S. Open-file Report. 65 p.

Yeats, R. S., et al., 1976. Initial Reports of the Deep Sea Drilling Project. Vol. 34. National Sci. Found., Washington, D.C. 814 p.

Zeigler, J. M., W. D. Athearn, and H. Small, 1957. Profiles across the Peru-Chile Trench. Deep-Sea Res. 4:238-249.

# APPENDICES

# Appendix I: Computer Program RAYTRACE

# Description of Program RAYTRACE

## General Description

Program RAYTRACE traces body wave ray paths through a possibly complex two-dimensional geological model represented as a mosaic of quadrilateral cells, each of constant velocity. The computer program allows a user to specify a source point anywhere on or within a model in order to simulate either an artificial explosion or an earthquake. Rays are traced for reflections from a layer interface or as refractions along a layer interface (headwave). All rays are traced from a source point to a designated layer, then back to the uppermost surface. Rays exiting through the sides of the model do not contribute to the travel time.

The ray tracing technique is based on a number of assumptions. A model is assumed to consist of layers that are continuous and extend from one end to the other. This assumption is relaxed somewhat when the layer velocities are allowed to vary in the horizontal as well as the vertical directions. This allows for more complicated modeling of geological structure than is seen in simple layered models. In addition, it is possible to assign an interface velocity different from the cell velocity for vertically refracted waves. Ray theory requires the additional assumptions that in a homogeneous, isotropic half-space, seismic waves propagate in the ray direction normal to the wavefront, that there is no dispersion of the waves under consideration, that the travel time will be the same if the source and the receiver are interchanged, that the source is not on a boundary, and that Snell's law applies at the boundaries between different velocity cells (Grant and West, 1965; Cerveny and Ravindra, 1971).

Marine geological models are composed of rock or sediment units overlain by a water layer. The rock and sediment units are assumed to be isotropic, perfectly elastic, homogeneous with two-dimensional geometry. The two-dimensional restriction assumes that all ray paths are within the model plane. Since the seismic refraction first arrivals are mainly used, body wave conversions (P to S, S to P) at interfaces are not considered because rays that travel strictly as P-waves will arrive first due to their higher velocities. The initial explosive source is generated in a liquid medium and is considered a source of compressional body waves. The above statements lead to geological models represented by areas of constant P-wave velocities delineated by plane boundaries that extend perpendicular to the plane of the model.

## Main Program RAYTRACE

Computer program RAYTRACE is the main program for subprograms RAYMOD, RAYPL, RAYGUN, and RAYHEAD, and subroutines RAYGN, RAYDN, RAYUP, and RAYSH, all of which are coded in an extended FORTRAN IV for use on a DATA GENERAL NOVA 1200 which is a 16 bit word minicomputer. Each subroutine is discussed under its own heading.

Main program RAYTRACE serves as the communication link between the user and the special purpose subprograms and subroutines. Typing the name RAYTRACE at the system console initializes the program (see I/0 example). The main program queries the user for the model file name. The program reads the two-dimensional digital representation of the geological model into its COMMON block and checks for format errors in the process. RAYTRACE then calls subroutine RAYMOD whose purpose is to compute the unit normals to all surfaces in the model. The program questions the user concerning a number of options which include: listing of the model coordinates; a travel time versus distances listing for reflection or critical refraction ray tracing; a travel time plot display; and a model plot with or without visual ray tracing.

The next section of the main program proceeds under control of control codes entered at the console. These codes are:

Code = 0 Stop Program
= 44 Airgun profiler simulation
= 55 Reflection ray trace
= 66 Critically refracted ray trace
= 77 Change shot point position

= 88 Give present shot point position

= 99 Selected other printing and plotting options.

The airgun profiler simulation will be discussed under subprogram RAYGUN and the critically refracted ray trace will be discussed under subprogram RAYHEAD.

Main program RAYTRACE contains the console I/O coding for reflection modeling. Here the user must specify a starting angle, stopping angle and stepping angle increment at the console. The range of angles measured from the positive z axis is from 0° to 180° and from 0° to -180° with positive and negative stepping increments respectively. The absolute value of the ending angle must always be larger than the absolute value of the starting angle. The reflecting layer is individually selected from 1 to the maximum number of layers in the model. Specification of reflecting layer 0 returns the user to the CODE input mode. Layer reflections are generated until the stopping angle is exceeded or a critical refraction angle is exceeded for a layer above the reflecting layer. In the latter case the value of the angle at the source point and the layer number are printed on the console. No reflections will occur from layer interfaces separating equal velocities.

Subprogram RAYMOD

Subprogram RAYMOD generates the unit normal vectors for all of the model interfaces. The model is specified by a grid of quarilateral cells whose upper and lower interfaces join together to form continuous layers while the remaining two interfaces form cell walls. Each quadrilateral cell may be assigned a velocity. The unit vectors are systematically computed for all the layer and cell wall interfaces in order to avoid redundant calculations. The present program allows 7 layers by 25 cells per layer. The bottom layer represents a half-space subdivided by cell walls parallel to the vertical axis. The vertical axis (z) is defined as positive down while the horizontal axis (x) is defined positive to the right.

Subprogram RAYPL

Subprogram RAYPL is used to plot either the model or a set of axes for travel time plots. The model plotting section permits three options: (1) plot only the axes; (2) plot axes and model layers; and (3) plot axes, model layers and model cell walls. The total model must be plotted in a horizontal length of 20 inches or less. The vertical axis length in inches is not limited.

The travel time curve plotting section limits the horizontal distance axis to 20 inches or less. It is possible to specify the right and left hand limits of this axis in kilometers so that a total plot can be made in sections. There is no limit to the number of seconds per inch on the vertical time axis. Due to the flexibility of plotting travel time plot axes, it is possible to make direct overlays of any size for seismic time sections.

Subprogram RAYHEAD

Subprogram RAYHEAD is used to find and ray trace critically refracted rays through a given model. To operate RAYHEAD, the user must specify at the console the refraction layer and direction of ray path travel along the layer (right or left). A search is conducted for the particular angle of incidence at the source which will produce a critical refraction on the layer specified. For a successful search, the user is asked to enter a stepping increment and an ending distance. The stepping increment is used to determine the incremental distance a critically refracted ray must travel along its interface before returning to the surface. The ending distance is the maximum model coordinate distance on the layer interface specified that a critically refracted ray will travel to. Any layer within the model may be traced in this manner. In the case of equal velocities or a velocity inversion between two layers, the user is notified and asked to specify a new layer number. Specification of layer 0 returns the program control to RAYTRACE.

## Subprogram RAYGUN

Subprogram RAYGUN is a computer simulation of a seismic reflection profiler. RAYGUN converts the velocity-depth model of RAYTRACE into a nonmigrated two-way reflection time model. The user specifies the starting and ending horizontal coordinates for the profile. A minimum and maximum reflection time can be specified also, in order to limit the area of interest. This is particularly useful in deep ocean modeling where much of the travel time is spent in the water column. The shot point and detector are assumed to be at a sea level (z = 0) datum. A detector length and position relative to a shot point is specified along with a shot point starting, ending and incremental stepping values. In order to conserve computer time, a reflection beam width and stepping angle within the beam must be given. This feature is needed because only those returning rays that lie within the detector length are used in the solution. Again the user must specify the reflecting layer number. Example of the output of this program is shown in Figure 9.

## Subroutine RAYGN

Subroutine RAYGN generates the initial x and z unit ray vectors from a given angle (-180° to 180°). This subroutine is called by RAYTRACE, RAYHEAD, and RAYGUN.

## Subroutine RAYDN

Subroutine RAYDN computes the distance, travel time and coordinates of a downgoing ray to a designated reflecting or critically refracting layer. This subroutine is based upon equations (22) to (25). At each layer interface checks are made to determine if the critical angle is exceeded and to determine if the ray has traveled through a cell wall. In either case the proper flags are set and control is returned to the calling program. Control is also returned to the calling program whenever an interface separates equal velocities. In cases where the ray does reach the designated layer, then control is returned to the calling program. Subroutine RAYDN can be called by RAYTRACE, RAYHEAD, and RAYGUN.

## Subroutine RAYSH

Subroutine RAYSH relocates a ray that has moved through a cell wall. Determinations are made first to determine which wall has been crossed and whether the ray has passed through either end of the model; if so, then appropriate flags are set and control is returned to the calling program. If the ray is still within the model, then the distance, travel time, and coordinates from the layer to the cell wall are computed. For cases where velocities differ across cell walls, then a new ray unit vector is computed provided the critical angle is not exceeded; if it is, then flags are set and control is returned to the calling program. The distance, travel time and new coordinates from the cell wall to the lower or upper layer, or to the next cell wall are computed. The proper ray path is determined from the new ray vector and according to which path is shortest. Control is returned to the calling program when the new ray is located on a layer interface; otherwise subroutine RAYSH continues. Subroutine RAYSH can be called by RAYTRACE, RAYHEAD, and RAYGUN.

FLOW CHART TO PROGRAM RAYTRACE

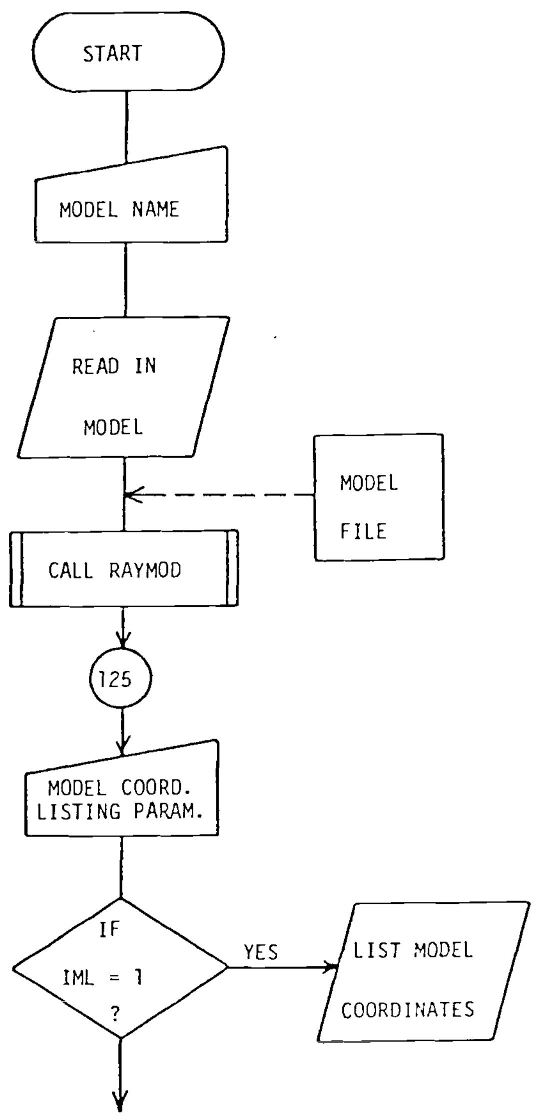

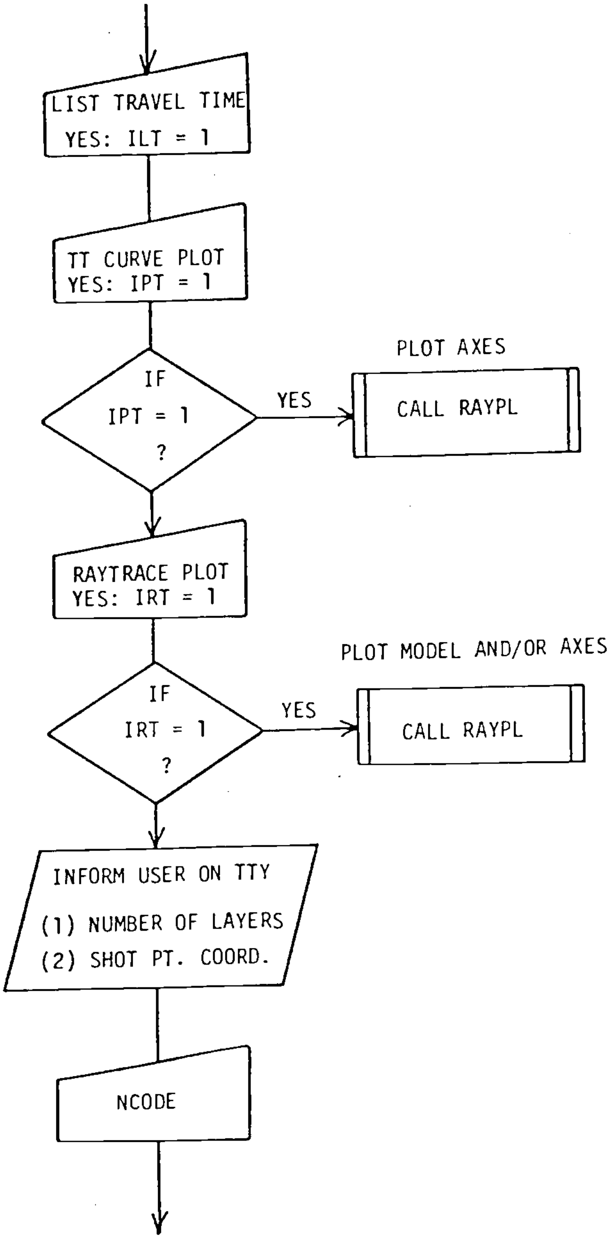
LIST TRAVEL TIME
YES: ILT = 1
TT CURVE PLOT
YES: IPT = 1
IF
IPT = 1
?
YES
PLOT AXES
CALL RAYPL
RAYTRACE PLOT
YES: IRT = 1
IF
IRT = 1
?
YES
PLOT MODEL AND/OR AXES
CALL RAYPL
INFORM USER ON TTY
(1) NUMBER OF LAYERS
(2) SHOT PT. COORD.
NCODE

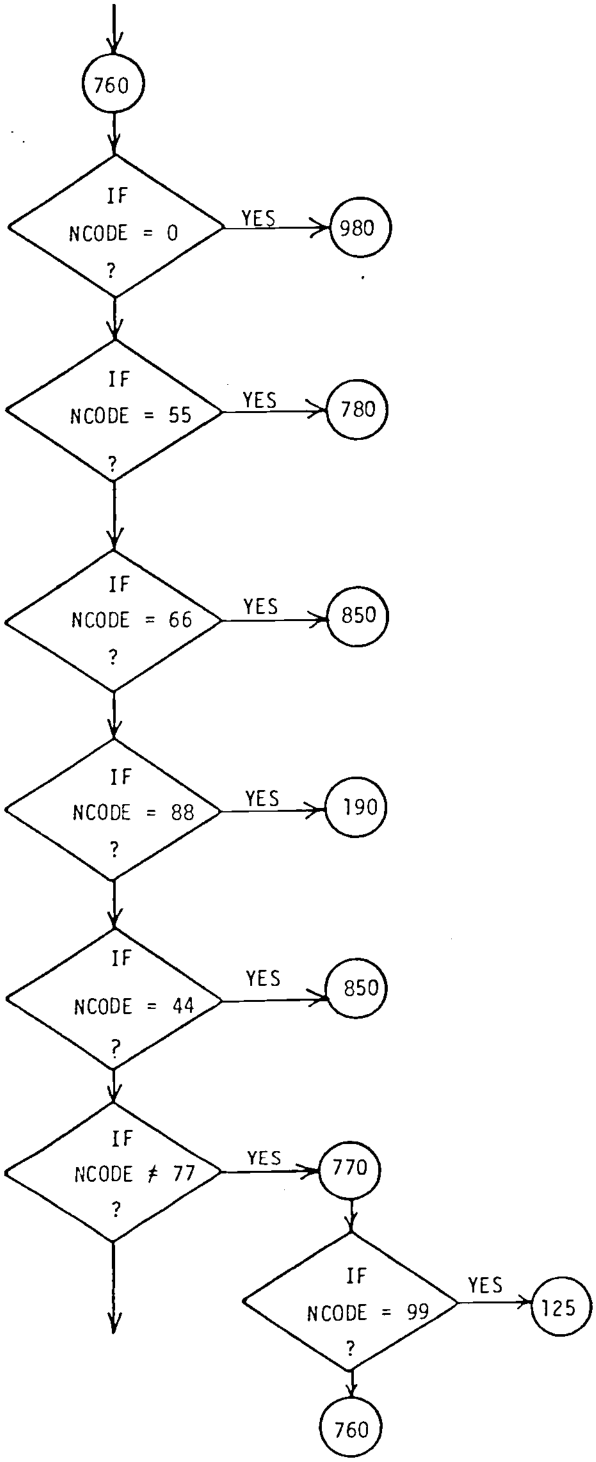
760
IF NCODE = 0 ?
YES
980
IF NCODE = 55 ?
YES
780
IF NCODE = 66 ?
YES
850
IF NCODE = 88 ?
YES
190
IF NCODE = 44 ?
YES
850
IF NCODE ≠ 77 ?
YES
770
IF NCODE = 99 ?
YES
125
760

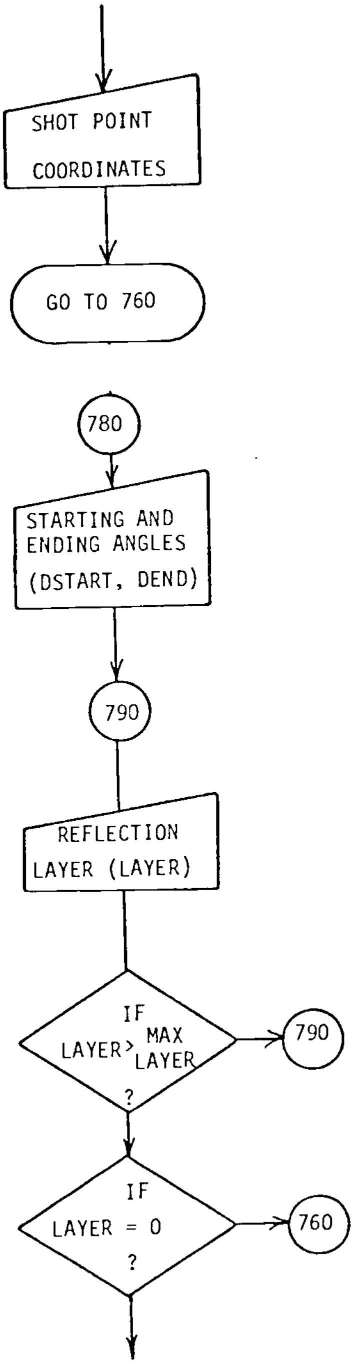
SHOT POINT
COORDINATES
GO TO 760
780
STARTING AND
ENDING ANGLES
(DSTART, DEND)
790
REFLECTION
LAYER (LAYER)
IF
LAYER > MAX LAYER
?
790
IF
LAYER = 0
?
760

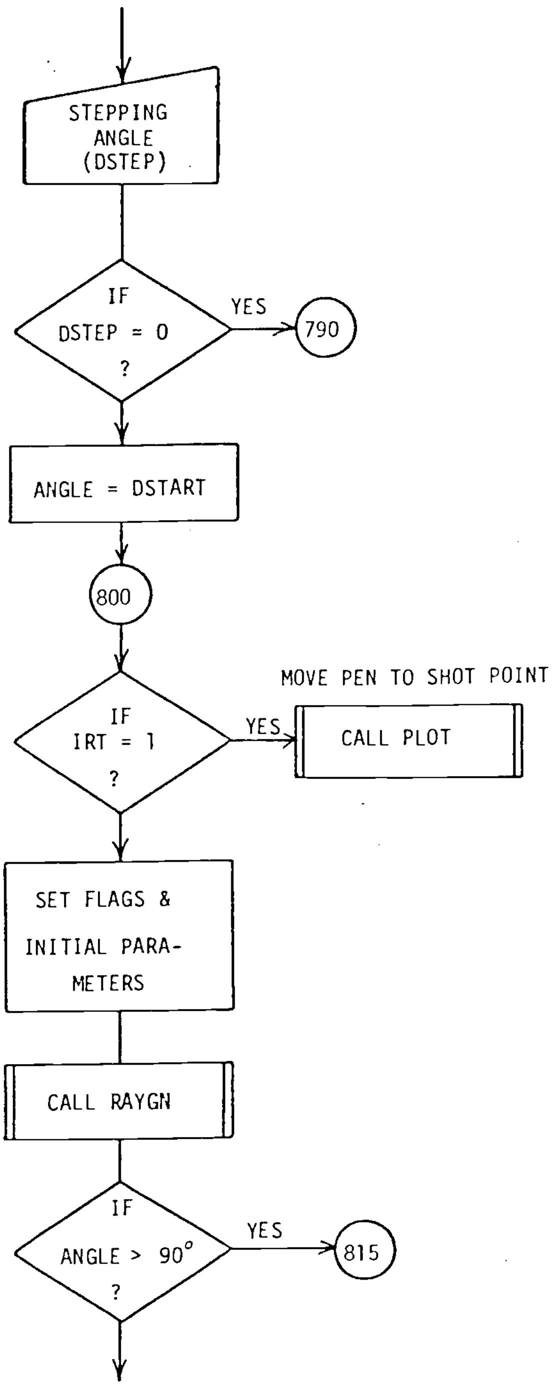
STEPPING ANGLE (DSTEP)
IF DSTEP = 0 ?
YES
790
ANGLE = DSTART
800
IF IRT = 1 ?
YES
MOVE PEN TO SHOT POINT
CALL PLOT
SET FLAGS & INITIAL PARA- METERS
CALL RAYGN
IF ANGLE > 90° ?
YES
815

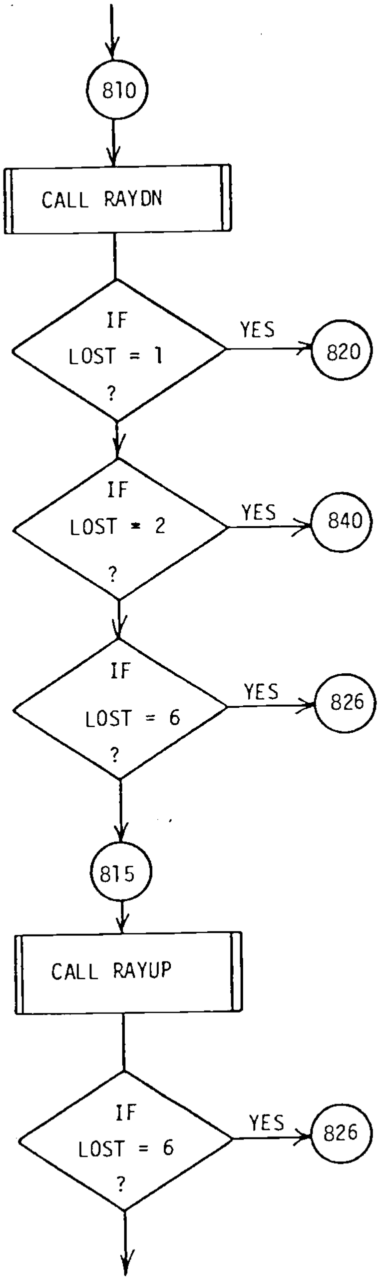
810
CALL RAYDN
IF
LOST = 1
?
YES
820
IF
LOST = 2
?
YES
840
IF
LOST = 6
?
YES
826
815
CALL RAYUP
IF
LOST = 6
?
YES
826

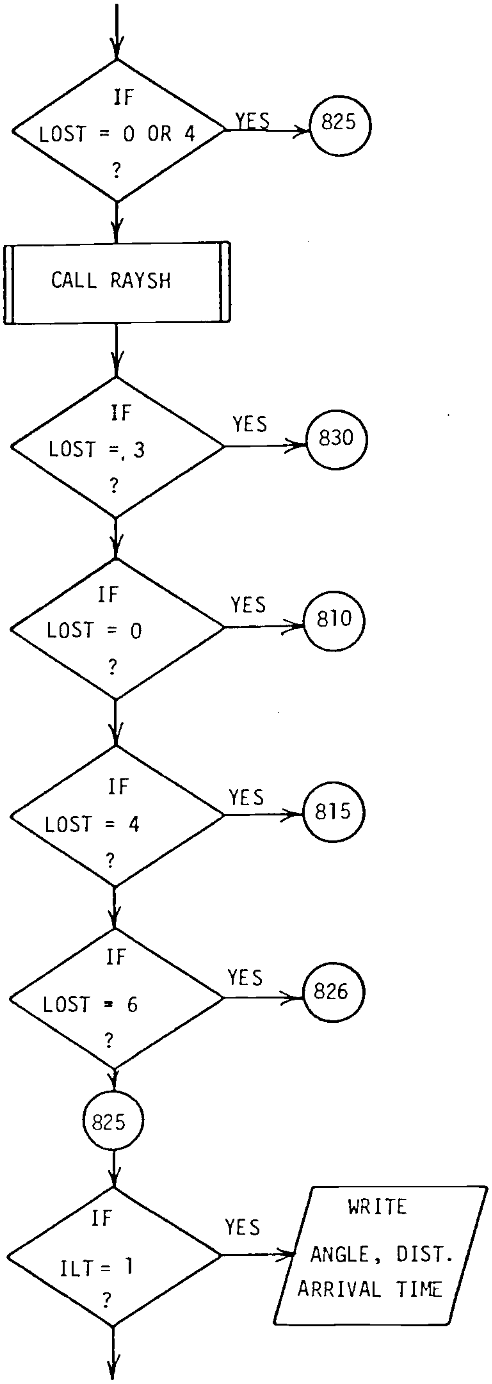
IF
LOST = 0 OR 4
?
YES
825
CALL RAYSH
IF
LOST =. 3
?
YES
830
IF
LOST = 0
?
YES
810
IF
LOST = 4
?
YES
815
IF
LOST = 6
?
YES
826
825
IF
ILT = 1
?
YES
WRITE
ANGLE, DIST.
ARRIVAL TIME

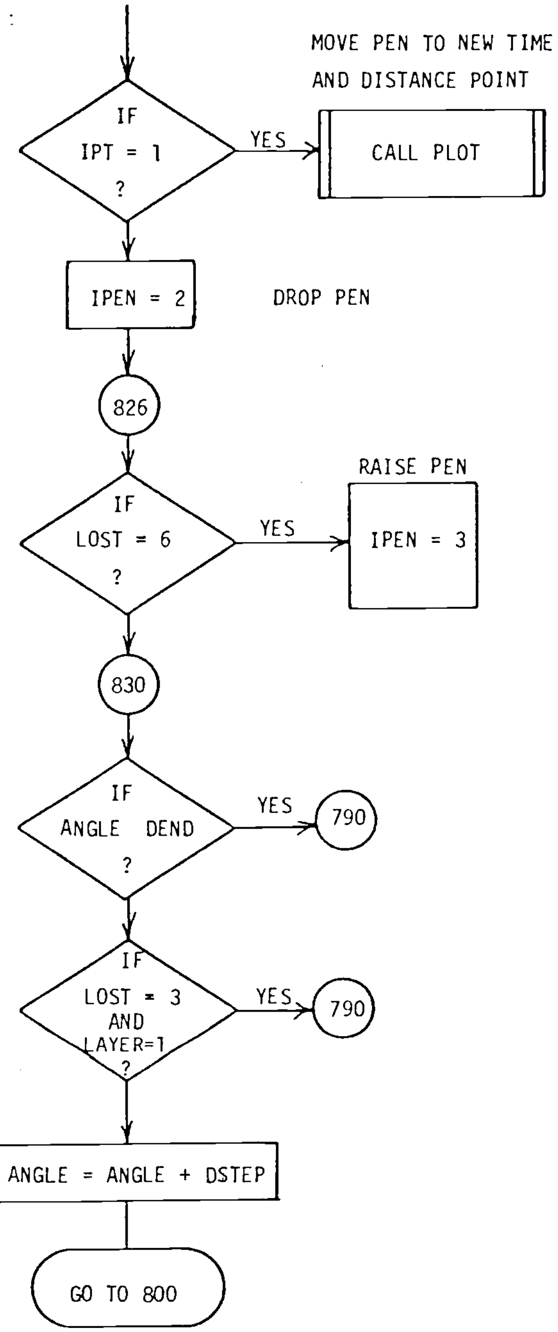
MOVE PEN TO NEW TIME
AND DISTANCE POINT
IF
IPT = 1
?
YES
CALL PLOT
IPEN = 2
DROP PEN
826
RAISE PEN
IF
LOST = 6
?
YES
IPEN = 3
830
IF
ANGLE DEND
?
YES
790
IF
LOST = 3
AND
LAYER=1
?
YES
790
ANGLE = ANGLE + DSTEP
GO TO 800

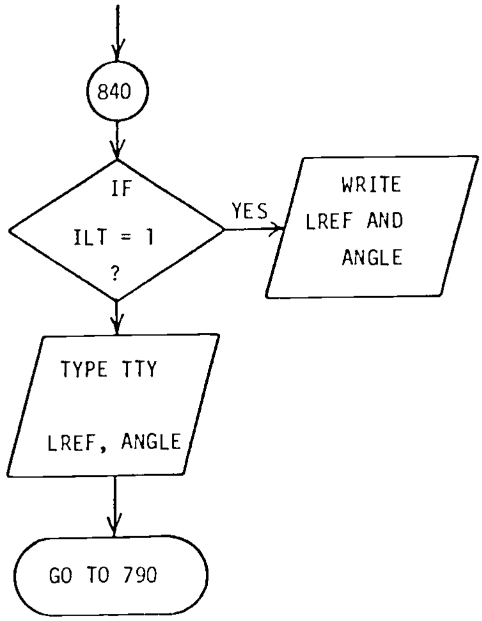
840
IF
ILT = 1
?
YES
WRITE
LREF AND
ANGLE
TYPE TTY
LREF, ANGLE
GO TO 790

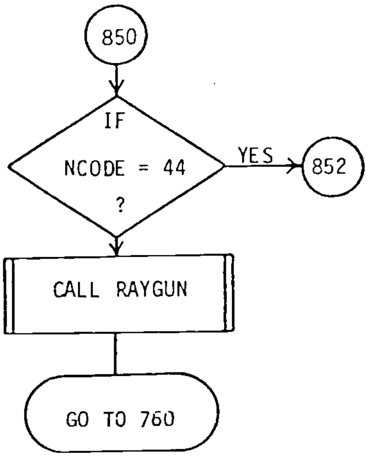
850
IF
NCODE = 44
?
YES
852
CALL RAYGUN
GO TO 760

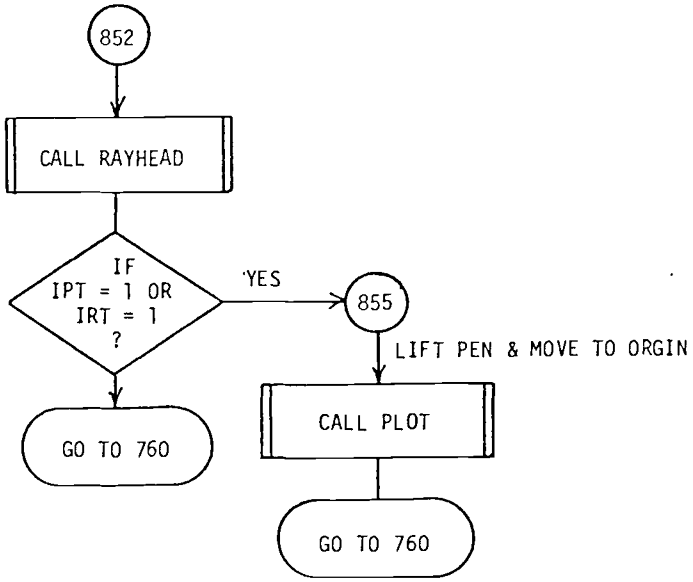
852
CALL RAYHEAD
IF
IPT = 1 OR
IRT = 1
?
YES
855
LIFT PEN & MOVE TO ORGIN
CALL PLOT
GO TO 760
GO TO 760

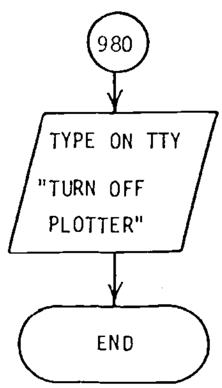
980
TYPE ON TTY
"TURN OFF
PLOTTER"
END

## Program Parameters

Definition of Variables Used in Program RAYTRACE

NCELLS = number of cells.

NLAYER = number of layers.

J = interger counter for cells, J = 1,2,3,... .

LAYER = bottom interface of reflection or refraction layer, LAYER = 1,2,3,..., NLAYER.

X(I,J) =
Z(I,J) = } x,z coordinates of upper L.H. corner of layer I and cell J.

V(I,J) = velocity of layer I and cell J.

UNORMX(I,J) =
UNORMZ(I,J) = } x,z unit normal vectors of layer (I-1) belonging to cell J.

FACEX(I,J) =
FACEZ(I,J) = } x,z unit normal vectors of the R.H. wall of cell J and layer I.

RAYX(I,J) =
RAYZ(I,J) = } x,z reflected and refracted unit rays $\hat{p}_{ij}$ for layer I and cell J.

DSTART = starting angle.

DEND = ending angle.

DSTEP = stepping angle.

HOR = horizontal distance traveled by ray.

VERT = vertical distance traveled by ray.

TIME = travel time of ray.

ANGLE = initial ray starting angle at shot point. Angle is measured in degrees from the positive z-axis.

LSTART = starting layer location flag.

LREF = last known layer location flat.

LOST = RAYTRACE logic parameters (see list).

IRT = flag for plotting ray trace model and rays.

IPT = flag for plotting travel time curves.

IML = flag for model coordinate listing.

ILT = flag for travel time listing.

XMAX = km value of upper R.H. coordinate on x-axis.

XMIN = km value of upper L.H. coordinate on z-axis.

XSIZE = horizontal size in inches of TT or RT plot.

TSIZE = vertical size in inches of TT or RT plot.

TSCALE = vertical scale in sec or km for TT or RT plot.

XSP = x coordinate of shot point.

ZSP = z coordinate of shot point.

LSP = layer containing shot point.

JSP = cell containing shot point.

TEMP1 = horizontal distance of ray upon reaching a layer interface.

ICRIT = angle at shot point which produces a critical refraction.

CHOR = horizontal distance traveled along layer interface before returning to surface layer.

RAYTRACE Logic Parameters for flag 'LOST'

LOST = 0 Ray is refracted downward and is still within cell upon reaching designated layer LAYER.

= 1 Downgoing ray has left cell J at layer (LREF+1).

= 2 Ray has reached a critical refracting angle at layer LREF before reaching layer LAYER.

= 3 Ray is outside of model.

= 4 Ray is refracted upward and is still within cell.

= 5 Upgoing ray has left cell.

= 6 Angle of critical refraction is exceeded at cell wall or at layer interface by an upgoing ray or velocities are equal across layer boundary. This parameter causes a 'penup' plot command.

```
      RAYTRACE                         7/24/78  16:20:35      PAGE  1
C     PROGRAM RAYTRACE
C     RAYTRACING PROGRAM FOR MULTI-CELL, MULTI-LAYER MODELS
C     AUTHOR: P.R. JONES, 26 MARCH 76   VERSION 6, 11 MARCH 77
      DIMENSION IHEADER(40),IFILE(6)
      COMMON NCELLS,NLAYER,J,TEMP1,X(7,26),Z(7,26),V(7,25),
     1  FACEX(6,26),FACEZ(6,26),UNORMX(7,25),UNORMZ(7,25),
     2  RAYX(6,25),RAYZ(6,25),XMAX,XMIN,ICRIT,CHOR,
     3  LSTART,LAYER,LREF,LOST,ZSP,XSP,LSP,JSP,IPT,ILT,HOR,
     4  VERT,TIME,ANGLE,IRT,XSIZE,TSIZE,TSCALE
      COMMON/PLABEL/LBLX(2),LBLY(2)
      DATA LBLX/' KM '/
      DATA LBLY/' SEC'/
      CALL FOPEN(6,"$PLT")
      TYPE "NAME OF MODEL"
      READ(11,520) IFILE(1)
  520 FORMAT(S10)
      CALL FOPEN(1,IFILE)
      READ(1,500) IHEADER
  500 FORMAT(40A2)
C  READ IN THE NUMBER OF CELLS AND LAYERS
      READ(1,501) NCELLS,NLAYER
  501 FORMAT(2I2)
C  READ IN THE CELL COORDINATES BY LAYERS FROM L.H. CELL
C  TO R.H. CELL
      NLP1=NLAYER + 1
      NCP1=NCELLS + 1
      DO 110 I=1,NLP1
      DO 100 K=1,NCP1
C  THIS PROGRAM USES THE Z-COORDINATE AS POSITIVE BELOW S.L.
  100 READ(1,502) X(I,K),Z(I,K)
  502 FORMAT(2F8.3)
  110 CONTINUE
C  READ IN CELL VELOCITIES BY EACH LAYER
      DO 130 I=1,NLP1
      DO 120 K=1,NCELLS
  120 READ(1,504,END=990) V(I,K)
  504 FORMAT(F8.3)
  130 CONTINUE
      CALL FSWAP("RAYMOD.SV")
      XMAX=X(1,NCP1)
      XMIN=X(1,1)
      XSP=X(1,1)
      ZSP=Z(1,1)
      LSP=1
      JSP=1
  125 IRT=0
      IPT=0
      ACCEPT "LIST MODEL COORDINATES?,YES=1 ",IML
      IF(IML.NE.1) GO TO 172
      WRITE(12,519) IHEADER
  519 FORMAT(1H1,40A2)
      WRITE(12,512)
  512 FORMAT(1H0,'MODEL COORDINATES,X,Z')
      DO 150 I=1,NLP1
      DO 140 K=1,NCP1
  140 WRITE(12,513) X(I,K),Z(I,K)
  150 CONTINUE
      WRITE(12,514)
```

```
      DO 170 I=1,NLP1
      DO 160 K=1,NCELLS
  160 WRITE(12,515) K,I,V(I,K)
  170 CONTINUE
  513 FORMAT(1H ,2F8.3)
  514 FORMAT(1H ,'CELL',2X,'LAYER',2X,'VELOCITY')
  515 FORMAT(1H ,2X,I2,3X,I2,1X,F8.3)
  172 ACCEPT "TT CURVE LISTING?,YES=1 ",ILT
      IF(ILT.EQ.1) WRITE(12,519) IHEADER
      ACCEPT "TT CURVE PLOT?,YES=1 ",IPT
      IF(IPT.NE.1)  GO TO 175
      CALL FSWAP("RAYPL.SV")
      CALL INITIAL(6,100,0.,0.)
      CALL PLOT(0.,0.,-3)
      GO TO 185
  175 ACCEPT "RAYTRACE PLOT?,YES=1 ",IRT
      IF(IRT.NE.1) GO TO 185
      CALL FSWAP("RAYPL.SV")
      CALL INITIAL(6,100,0.,0.)
      CALL PLOT(0.,0.,-3)
      XRT=(XSP-X(1,1))/(X(1,NCP1)-X(1,1))*XSIZE
      ZRT=TSIZE-ZSP/TSCALE*TSIZE
  185 TYPE NLAYER," LAYER MODEL"
  190 WRITE(10,517) XSP,ZSP,LSP,JSP
  517 FORMAT(1H0,'PRESENT SHOT POINT COORDINATES ARE:',/,' X=',
     1  F8.3,/,' Z=',F8.3,/,' LAYER=',I3,/,' CELL=',I3)
C
C  IF NCODE=0:  STOP PROGRAM
C            =44:  AIRGUN PROFILER
C            =55:  REFLECTION RAYTRACE
C            =66:  CRITICALLY REFRACTED RAYTRACE
C            =77:  CHANGE SHOT POINT POSITION
C            =88:  GIVE PRESENT SHOT POINT POSITION
C            =99:  ACCEPT OTHER PRINTING AND PLOTTING OPTIONS
C
C
  760 IF(IRT.EQ.1) CALL PLOT(XRT,ZRT,3)
      IF(IPT.EQ.1) CALL PLOT(0.,0.,3)
      ACCEPT "CODE? ",NCODE
      IF(NCODE.EQ.0) GO TO 980
      IF(NCODE.EQ.55) GO TO 780
      IF(NCODE.EQ.66) GO TO 850
      IF(NCODE.EQ.88) GO TO 190
      IF(NCODE.EQ.44) GO TO 850
      IF(NCODE.NE.77) GO TO 770
      ACCEPT "S.P. HOR.= ",XSP
      ACCEPT "S.P. VERT.= ",ZSP
      ACCEPT "S.P. LAYER= ",LSP
      ACCEPT "S.P. CELL= ",JSP
      XRT=(XSP-X(1,1))/(X(1,NCP1)-X(1,1))*XSIZE
      ZRT=TSIZE-ZSP/TSCALE*TSIZE
      GO TO 760
  770 IF(NCODE.EQ.99) GO TO 125
      GO TO 760
  780 ACCEPT "STARTING ANGLE? ",DSTART
      ACCEPT "ENDING ANGLE? ",DEND
  790 IF(IPT.EQ.1) CALL PENUP
      ACCEPT "REFLECTING LAYER? ",LAYER
```

```
      IF(LAYER.GT.NLAYER) GO TO 790
      IF(LAYER.EQ.0) GO TO 760
      ACCEPT 'STEPPING ANGLE? ',DSTEP
      IF(DSTEP.EQ.0.) GO TO 790
      IF(ILT.EQ.1) WRITE(12,583) LAYER
  583 FORMAT(1H0,'LAYER NUMBER',I2,' REFLECTION')
      IF(ILT.EQ.1) WRITE(12,516)
  516 FORMAT(1H ,'    ANGLE',4X,'DISTANCE',4X,'TIME')
C  START THE RAY TRACE
      ANGLE=DSTART
      IPEN=3
  800 IF(IRT.EQ.1) CALL PLOT(XRT,ZRT,3)
      TIME=0.
      VERT=ZSP
      HOR=XSP
      LOST=0
      LSTART=LSP
      LREF=0
      J=JSP
      ICRIT=0
      CALL RAYGN
C  CHECK FOR UPWARD STARTING INITIAL RAYS
      IF(ABS(ANGLE).GT.90.) GO TO 815
C
C
C  RAYTRACE LOGIC PARAMETERS
C  IF LOST=0, DN RAY IS STILL W/IN CELL UPON REACHING 'LAYER'
C          =1: DN RAY HAS LEFT CELL J @ LAYER 'LREF+1'
C          =2, RAY HAS REACHED CRIT. REFR. ANGLE @ LAYER 'LREF'
C          =3, RAY IS OUTSIDE OF MODEL
C          =4, RAY IS REFRACTED UP AND STILL W/IN CELL
C          =5: UP RAY HAS LEFT CELL
C          =6: CRIT. REFR. AT CELL WALL OR DURING UPWARD PATH
C              OR NO REFLECTOR (EQUAL VELOCITIES ABOVE AND BELOW)
C
C
C  TRACE RAY DOWN TO DESIRED REFLECTOR
  810 CALL DOWN
C  CHECK IF RAY HAS LEFT CELL J BEFORE REACHING REFLECTOR
      IF(LOST.EQ.1) GO TO 820
C  CHECK FOR A POSSIBLE CRITICAL REFRACTION
      IF(LOST.EQ.2) GO TO 840
C  CHECK FOR NO REFLECTION
      IF(LOST.EQ.6) GO TO 826
C  TRACE RAY UP TO SURFACE
  815 CALL UP
C  CHECK FOR CRITICAL REFRACTION OF UP RAY
      IF(LOST.EQ.6) GO TO 826
C  CHECK IF RAY HAS NOT LEFT CELL J BEFORE REACHING SURFACE
      IF(LOST.EQ.0.OR.LOST.EQ.4) GO TO 825
C  USE SEARCH SUBROUTINE TO LOCATE RAY OUTSIDE OF CELL J
  820 CALL SEARCH
C  CHECK IF RAY IS OUTSIDE OF MODEL
      IF(LOST.EQ.3) GO TO 830
C  CHECK IF RAY IS STILL DOWN GOING
      IF(LOST.EQ.0) GO TO 810
C  CHECK IF RAY IS UP GOING
      IF(LOST.EQ.4) GO TO 815
```

```
      RAYTRACE                    7/24/78  16.20.35      PAGE  4
C  CHECK FOR CRITICAL REFRACTION ON CELL WALL
      IF(LOST.EQ.6) GO TO 826
  825 IF(ILT.EQ.1) WRITE(12,510) ANGLE,HOR,TIME
  510 FORMAT(1H ,3F10.3)
      IF(IPT.NE.1) GO TO 830
      IF(HOR.GT.XMAX) GO TO 830
      IF(HOR.LT.XMIN) GO TO 830
      IF(TIME.GT.TSCALE) GO TO 830
      PHOR=(HOR-XMIN)/(XMAX-XMIN)*XSIZE
      PTIME=TIME/TSCALE*TSIZE
      CALL PLOT(PHOR,PTIME,IPEN)
      IPEN=2
  826 IF(LOST.EQ.6) IPEN=3
  830 IF(ABS(ANGLE).GE.ABS(DEND)) GO TO 790
      IF(LOST.EQ.3.AND.LAYER.EQ.1) GO TO 790
      ANGLE=ANGLE+DSTEP
      GO TO 800
  840 IF(ILT.EQ.1) WRITE(12,511) LREF,ANGLE
  511 FORMAT(1H ,'CRITICAL REFRACTION AT LAYER',1X,I2,
     1  ', APPROXIMATE ANGLE=',F6.3)
      TYPE "CRITICAL REFR. AT LAYER",LREF,"     APPROX. ANGLE",ANGLE
      GO TO 790
  850 IF(IPT.EQ.1.OR.IRT.EQ.1) CALL PLOT(0.,0.,3)
      IF(NCODE.NE.44) GO TO 852
      CALL FSWAP("RAYGUN.SV")
      GO TO 760
  852 CALL FSWAP("RAYHEAD.SV")
      IF(IPT.EQ.1.OR.IRT.EQ.1) GO TO 855
      GO TO 760
  855 CALL INITIAL(6,100,0.,0.)
      CALL PLOT(0.,0.,3)
      GO TO 760
  980 TYPE "TURN OFF PLOTTER"
      STOP
  990 STOP ERROR IN MODEL FILE
      END
```

```
C     RAYGUN
C     SUBROUTINE SIMULATES AN AIRGUN PROFILER SYSTEM
C     VERSION 1,  22 MAY 77     REVISED, 23 NOV 77
      COMMON NCELLS,NLAYER,J,TEMP1,X(7,26),Z(7,26),V(7,25),
     1 FACEX(6,26),FACEZ(6,26),UNORMX(7,25),UNORMZ(7,25),
     2 RAYX(6,25),RAYZ(6,25),XMAX,XMIN,ICRIT,CHOR,
     3 LSTART,LAYER,LREF,LOST,ZSP,XSP,LSP,JSP,IPT,ILT,HOR,
     4 VERT,TIME,ANGLE,IRT,XSIZE,TSIZE,TSCALE
      COMMON/PLABEL/LBLX(2),LBLY(2)
      DATA LBLX/' KM '/
      DATA LBLY/' SEC'/
      CALL FOPEN(6,"$PLT")
      CALL INITIAL(6,100,0.,0.)
      ACCEPT "DISTANCE SCALE(INCHES)? ",XSIZE
      ACCEPT "LEFT EDGE(KM)? ",XMIN
      ACCEPT "RIGHT EDGE(KM)? ",XMAX
      ACCEPT "TIME SCALE(INCHES)? ",TSIZE
      ACCEPT "MIN. TIME SCALE(SEC.)? ",TMIN
      ACCEPT "MAX. TIME SCALE(SEC.)? ",TMAX
      ACCEPT "AUTO-ORIGIN?,YES=1 ",IAUTO
      XMX=XMAX-XMIN
      XMN=XMIN/XMX*XSIZE
      DSX=XMX/XSIZE
      TSCALE=TMAX-TMIN
      DSY=TSCALE/TSIZE
      PAUSE: TURN ON PLOTTER
      IF(IAUTO.NE.1) GO TO 600
      CALL PLOT(.75,0.,-3)
  600 CALL AXIS(0.,TSIZE,LBLX,4,XSIZE,0.,XMIN,DSX,2)
      CALL AXIS(0.,TSIZE,LBLY,-4,TSIZE,270.,TMIN,DSY,2)
  700 ACCEPT "DETECTOR LENGTH LEFT OF S.P.= ",SPL
      ACCEPT "DETECTOR LENGTH RIGHT OF S.P.= ",SPR
      ACCEPT "START SHOT POINT AT X= ",XSPS
      ACCEPT "END SHOT POINT AT X= ",XSPE
      ACCEPT "SHOT POINT STEPPING INCREMENT= ",XSPI
      ACCEPT "MARK S.P. POSITIONS, YES=1 ",MSP
      ACCEPT "GIVE INCLUDED ANGLE OF BEAM ",BA
      ACCEPT "GIVE STEPPING ANGLE IN BEAM ",DSTEP
      DSTART=-BA/2.
      DEND=BA/2.
C  START FIRING AIRGUN
  800 ACCEPT "REFLECTING LAYER= ",LAYER
      IF(LAYER.EQ.0) GO TO 999
      IF(LAYER.EQ.99) GO TO 700
      IF(LAYER.GT.NLAYER) GO TO 800
      XSP=XSPS
      JSP=1
      HMIN=XSP-SPL
      HMAX=XSP+SPR
  900 ANGLE=DSTART
      I=JSP
  910 IF(XSP.GE.X(1,I).AND.XSP.LE.X(1,I+1)) GO TO 920
      I=I+1
      IF(I.GT.NCELLS) GO TO 800
      GO TO 910
  920 JSP=I
      IF(MSP.NE.1) GO TO 930
      SPX=(XSP-XMIN)/(XMX)*XSIZE
```

```
      CALL PLOT(SPX,TSIZE,3)
      CALL MARKER(1)
  930 IPEN=3
  100 TIME=0.
      HOR=XSP
      VERT=0.
      LOST=0
      LSTART=1
      LREF=0
      J=JSP
      ICRIT=0
      CALL RAYGN
  110 CALL DOWN
      IF(LOST.EQ.1) GO TO 120
      IF(LOST.EQ.2) GO TO 130
      IF(LOST.EQ.6) GO TO 126
  115 CALL UP
      IF(LOST.EQ.6) GO TO 126
      IF(LOST.EQ.0.OR.LOST.EQ.4) GO TO 125
  120 CALL SEARCH
      IF(LOST.EQ.3) GO TO 130
      IF(LOST.EQ.0) GO TO 110
      IF(LOST.EQ.4) GO TO 115
      IF(LOST.EQ.6) GO TO 126
C  PLOT REFLECTION POINT IN TIME DOMAIN
  125 IF(HOR.GT.XMAX.OR.HOR.GT.HMAX) GO TO 130
      IF(HOR.LT.XMIN.OR.HOR.LT.HMIN) GO TO 130
      IF(TIME.LT.TMIN.OR.TIME.GT.TMAX) GO TO 130
      PHOR=(HOR-XMIN)/(XMX)*XSIZE
      PTIME=TSIZE-(TIME-TMIN)/TSCALE*TSIZE
      CALL PLOT(PHOR,PTIME,IPEN)
      IPEN=2
  126 IF(LOST.EQ.6) IPEN=3
  130 ANGLE=ANGLE+DSTEP
      IF(ABS(ANGLE).GT.ABS(DEND)) GO TO 140
      GO TO 100
C  MOVE S.P. TO NEXT INCREMENT
  140 XSP=XSP+XSPI
      IF(XSP.GT.XSPE) GO TO 800
      IF(XSP.GT.XMAX) GO TO 800
      HMIN=XSP-SPL
      HMAX=XSP+SPR
      GO TO 900
  999 CALL FEACK
      END
```

```
RAYMOD                                7/24/78  16:20.35       PAGE  1
C     PROGRAM RAYMOD
C     GENERATES UNIT VECTORS FOR INTERFACES OF MODEL
      COMMON NCELLS,NLAYER,J,TEMP1,X(7,26),Z(7,26),V(7,25),
     1  FACEX(6,26),FACEZ(6,26),UNORMX(7,25),UNORMZ(7,25),
     2  RAYX(6,25),RAYZ(6,25),XMAX,XMIN,ICRIT,CHOR,
     3  LSTART,LAYER,LREF,LOST,ZSP,XSP,LSP,JSP,IPT,ILT,HOR,
     4  VERT,TIME,ANGLE,IRT,XSIZE,TSIZE,TSCALE
      NLP1=NLAYER+1
      NCP1=NCELLS+1
C  COMPUTATION OF HORIZONTAL INTERFACE UNIT NORMALS
      DO 60 I=1,NLP1
      DO 50 K=1,NCELLS
      TEMPX=X(I,K+1)-X(I,K)
      TEMPZ=Z(I,K+1)-Z(I,K)
      UNORM=SQRT(TEMPX*TEMPX+TEMPZ*TEMPZ)
      UNORMZ(I,K)=-TEMPX/UNORM
   50 UNORMX(I,K)=TEMPZ/UNORM
   60 CONTINUE
C  COMPUTATION OF UNIT NORMAL WALL VECTORS
      DO 80 I=1,NLAYER
      DO 70 K=1,NCP1
      TEMPX=X(I+1,K)-X(I,K)
      TEMPZ=Z(I+1,K)-Z(I,K)
      UNORM=SQRT(TEMPX*TEMPX+TEMPZ*TEMPZ)
      FACEX(I,K)=TEMPZ/UNORM
   70 FACEZ(I,K)=-TEMPX/UNORM
   80 CONTINUE
      CALL FEACK
      END
```

```
RAYPL   :                        7/24/78  16.20.35      PAGE  1
C      RAYPL
C      MODEL PLOTTING PROGRAM FOR RAYTRACE
       COMMON NCELLS,NLAYER,J,TEMP1,X(7,26),Z(7,26),V(7,25),
      1  FACEX(6,26),FACEZ(6,26),UNORMX(7,25),UNORMZ(7,25),
      2  RAYX(6,25),RAYZ(6,25),XMAX,XMIN,ICRIT,CHOR,
      3  LSTART,LAYER,LREF,LOST,ZSP,XSP,LSP,JSP,IPT,ILT,HOR,
      4  VERT,TIME,ANGLE,IRT,XSIZE,TSIZE,TSCALE
       COMMON/PLABEL/LBLX(2),LBLY(2)
       DATA LBLX/' KM '/
       DATA LBLY/' SEC'/
       CALL FOPEN(6,"$PLT")
       CALL INITIAL(6,100,0.,0.)
       IF(IRT.EQ.1) GO TO 9
C  PLOT AXES OF TT CURVE
       ACCEPT "DISTANCE SCALE(INCHES)? ",XSIZE
       ACCEPT "LEFT EDGE(KM)? ",XMIN
       ACCEPT "RIGHT EDGE(KM)? ",XMAX
       ACCEPT "TIME SCALE(INCHES)? ",TSIZE
       ACCEPT "TIME SCALE(SEC.)? ",TSCALE
       ACCEPT "AUTO-ORIGIN?,YES=1 ",IAUTO
       XMX=XMAX-XMIN
       XMN=XMIN/XMX*XSIZE
       PAUSE:  TURH ON PLOTTER
       DSX=XMX/XSIZE
       DSY=TSCALE/TSIZE
       IF(IAUTO.NE.1) GO TO 8
       CALL PLOT(.75,0.,-3)
     8 CALL AXIS(0.,0.,LBLX,-4,XSIZE,0.,XMIN,DSX,2)
       CALL AXIS(0.,0.,LBLY,4,TSIZE,90.,0.,DSY,2)
       GO TO 50
C  PLOT AXES AND MODEL FOR RAYTRACE PLOT
     9 ACCEPT "HORIZONTAL SCALE(INCHES)? ",XSIZE
       ACCEPT "VERTICAL SCALE(INCHES)? ",TSIZE
       ACCEPT "VERTICAL SCALE(KM)? ",TSCALE
       ACCEPT "AUTO-ORGIN?,YES=1 ",IAUTO
       NLP1=NLAYER+1
       NCP1=NCELLS+1
       XMX=X(1,NCP1)-X(1,1)
       XMN=X(1,1)/XMX*XSIZE
       DSX=XMX/XSIZE
       DSY=TSCALE/TSIZE
       PAUSE:  TURN ON PLOTTER
       IF(IAUTO.NE.1) GO TO 11
       CALL PLOT(.75,0.,-3)
    11 CALL AXIS(0.,0.,LBLX,-4,XSIZE,0.,X(1,1),DSX,2)
       CALL AXIS(0.,TSIZE,LBLX,-4,TSIZE,270.,0.,DSY,2)
       ACCEPT "PLOT MODEL LAYERS?, 1=YES ",IPM
       IF(IPM.NE.1) GO TO 50
       CALL PLOT(0.,TSIZE,3)
       DO 20 I=1,NLP1
       DO 10 K=1,NCP1
       PX=(X(I,K)-X(1,1))/XMX*XSIZE
       PZ=TSIZE-Z(I,K)/TSCALE*TSIZE
    10 CALL PLOT(PX,PZ,2)
       IF(I.EQ.NLP1) GO TO 20
       PZ=TSIZE-Z(I+1,1)/TSCALE*TSIZE
       CALL PLOT(0.,PZ,3)
    20 CONTINUE
```

```
      RAYPL                              7/24/78  16:20:35      PAGE  2
C     NEXT PLOT THE CELL WALLS
         ACCEPT "PLOT CELL WALLS? ",ICW
         IF(ICW.NE.1) GO TO 50
         CALL PLOT(0.,TSIZE,3)
         DO 40 K=1,NCP1
         DO 30 I=1,NLP1
         PX=(X(I,K)-X(1,1))/XMX*XSIZE
         PZ=TSIZE-Z(I,K)/TSCALE*TSIZE
      30 CALL PLOT(PX,PZ,2)
         IF(K.EQ.NCP1) GO TO 40
         PX=(X(1,K+1)-X(1,1))/XMX*XSIZE
         PZ=TSIZE-Z(1,K+1)/TSCALE*TSIZE
         CALL PLOT(PX,PZ,3)
      40 CONTINUE
      50 CONTINUE
         CALL PLOT(0.,0.,3)
         CALL FEACK
         END
```

```
     RAYHEAD                        7/24/78  16.20.35      PAGE  1
C        RAYHEAD
C        SUBROUTINE TRACES CRITICALLY REFRACTED RAY PATH
         COMMON NCELLS,NLAYER,J,TEMP1,X(7,26),Z(7,26),V(7,25),
        1  FACEX(6,26),FACEZ(6,26),UNORMX(7,25),UNORMZ(7,25),
        2  RAYX(6,25),RAYZ(6,25),XMAX,XMIN,ICRIT,CHOR,
        3  LSTART,LAYER,LREF,LOST,ZSP,XSP,LSP,JSP,IPT,ILT,HOR,
        4  VERT,TIME,ANGLE,IRT,XSIZE,TSIZE,TSCALE
         XMX=X(1,NCELLS+1)-X(1,1)
         XRT=(XSP-X(1,1))/(X(1,NCELLS+1)-X(1,1))*XSIZE
         ZRT=TSIZE-ZSP/TSCALE*TSIZE
         IF(IPT.EQ.1.OR.IRT.EQ.1) GO TO 90
         GO TO 100
     90  CALL FOPEN(6,"$PLT")
         CALL INITIAL(6,100,0.,0.)
         CALL PLOT(0.,0.,-3)
         IF(IRT.EQ.1) CALL PLOT(XRT,ZRT,3)
    100  IF(IPT.EQ.1) CALL PENUP
C    INPUT REFRACTING LAYER
         ACCEPT "REFRACTING LAYER? ",LAYER
         IF(LAYER.EQ.0) GO TO 900
         IF(LAYER.GT.NLAYER) GO TO 100
C    FORWARD SHOOTING IS FROM LEFT TO RIGHT
         ACCEPT "SHOOTING LEFT TO RIGHT?,YES=1 ",LINE
         S=1.
         IF(LINE.NE.1) S=-1.
         IF(IRT.NE.1) GO TO 105
         PHOR=(XSP-X(1,1))/XMX*XSIZE
         PVERT=TSIZE-ZSP/TSCALE*TSIZE
         CALL PLOT(PHOR,PVERT,3)
X        CALL MARKER(2)
C    INITIAL SEARCHING ANGLE INCREMENT=DEL
    105  DEL=S
         LEFT=1
         IRTS=0
C    SEARCH STARTING ANGLE=0.
         ANGLE=0.
         IPEN=3
         IF(IRT.EQ.1) IRTS=1
    110  TIME=0.
         VERT=ZSP
         HOR=XSP
         LSTART=LSP
         LREF=0
         LOST=0
         J=JSP
         IRT=0
         ICRIT=1
         CALL RAYGN
C    TRACE RAY DOWN TO DESIRED LAYER
    115  CALL DOWN
C    CHECK IF RAY HAS LEFT CELL BEFORE REACHING LAYER
         IF(LOST.EQ.1) GO TO 120
C    CHECK FOR CRITICAL REFRACTION BEFORE REACHING LAYER
         IF(LOST.EQ.2) GO TO 125
         GO TO 130
C    USE SEARCH TO LOCATE RAY OUTSIDE OF MODEL
    120  CALL SEARCH
         IF(LOST.EQ.6) GO TO 135
```

```
      IF(LOST.NE.3) GO TO 115
  125 TYPE "CRIT. REFR. AT LAYER",LREF," APPROX. ANGLE",ANGLE
      IRT=IRTS
      GO TO 100
C  CHECK FOR CRITICAL REFRACTION ON LAYER
  130 IF(ICRIT.NE.2) GO TO 135
      LEFT=LEFT+1
      IF(LEFT.GE.3) GO TO 140
      ANGLE=ANGLE-DEL
C  DECREASE ANGLE INCREMENT TO 1/20 OF DEL
      DEL=DEL/20.
      GO TO 110
  135 IF(ABS(ANGLE).LT.90.) GO TO 136
      IRT=IRTS
      GO TO 100
  136 ANGLE=ANGLE+DEL
      GO TO 110
C  STORE THE CRITICAL ANGLE
  140 ANGLE=ANGLE-DEL
      IRT=IRTS
      CDIS=0.
      IF(ILT.EQ.1) WRITE(12,500) LAYER
  500 FORMAT(1H0,'CRITICAL REFRACTING LAYER ',I2,/,
     1  3X,'DISTANCE',6X,'TIME')
      ACCEPT "REFR. INCREMENT(KM)? ",DIS
      ACCEPT "END OF REFR. LAYER(KM)? ",SDIS
      TIME=0.
      VERT=ZSP
      HOR=XSP
      LSTART=LSP
      LREF=0
      LOST=0
      J=JSP
      ICRIT=0
C  TRACE CRITICAL REFRACTION PATHS
  145 CALL DOWN
      IF(LOST.EQ.1) GO TO 150
      IF(LOST.EQ.6) GO TO 100
      GO TO 155
  150 CALL SEARCH
      GO TO 145
  155 L=LAYER
      LP1=L+1
      JC=J
      CRAYX=RAYX(L,J)
      CRAYZ=RAYZ(L,J)
      CTIME=TIME
      CHOR=HOR
      CVERT=VERT
C  FIND THE UNIT RAY VECTOR ALONG THE REFRACTOR
      S=1.
      IF(RAYX(L,J).LT.0.) S=-1.
      HRX=S*ABS(UNORMZ(LP1,J))
      HRZ=S*UNORMX(LP1,J)
  160 J=JC
      LOST=0
C  FIND THE NEW POSITION ON THE REFRACTING LAYER
      TEMP1=CHOR+CDIS*HRX
```

```
C  FIRST CHECK IF RAY IS BEYOND END OF REFRACTION LINE
      IF(S.EQ.1..AND.TEMP1.GT.SDIS) GO TO 100
      IF(S.EQ.-1..AND.TEMP1.LT.SDIS) GO TO 100
C  CHECK IF RAY IS OUTSIDE OF CELL J
      IF(TEMP1.GT.X(LP1,J+1)) GO TO 165
      IF(TEMP1.LT.X(LP1,J)) GO TO 165
      CHOR=TEMP1
      CVERT=CVERT+CDIS*HRZ
      CTIME=CTIME+CDIS/V(LP1,J)
      GO TO 180
C  LOCATE HEAD WAVE IN NEW CELL
  165 IF(TEMP1.GT.X(LP1,J+1)) JP1=J+1
      IF(TEMP1.LT.X(LP1,J)) JP1=J-1
C  CHECK IF RAY WILL BE OUTSIDE OF MODEL
      IF(JP1.GT.NCELLS) GO TO 100
      IF(JP1.LT.1) GO TO 100
C  CHECK IF VELOCITIES ARE THE SAME ABOVE AND BELOW LAYER
      IF(V(L,JP1).LT.V(LP1,JP1)) GO TO 170
      TYPE "STOP REFRACTION, VELOCITIES EQUAL OR INVERTED"
      GO TO 100
C  FIND NEW UNIT RAY VECTOR
  170 IF(JP1.GT.J) JJJ=J+1
      IF(JP1.LT.J) JJJ=J
      HRX=S*ABS(UNORMZ(LP1,JP1))
      HRZ=S*UNORMX(LPI,JP1)
      JS=J
      J=JP1
C  FIND NEW INCIDENT UNIT RAY
      VR=V(L,J)/V(LP1,J)
      CRAYX=S*VR
      ARG=-UNORMX(LP1,J)
      THETA=ATAN(ARG/SQRT(1.-ARG*ARG))
      PHI=ATAN(CRAYX/SQRT(1.-CRAYX*CRAYX))
      ETA=THETA+PHI
      CRAYX=SIN(ETA)
      CRAYZ=COS(ETA)
      UN=SQRT(CRAYX**2+CRAYZ**2)
      CRAYX=CRAYX/UN
      CRAYZ=CRAYZ/UN
      D=SQRT((CHOR-X(LP1,JJJ))**2+(CVERT-Z(LP1,JJJ))**2)
      CTIME=CTIME+D/V(LP1,JS)
      CHOR=X(LP1,JJJ)
      CVERT=Z(LP1,JJJ)
      IPEN=3
  180 JC=J
      TIME=CTIME
      HOR=CHOR
      VERT=CVERT
      RAYX(L,J)=CRAYX
      RAYZ(L,J)=CRAYZ
      IF(IRT.NE.1) GO TO 185
      PHOR=(CHOR-X(1,1))/XMX*XSIZE
      PVERT=TSIZE-CVERT/TSCALE*TSIZE
      PH=PHOR
      PV=PVERT
      CALL PLOT(PHOR,PVERT,2)
X     CALL MARKER(2)
C  TRACE RAY BACK TO SURFACE
```

```
  185 CALL UP
      IF(LOST.EQ.6) GO TO 195
      IF(LOST.EQ.0.OR.LOST.EQ.4) GO TO 190
      CALL SEARCH
      IF(LOST.EQ.3) GO TO 195
      IF(LOST.EQ.6) GO TO 195
      GO TO 185
  190 IF(IPT.NE.1) GO TO 195
      IF(HOR.GT.XMAX) GO TO 195
      IF(HOR.LT.XMIN) GO TO 195
      IF(TIME.GT.TSCALE) GO TO 195
      PHOR=(HOR-XMIN)/(XMAX-XMIN)*XSIZE
      PTIME=TIME/TSCALE*TSIZE
      CALL PLOT(PHOR,PTIME,IPEN)
X     CALL MARKER(1)
      IPEN=2
  195 IF(LOST.EQ.6) IPEN=3
      CDIS=DIS
      IF(IRT.EQ.1) CALL PLOT(PH,PV,3)
      IF(ILT.EQ.1) WRITE(12,505) HOR,TIME
  505 FORMAT(1H ,2F10.3)
      GO TO 160
  900 CONTINUE
      IRT=IRTS
      IF(IPT.EQ.1.OR.IRT.EQ.1) CALL PLOT(0.,0.,3)
      CALL FBACK
      END
```

```
      RAYGN                          7/24/78  16:28:35      PAGE  1
      SUBROUTINE RAYGN
C     GENERATES STARTING RAY VECTORS
      COMMON NCELLS,NLAYER,J,TEMP1,X(7,26),Z(7,26),V(7,25),
     1  FACEX(6,26),FACEZ(6,26),UNORMX(7,25),UNORMZ(7,25),
     2  RAYX(6,25),RAYZ(6,25),XMAX,XMIN,ICRIT,CHOR,
     3  LSTART,LAYER,LREF,LOST,ZSP,XSP,LSP,JSP,IPT,ILT,HOR,
     4  VERT,TIME,ANGLE,IRT,XSIZE,TSIZE,TSCALE
C  GENERATE RAY
      S=1.
      IF(ABS(ANGLE).GT.90.) S=-1.
      L=LSTART
      RADCON=3.14159/180.
      RAYX(L,J)=ABS(TAN(RADCON*ANGLE))
      RAYZ(L,J)=1.
      RAYNORM=SQRT(1.+RAYX(L,J)**2)
      RAYX(L,J)=SIGN(1.,ANGLE)*RAYX(L,J)/RAYNORM
      RAYZ(L,J)=S*RAYZ(L,J)/RAYNORM
      RETURN
      END
```

```
RAYDH                    7/24/78  16:28:35      PAGE  1
C     RAYDH
      SUBROUTINE DOWN
C     TRACES DOWNWARD RAY PATH THROUGH MODEL
      COMMON NCELLS,NLAYER,J,TEMP1,X(7,26),Z(7,26),V(7,25),
     1  FACEX(6,26),FACEZ(6,26),UNORMX(7,25),UNORMZ(7,25),
     2  RAYX(6,25),RAYZ(6,25),XMAX,XMIN,ICRIT,CHOR,
     3  LSTART,LAYER,LREF,LOST,ZSP,XSP,LSP,JSP,IPT,ILT,HOR,
     4  VERT,TIME,ANGLE,IRT,XSIZE,TSIZE,TSCALE
      XMX=X(1,NCELLS+1)-X(1,1)
C  COMPUTE MAGNITUDE OF FIRST LAYER RAY
      IF(LREF.NE.0) GO TO 2
      I=LSTART-1
      L=LSTART
      LP1=L+1
      TEMP=UNORMX(LP1,J)*(X(LP1,J)-HOR)+UNORMZ(LP1,J)*(Z(LP1,J)-VERT)
      PDOTN=UNORMX(LP1,J)*RAYX(L,J)+UNORMZ(LP1,J)*RAYZ(L,J)
      TEMP=ABS(TEMP/PDOTN)
      TEMP1=HOR+TEMP*RAYX(L,J)
C  CHECK TO SEE IF RAY IS OUTSIDE OF CELL J
      IF(TEMP1.GT.X(LP1,J+1)) GO TO 25
      IF(TEMP1.LT.X(LP1,J)) GO TO 25
      HOR=TEMP1
      VERT=VERT+TEMP*RAYZ(L,J)
      IF(IRT.NE.1) GO TO 3
      PHOR=(HOR-X(1,1))/XMX*XSIZE
      PVERT=TSIZE-VERT/TSCALE*TSIZE
      CALL PLOT(PHOR,PVERT,2)
X     CALL MARKER(2)
    3 TIME=TIME+TEMP/V(L,J)
      IF(LAYER.EQ.L) GO TO 30
C  FOLLOW DOWNWARD REFRACTED RAY TO LAYER DESIRED
    2 IF(LREF.EQ.LAYER) GO TO 30
      LM1=LAYER-1
      DO 10 I=LSTART,LM1
      IP1=I+1
      IP2=I+2
C  CHECK FOR POSSIBLE CRITICAL REFRACTION
C  STOP IF CRIT. REFRACTION OCCURS BEFORE REACHING REFLECTOR
      PDOTN=RAYX(I,J)*UNORMX(IP1,J)+RAYZ(I,J)*UNORMZ(IP1,J)
      CHECK=1.-(V(I,J)/V(IP1,J))**2
      IF(PDOTN**2.GT.CHECK) GO TO 5
      LREF=I
      LOST=2
      GO TO 40
    5 PMAG=ABS(PDOTN**2-(V(IP1,J)**2-V(I,J)**2)/V(IP1,J)**2)
      PMAG=SQRT(PMAG)
      PMAG=(V(IP1,J)/V(I,J))*(PDOTN-SIGN(1.,PDOTN)*PMAG)
      TEMPX=V(IP1,J)/V(I,J)*RAYX(I,J)-PMAG*UNORMX(IP1,J)
      TEMPZ=V(IP1,J)/V(I,J)*RAYZ(I,J)-PMAG*UNORMZ(IP1,J)
C  NORMALIZE THE RAYS TO FORM UNIT VECTORS
      RAYNORM=SQRT(TEMPX**2+TEMPZ**2)
      RAYX(IP1,J)=TEMPX/RAYNORM
      RAYZ(IP1,J)=TEMPZ/RAYNORM
C  FIND THE PATH LENGTH OF EACH DOWNWARD REFRACTED VECTOR
      TEMP=UNORMZ(IP2,J)*(Z(IP2,J)-VERT)+UNORMX(IP2,J)*(X(IP2,J)-HOR)
      PDOTN=UNORMX(IP2,J)*RAYX(IP1,J)+UNORMZ(IP2,J)*RAYZ(IP1,J)
      TEMP=ABS(TEMP/PDOTN)
      TEMP1=HOR+TEMP*RAYX(IP1,J)
```

```
RAYDN          :                    7/24/78  16:20:35      PAGE  2
C  CHECK TO SEE IF RAY IS OUTSIDE OF CELL J
      IF(TEMP1.GT.X(IP2,J+1)) GO TO 25
      IF(TEMP1.LT.X(IP2,J)) GO TO 25
      TIME=TIME+TEMP/V(IP1,J)
      HOR=TEMP1
      VERT=VERT+TEMP*RAYZ(IP1,J)
      IF(IRT.NE.1) GO TO 10
      PHOR=(HOR-X(1,1))/XMX*XSIZE
      PVERT=TSIZE-VERT/TSCALE*TSIZE
      CALL PLOT(PHOR,PVERT,2)
X     CALL MARKER(2)
   10 CONTINUE
      GO TO 30
   25 LOST=1
      LREF=I
      LSTART=I+1
      GO TO 40
   30 CONTINUE
C  CHECK FOR EQUAL VELOCITIES ABOVE AND BELOW REFLECTOR
      IF(V(I+1,J).NE.V(I+2,J)) GO TO 35
      LOST=6
      GO TO 40
   35 IF(ICRIT.EQ.0) GO TO 40
C  CHECK FOR CRITICAL REFRACTION ON REFLECTING LAYER
      L=LAYER
      L1=L+1
      PDOTN=RAYX(L,J)*UNORMX(L1,J)+RAYZ(L,J)*UNORMZ(L1,J)
      CHECK=1.-(V(L,J)/V(L1,J))**2
      IF(PDOTN**2.GT.CHECK) GO TO 40
      ICRIT=2
   40 CONTINUE
      RETURN
      END
```

```
      RAYUP       :                    7/24/78  16.28.35      PAGE  1
C     RAYUP
      SUBROUTINE UP
C     TRACES UPWARD RAY PATH THROUGH MODEL
      COMMON NCELLS,NLAYER,J,TEMP1,X(7,26),Z(7,26),V(7,25),
     1  FACEX(6,26),FACEZ(6,26),UNORMX(7,25),UNORMZ(7,25),
     2  RAYX(6,25),RAYZ(6,25),XMAX,XMIN,ICRIT,CHOR,
     3  LSTART,LAYER,LREF,LOST,ZSP,XSP,LSP,JSP,IPT,ILT,HOR,
     4  VERT,TIME,ANGLE,IRT,XSIZE,TSIZE,TSCALE
      XMX=X(1,NCELLS+1)-X(1,1)
      L=LAYER
C  CHECK IF INITIAL RAY IS NOT A REFLECTING RAY
      IF(LOST.EQ.0.AND.ABS(ANGLE).GT.90.) GO TO 2
C  CHECK IF REFLECTION VECTOR IS TO BE FOUND
      IF(LOST.EQ.4) GO TO 5
C  FIND UNIT REFLECTION VECTOR
      LP1=LAYER+1
      PDOTN=RAYX(L,J)*UNORMX(LP1,J)+RAYZ(L,J)*UNORMZ(LP1,J)
      TEMPX=RAYX(L,J)-2.*PDOTN*UNORMX(LP1,J)
      TEMPZ=RAYZ(L,J)-2.*PDOTN*UNORMZ(LP1,J)
      RAYNORM=SQRT(TEMPX**2+TEMPZ**2)
      RAYX(L,J)=TEMPX/RAYNORM
      RAYZ(L,J)=TEMPZ/RAYNORM
C  FIRST FIND PATH LENGTH OF REFLECTED VECTOR
    2 TEMP=UNORMZ(L,J)*(Z(L,J)-VERT)+UNORMX(L,J)*(X(L,J)-HOR)
      PDOTN=UNORMX(L,J)*RAYX(L,J)+UNORMZ(L,J)*RAYZ(L,J)
      TEMP=ABS(TEMP/PDOTN)
      TEMP1=HOR+TEMP*RAYX(L,J)
C  CHECK TO SEE IF RAY IS OUTSIDE OF CELL
      IF(TEMP1.GT.X(L,J+1)) GO TO 25
      IF(TEMP1.LT.X(L,J)) GO TO 25
      HOR=TEMP1
      VERT=VERT+TEMP*RAYZ(L,J)
      IF(IRT.NE.1) GO TO 1
      PHOR=(HOR-X(1,1))/XMX*XSIZE
      PVERT=TSIZE-VERT/TSCALE*TSIZE
      CALL PLOT(PHOR,PVERT,2)
X     CALL MARKER(2)
    1 TIME=TIME+TEMP/V(L,J)
      IF(L.EQ.1) GO TO 30
      LREF=LAYER
C  TRACE REFLECTED RAY BACK TO SURFACE
    5 IF(LREF.EQ.1) GO TO 30
      LREFM1=LREF-1
      DO 10 II=1,LREFM1
      L=LREF-II+1
      LM1=L-1
      PDOTN=RAYX(L,J)*UNORMX(L,J)+RAYZ(L,J)*UNORMZ(L,J)
C  CHECK FOR CRITICAL REFRACTION OF RAY
C  IF CRITICAL REFRACTION OCCURS THEN FURTHER UPWARD REFRACTION
C  IS NOT POSSIBLE
      CHECK=1.-(V(L,J)/V(LM1,J))**2
      IF(PDOTN**2.GT.CHECK) GO TO 6
      LREF=L
      LOST=6
      GO TO 30
    6 PMAG=ABS(PDOTN**2-(V(LM1,J)**2-V(L,J)**2)/V(LM1,J)**2)
      PMAG=SQRT(PMAG)
      PMAG=(V(LM1,J)/V(L,J))*(PDOTN-SIGN(1.,PDOTN)*PMAG)
```

```
      TEMPX=RAYX(L,J)*V(LM1,J)/V(L,J)-PMAG*UNORMX(L,J)
      TEMPZ=RAYZ(L,J)*V(LM1,J)/V(L,J)-PMAG*UNORMZ(L,J)
C  NORMALIZE THE RAYS TO FORM UNIT VECTORS
      RAYNORM=SQRT(TEMPX**2+TEMPZ**2)
      RAYX(LM1,J)=TEMPX/RAYNORM
      RAYZ(LM1,J)=TEMPZ/RAYNORM
C  FIND PATH LENGTH OF EACH UPWARD REFRACTED VECTOR
      TEMPX=UNORMX(LM1,J)*(X(LM1,J)-HOR)
      TEMPZ=UNORMZ(LM1,J)*(Z(LM1,J)-VERT)
      PDOTN=UNORMX(LM1,J)*RAYX(LM1,J)+UNORMZ(LM1,J)*RAYZ(LM1,J)
      TEMP=ABS((TEMPX+TEMPZ)/PDOTN)
      TEMP1=HOR+TEMP*RAYX(LM1,J)
C  CHECK TO SEE IF RAY IS OUTSIDE OF CELL
      IF(TEMP1.GT.X(LM1,J+1)) GO TO 20
      IF(TEMP1.LT.X(LM1,J)) GO TO 20
      HOR=TEMP1
      VERT=VERT+TEMP*RAYZ(LM1,J)
      IF(IRT.NE.1) GO TO 7
      PHOR=(HOR-X(1,1))/XMX*XSIZE
      PVERT=TSIZE-VERT/TSCALE*TSIZE
      CALL PLOT(PHOR,PVERT,2)
X     CALL MARKER(2)
    7 TIME=TIME+TEMP/V(LM1,J)
   10 CONTINUE
      GO TO 30
   20 LOST=5
      LREF=L
      LSTART=LM1
      GO TO 30
   25 LOST=5
      LREF=L+1
      LSTART=L
   30 CONTINUE
      RETURN
      END
```

```
     RAYSH                        7/24/78  16:28:35      PAGE  1
C       RAYSH
        SUBROUTINE SEARCH
C       RELOCATES RAY AFTER MOVING THROUGH CELL WALL
        COMMON NCELLS,NLAYER,J,TEMP1,X(7,26),Z(7,26),V(7,25),
       1  FACEX(6,26),FACEZ(6,26),UNORMX(7,25),UNORMZ(7,25),
       2  RAYX(6,25),RAYZ(6,25),XMAX,XMIN,ICRIT,CHOR,
       3  LSTART,LAYER,LREF,LOST,ZSP,XSP,LSP,JSP,IPT,ILT,HOR,
       4  VERT,TIME,ANGLE,IRT,XSIZE,TSIZE,TSCALE
        XMX=X(1,NCELLS+1)-X(1,1)
C   CALCULATE PATH LENGTH FROM LREF TO CELL WALL
        L=LSTART
        LP1=L+1
        IF(LOST.EQ.5) LP1=L
C   DETERMINE WHICH WALL THE RAY WILL MOVE THROUGH
        IF(TEMP1.GT.X(LP1,J+1)) JP1=J+1
        IF(TEMP1.LT.X(LP1,J)) JP1=J-1
C   CHECK TO SEE IF RAY WILL BE OUTSIDE OF MODEL
        IF(JP1.GT.NCELLS) GO TO 2
        IF(JP1.LT.1) GO TO 2
        GO TO 3
      2 LOST=3
        GO TO 50
      3 IF(LOST.EQ.1) LP1=L
        IF(LOST.EQ.5) LP1=L+1
        JJ=J+1
        IF(J.GT.JP1) JJ=J
        XL=X(LP1,JJ)-HOR
        ZL=Z(LP1,JJ)-VERT
        TEMP=XL*FACEX(L,JJ)+ZL*FACEZ(L,JJ)
        TEMPD=RAYX(L,J)*FACEX(L,JJ)+RAYZ(L,J)*FACEZ(L,JJ)
        TEMP=ABS(TEMP/TEMPD)
C   FIND HOR. AND VERT. DISTANCES THUS TRAVELLED TO WALL OF CELL J
        HOR=HOR+TEMP*RAYX(L,J)
        VERT=VERT+TEMP*RAYZ(L,J)
        IF(IRT.NE.1) GO TO 8
        IF(HOR.LT.X(1,1)) GO TO 8
        PHOR=(HOR-X(1,1))/XMX*XSIZE
        PVERT=TSIZE-VERT/TSCALE*TSIZE
        CALL PLOT(PHOR,PVERT,2)
X       CALL MARKER(2)
C   FIND TRAVEL TIME WITHIN CELL J TO WHERE RAY LEAVES CELL
      8 TIME=TIME+TEMP/V(L,J)
C   FIND NEW RAY VECTOR IN CELL JP1, LAYER L
     15 IF(V(L,J).NE.V(L,JP1)) GO TO 20
        RAYX(L,JP1)=RAYX(L,J)
        RAYZ(L,JP1)=RAYZ(L,J)
        GO TO 22
     20 PDOTF=RAYX(L,J)*FACEX(L,JJ)+RAYZ(L,J)*FACEZ(L,JJ)
C   CHECK FOR CRITICAL REFRACTION ACROSS CELL WALL
        CHECK=1.-(V(L,J)/V(L,JP1))**2
        IF(PDOTF**2.GT.CHECK) GO TO 21
        LOST=6
        GO TO 50
     21 PMAG=ABS(PDOTF**2-(V(L,JP1)**2-V(L,J)**2)/V(L,JP1)**2)
        PMAG=SQRT(PMAG)
        PMAG=(V(L,JP1)/V(L,J))*(PDOTF-SIGN(1.,PDOTF)*PMAG)
        TEMPX=V(L,JP1)/V(L,J)*RAYX(L,J)-PMAG*FACEX(L,JJ)
        TEMPZ=V(L,JP1)/V(L,J)*RAYZ(L,J)-PMAG*FACEZ(L,JJ)
```

```
C  NORMALIZE THE NEW RAY TO FORM A UNIT VECTOR
       RAYNORM=SQRT(TEMPX**2+TEMPZ**2)
       RAYX(L,JP1)=TEMPX/RAYNORM
       RAYZ(L,JP1)=TEMPZ/RAYNORM
C  FIND THE PATH LENGTH OF THE NEW RAY IN CELL
C  FIRST FIND WHICH INTERFACE THE RAY MAY INTERSECT
   22 JS=JP1
       IF(J.GT.JP1) JP1=JP1-1
       IF(J.LT.JP1) JP1=JP1+1
       IF(JJ.EQ.J) JJ=JS
       IF(JJ.GT.J) JJ=JS+1
       J=JS
       JJJ=J+1
       IF(J.GT.JP1) JJJ=J
       LP1=L+1
       PDOTH=RAYX(L,J)*UNORMX(LP1,J)+RAYZ(L,J)*UNORMZ(LP1,J)
       IF(PDOTH.GT.0) GO TO 30
C  THE RAY MAY INTERSECT THE LOWER INTERFACE OR NEXT CELL WALL
C  FIRST CALCULATE THE PATH LENGTH IF RAY INTERSECTS LOWER LAYER
       XL=X(LP1,JJ)-HOR
       ZL=Z(LP1,JJ)-VERT
       FACEL=XL*UNORMX(LP1,J)+ZL*UNORMZ(LP1,J)
       TEMPD=RAYX(L,J)*UNORMX(LP1,J)+RAYZ(L,J)*UNORMZ(LP1,J)
       FACEL=ABS(FACEL/TEMPD)
C  NEXT DOUBLE CHECK WITH LENGTH TO UPPER LAYER
       IF(LOST.EQ.1) GO TO 24
       XU=X(L,JJ)-HOR
       ZU=Z(L,JJ)-VERT
       FACE=XU*UNORMX(L,J)+ZU*UNORMZ(L,J)
       TEMP1=RAYX(L,J)*UNORMX(L,J)+RAYZ(L,J)*UNORMZ(L,J)
       FACE=ABS(FACE/TEMP1)
       IF(FACE.LE.FACEL) GO TO 31
C  NEXT CALCULATE THE PATH LENGTH IF RAY INTERSECTS FAR WALL
   24 XL=X(LP1,JJJ)-HOR
       ZL=Z(LP1,JJJ)-VERT
       P=-FACEZ(L,JJ)
       Q=FACEX(L,JJ)
       WALL=ABS((XL*Q-ZL*P)/(RAYX(L,J)*Q-RAYZ(L,J)*P))
C  CHOOSE THE SHORTER PATH LENGTH
       IF(WALL.LE.FACEL) GO TO 25
C  FIND NEW HOR. AND VERT. DISTANCES TRAVELLED TO LOWER LAYER
       HOR=HOR+FACEL*RAYX(L,J)
       VERT=VERT+FACEL*RAYZ(L,J)
       IF(IRT.NE.1) GO TO 23
       PHOR=(HOR-X(1,1))/XMX*XSIZE
       PVERT=TSIZE-VERT/TSCALE*TSIZE
       CALL PLOT(PHOR,PVERT,2)
X      CALL MARKER(2)
   23 TIME=TIME+FACEL/V(L,J)
       LOST=0
       LSTART=L
       LREF=L
       GO TO 50
C  FIND HOR. AND VERT. DISTANCES TRAVELLED THROUGH CELL
   25 HOR=HOR+WALL*RAYX(L,J)
       VERT=VERT+WALL*RAYZ(L,J)
       IF(IRT.NE.1) GO TO 26
       PHOR=(HOR-X(1,1))/XMX*XSIZE
```

```
      PVERT=TSIZE-VERT/TSCALE*TSIZE
      CALL PLOT(PHOR,PVERT,2)
X     CALL MARKER(2)
   26 TIME=TIME+WALL/V(L,J)
C  CHECK TO SEE IF RAY IS OUTSIDE OF MODEL
      IF(JP1.EQ.0) GO TO 27
      IF(JP1.EQ.NCELLS+1) GO TO 27
      GO TO 15
   27 LOST=3
      GO TO 50
C  CASE WHERE RAY MAY INTERSECT UPPER INTERFACE OR NEXT CELL WALL
C  FIRST FIND PATH LENGTH OF RAY THAT MAY INTERSECT UPPER LAYER
   30 XU=X(L,JJ)-HOR
      ZU=Z(L,JJ)-VERT
      FACE=XU*UNORMX(L,J)+ZU*UNORMZ(L,J)
      TEMP1=RAYX(L,J)*UNORMX(L,J)+RAYZ(L,J)*UNORMZ(L,J)
      FACE=ABS(FACE/TEMP1)
C  NEXT CALCULATE THE PATH LENGTH IF RAY INTERSECTS FAR WALL
   31 XL=X(LP1,JJJ)-HOR
      ZL=Z(LP1,JJJ)-VERT
      P=-FACEZ(L,JJ)
      Q=FACEX(L,JJ)
      WALL=ABS((XL*Q-ZL*P)/(RAYX(L,J)*Q-RAYZ(L,J)*P))
C  CHOOSE THE SHORTER PATH LENGTH OF UPWARD RAY
      IF(WALL.LE.FACE) GO TO 25
      HOR=HOR+FACE*RAYX(L,J)
      VERT=VERT+FACE*RAYZ(L,J)
      IF(IRT.NE.1) GO TO 35
      PHOR=(HOR-X(1,1))/XMX*XSIZE
      PVERT=TSIZE-VERT/TSCALE*TSIZE
      CALL PLOT(PHOR,PVERT,2)
X     CALL MARKER(2)
   35 TIME=TIME+FACE/V(L,J)
      LOST=4
      LSTART=L-1
      LREF=L
   50 CONTINUE
      RETURN
      END
```

```
FORT/B RAYTRACE
FORT/B RAYGUN
FORT/B RAYMOD
FORT/B RAYPL
FORT/B RAYHEAD
FORT/B RAYGN
FORT/B RAYDN
FORT/B RAYUP
FORT/B RAYSH
RLDR/M RAYMOD FORT.LB
RLDR/M RAYPL FORT.LB
RLDR/M RAYTRACE RAYGN RAYDN RAYUP RAYSH FORT.LB
RLDR/M RAYHEAD RAYGN RAYDN RAYUP RAYSH FORT.LB
RLDR/M RAYGUN RAYGN RAYDN RAYUP RAYSH FORT.LB
```

Console Example for RAYTRACE

NOTE: Console input is underlined

```
R
RAYTRACE
NAME OF MODEL
RAYTEST
LIST MODEL COORDINATES?,YES=1 1          see listing example
TT CURVE LISTING?,YES=1 0
TT CURVE PLOT?,YES=1 0
RAYTRACE PLOT?,YES=1 1                   see model plot example
HORIZONTAL SCALE(INCHES)? 2
VERTICAL SCALE(INCHES)? 2                dimensions of model plot
VERTICAL SCALE(KM)? 6
TURN ON PLOTTER
PAUSE                                    hit any key to start plotter
PLOT MODEL?, 1=YES 1
PLOT CELL WALLS? 1
      6 LAYER MODEL

PRESENT SHOT POINT COORDINATES ARE:
X=    0.000
Z=    0.000
LAYER=  1
CELL=  1
CODE? 55                                 reflection case
STARTING ANGLE? 0
ENDING ANGLE? 90
REFLECTING LAYER? 6
STEPPING ANGLE? 10
CRITICAL REFR. AT LAYER  5 APPROX. ANGLE 0.200000E  2
REFLECTING LAYER? 0
CODE? 66                                 refraction case
REFRACTING LAYER? 6
SHOOTING LEFT TO RIGHT?,YES=1 1
REFR. INCREMENT(KM)?    .5
END OF REFR. LAYER(KM)? 20
REFRACTING LAYER? 0
CODE? 99                                 select new options
LIST MODEL COORDINATES?,YES=1 0
TT CURVE LISTING?,YES=1 0
TT CURVE PLOT?,YES=1 1                   see TT plot example
DISTANCE SCALE(INCHES)? 2
LEFT EDGE(KM)? 0                         dimensions of travel time plot
RIGHT EDGE(KM)? 20
TIME SCALE(INCHES)? 2
TIME SCALE(SEC.)? 10
TURN ON PLOTTER
PAUSE
```

Console Example for RAYTRACE , cont.

```
6 LAYER MODEL

PRESENT SHOT POINT COORDINATES ARE:
X=    Ø.ØØØ
Z=    Ø.ØØØ
LAYER=  1
CELL=  1
CODE? 55 <-------------------------------- reflection case
STARTING ANGLE? Ø
ENDING ANGLE? 9Ø
REFLECTING LAYER? 1
STEPPING ANGLE? 2
REFLECTING LAYER? 2
STEPPING ANGLE? 2
CRITICAL REFR. AT LAYER 1  APPROX. ANGLE  Ø.5ØØØØØE  2
REFLECTING LAYER? 3
STEPPING ANGLE? 2
CRITICAL REFR. AT LAYER 2  APPROX. ANGLE  Ø.38ØØØØE  2
REFLECTING LAYER? 4
STEPPING ANGLE? 2
CRITICAL REFR. AT LAYER 3  APPROX. ANGLE  Ø.32ØØØØE  2
REFLECTING LAYER? 5
STEPPING ANGLE? 2
CRITICAL REFR. AT LAYER 4  APPROX. ANGLE  Ø.24ØØØØE  2
REFLECTING LAYER? 6
STEPPING ANGLE? 2
CRITICAL REFR. AT LAYER 5  APPROX. ANGLE  Ø.18ØØØØE  2
REFLECTING LAYER? Ø
CODE? 66 <-------------------------------- refraction case
REFRACTING LAYER? 1
SHOOTING LEFT TO RIGHT?,YES=1 1
REFR. INCREMENT(KM)? .5
END OF REFR. LAYER(KM)? 2Ø
REFRACTING LAYER? 2
SHOOTING LEFT TO RIGHT?,YES=1 1
REFR. INCREMENT(KM)? .25
END OF REFR. LAYER(KM)? 2Ø
REFRACTING LAYER? 3
SHOOTING LEFT TO RIGHT?,YES=1 1
REFR. INCREMENT(KM)? .25
END OF REFR. LAYER(KM)? 2Ø
REFRACTING LAYER? 4
SHOOTING LEFT TO RIGHT?,YES=1 1
REFR. INCREMENT(KM)? .25
END OF REFR. LAYER(KM)? 2Ø
```

Console Example for RAYTRACE, cont.

```
REFRACTING LAYER? 5
SHOOTING LEFT TO RIGHT?,YES=1 1
REFR. INCREMENT(KM)? .25
END OF REFR. LAYER(KM)? 20
REFRACTING LAYER? 6
SHOOTING LEFT TO RIGHT?,YES=1 1
REFR. INCREMENT(KM)? .25
END OF REFR. LAYER(KM)? 20
REFRACTING LAYER? 0
CODE? 0
TURN OFF PLOTTER
STOP
R
```

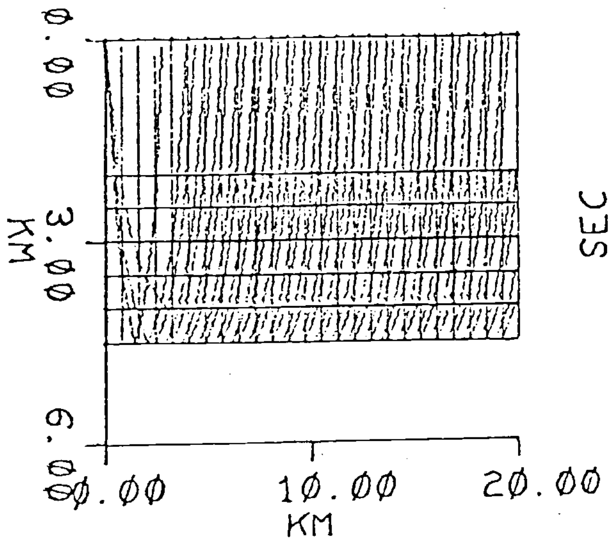


Model Plot Example

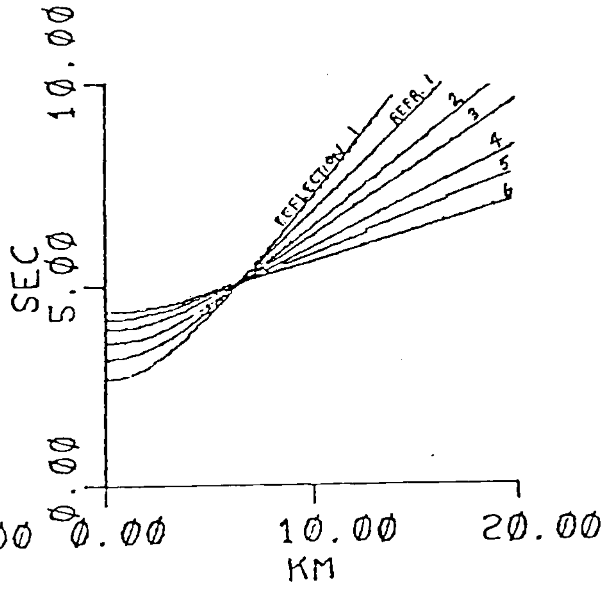


TT Curve Plot Example

# Model Listing to Console Example

PAGE 1

TEST OF NEW SYSTEM (#6.1)

MODEL COORDINATES,X,Z

| | |
|---|---|
| 0.000 | 0.000 |
| 0.800 | 0.000 |
| 1.600 | 0.000 |
| 2.400 | 0.000 |
| 3.200 | 0.000 |
| 4.000 | 0.000 |
| 4.800 | 0.000 |
| 5.600 | 0.000 |
| 6.400 | 0.000 |
| 7.200 | 0.000 |
| 8.000 | 0.000 |
| 8.800 | 0.000 |
| 9.600 | 0.000 |
| 10.400 | 0.000 |
| 11.200 | 0.000 |
| 12.000 | 0.000 |
| 12.800 | 0.000 |
| 13.600 | 0.000 |
| 14.400 | 0.000 |
| 15.200 | 0.000 |
| 16.000 | 0.000 |
| 16.800 | 0.000 |
| 17.600 | 0.000 |
| 18.400 | 0.000 |
| 19.200 | 0.000 |
| 20.000 | 0.000 |
| 0.000 | 2.000 |
| 0.800 | 2.000 |
| 1.600 | 2.000 |
| 2.400 | 2.000 |
| 3.200 | 2.000 |
| 4.000 | 2.000 |
| 4.800 | 2.000 |
| 5.600 | 2.000 |
| 6.400 | 2.000 |
| 7.200 | 2.000 |
| 8.000 | 2.000 |
| 8.800 | 2.000 |
| 9.600 | 2.000 |
| 10.400 | 2.000 |
| 11.200 | 2.000 |
| 12.000 | 2.000 |
| 12.800 | 2.000 |
| 13.600 | 2.000 |
| 14.400 | 2.000 |
| 15.200 | 2.000 |
| 16.000 | 2.000 |
| 16.800 | 2.000 |
| 17.600 | 2.000 |
| 18.400 | 2.000 |
| 19.200 | 2.000 |
| 20.000 | 2.000 |
| 0.000 | 2.500 |
| 0.800 | 2.500 |
| 1.600 | 2.500 |
| 2.400 | 2.500 |
| 3.200 | 2.500 |
| 4.000 | 2.500 |

PAGE 2

| | |
|---|---|
| 4.800 | 2.500 |
| 5.600 | 2.500 |
| 6.400 | 2.500 |
| 7.200 | 2.500 |
| 8.000 | 2.500 |
| 8.800 | 2.500 |
| 9.600 | 2.500 |
| 10.400 | 2.500 |
| 11.200 | 2.500 |
| 12.000 | 2.500 |
| 12.800 | 2.500 |
| 13.600 | 2.500 |
| 14.400 | 2.500 |
| 15.200 | 2.500 |
| 16.000 | 2.500 |
| 16.800 | 2.500 |
| 17.600 | 2.500 |
| 18.400 | 2.500 |
| 19.200 | 2.500 |
| 20.000 | 2.500 |
| 0.000 | 3.000 |
| 0.800 | 3.000 |
| 1.600 | 3.000 |
| 2.400 | 3.000 |
| 3.200 | 3.000 |
| 4.000 | 3.000 |
| 4.800 | 3.000 |
| 5.600 | 3.000 |
| 6.400 | 3.000 |
| 7.200 | 3.000 |
| 8.000 | 3.000 |
| 8.800 | 3.000 |
| 9.600 | 3.000 |
| 10.400 | 3.000 |
| 11.200 | 3.000 |
| 12.000 | 3.000 |
| 12.800 | 3.000 |
| 13.600 | 3.000 |
| 14.400 | 3.000 |
| 15.200 | 3.000 |
| 16.000 | 3.000 |
| 16.800 | 3.000 |
| 17.600 | 3.000 |
| 18.400 | 3.000 |
| 19.200 | 3.000 |
| 20.000 | 3.000 |
| 0.000 | 3.500 |
| 0.800 | 3.500 |
| 1.600 | 3.500 |
| 2.400 | 3.500 |
| 3.200 | 3.500 |
| 4.000 | 3.500 |
| 4.800 | 3.500 |
| 5.600 | 3.500 |
| 6.400 | 3.500 |
| 7.200 | 3.500 |
| 8.000 | 3.500 |
| 8.800 | 3.500 |
| 9.600 | 3.500 |
| 10.400 | 3.500 |
| 11.200 | 3.500 |

PAGE 3

| | |
|---|---|
| 12.000 | 3.500 |
| 12.800 | 3.500 |
| 13.600 | 3.500 |
| 14.400 | 3.500 |
| 15.200 | 3.500 |
| 16.000 | 3.500 |
| 16.800 | 3.500 |
| 17.600 | 3.500 |
| 18.400 | 3.500 |
| 19.200 | 3.500 |
| 20.000 | 3.500 |
| 0.000 | 4.000 |
| 0.800 | 4.000 |
| 1.600 | 4.000 |
| 2.400 | 4.000 |
| 3.200 | 4.000 |
| 4.000 | 4.000 |
| 4.800 | 4.000 |
| 5.600 | 4.000 |
| 6.400 | 4.000 |
| 7.200 | 4.000 |
| 8.000 | 4.000 |
| 8.800 | 4.000 |
| 9.600 | 4.000 |
| 10.400 | 4.000 |
| 11.200 | 4.000 |
| 12.000 | 4.000 |
| 12.800 | 4.000 |
| 13.600 | 4.000 |
| 14.400 | 4.000 |
| 15.200 | 4.000 |
| 16.000 | 4.000 |
| 16.800 | 4.000 |
| 17.600 | 4.000 |
| 18.400 | 4.000 |
| 19.200 | 4.000 |
| 20.000 | 4.000 |
| 0.000 | 4.500 |
| 0.800 | 4.500 |
| 1.600 | 4.500 |
| 2.400 | 4.500 |
| 3.200 | 4.500 |
| 4.000 | 4.500 |
| 4.800 | 4.500 |
| 5.600 | 4.500 |
| 6.400 | 4.500 |
| 7.200 | 4.500 |
| 8.000 | 4.500 |
| 8.800 | 4.500 |
| 9.600 | 4.500 |
| 10.400 | 4.500 |
| 11.200 | 4.500 |
| 12.000 | 4.500 |
| 12.800 | 4.500 |
| 13.600 | 4.500 |
| 14.400 | 4.500 |
| 15.200 | 4.500 |
| 16.000 | 4.500 |
| 16.800 | 4.500 |
| 17.600 | 4.500 |
| 18.400 | 4.500 |

# Model Listing to Console Example

PAGE 4

```
 19.200    4.500
 20.000    4.500
CELL   LAYER   VELOCITY
   1     1     1.500
   2     1     1.500
   3     1     1.500
   4     1     1.500
   5     1     1.500
   6     1     1.500
   7     1     1.500
   8     1     1.500
   9     1     1.500
  10     1     1.500
  11     1     1.500
  12     1     1.500
  13     1     1.500
  14     1     1.500
  15     1     1.500
  16     1     1.500
  17     1     1.500
  18     1     1.500
  19     1     1.500
  20     1     1.500
  21     1     1.500
  22     1     1.500
  23     1     1.500
  24     1     1.500
  25     1     1.500
   1     2     2.000
   2     2     2.000
   3     2     2.000
   4     2     2.000
   5     2     2.000
   6     2     2.000
   7     2     2.000
   8     2     2.000
   9     2     2.000
  10     2     2.000
  11     2     2.000
  12     2     2.000
  13     2     2.000
  14     2     2.000
  15     2     2.000
  16     2     2.000
  17     2     2.000
  18     2     2.000
  19     2     2.000
  20     2     2.000
  21     2     2.000
  22     2     2.000
  23     2     2.000
  24     2     2.000
  25     2     2.000
   1     3     2.500
   2     3     2.500
   3     3     2.500
   4     3     2.500
   5     3     2.500
   6     3     2.500
   7     3     2.500
   8     3     2.500
```

PAGE 5

```
   9     3     2.500
  10     3     2.500
  11     3     2.500
  12     3     2.500
  13     3     2.500
  14     3     2.500
  15     3     2.500
  16     3     2.500
  17     3     2.500
  18     3     2.500
  19     3     2.500
  20     3     2.500
  21     3     2.500
  22     3     2.500
  23     3     2.500
  24     3     2.500
  25     3     2.500
   1     4     3.000
   2     4     3.000
   3     4     3.000
   4     4     3.000
   5     4     3.000
   6     4     3.000
   7     4     3.000
   8     4     3.000
   9     4     3.000
  10     4     3.000
  11     4     3.000
  12     4     3.000
  13     4     3.000
  14     4     3.000
  15     4     3.000
  16     4     3.000
  17     4     3.000
  18     4     3.000
  19     4     3.000
  20     4     3.000
  21     4     3.000
  22     4     3.000
  23     4     3.000
  24     4     3.000
  25     4     3.000
   1     5     4.000
   2     5     4.000
   3     5     4.000
   4     5     4.000
   5     5     4.000
   6     5     4.000
   7     5     4.000
   8     5     4.000
   9     5     4.000
  10     5     4.000
  11     5     4.000
  12     5     4.000
  13     5     4.000
  14     5     4.000
  15     5     4.000
  16     5     4.000
  17     5     4.000
  18     5     4.000
  19     5     4.000
```

PAGE 6

```
  20     5     4.000
  21     5     4.000
  22     5     4.000
  23     5     4.000
  24     5     4.000
  25     5     4.000
   1     6     5.000
   2     6     5.000
   3     6     5.000
   4     6     5.000
   5     6     5.000
   6     6     5.000
   7     6     5.000
   8     6     5.000
   9     6     5.000
  10     6     5.000
  11     6     5.000
  12     6     5.000
  13     6     5.000
  14     6     5.000
  15     6     5.000
  16     6     5.000
  17     6     5.000
  18     6     5.000
  19     6     5.000
  20     6     5.000
  21     6     5.000
  22     6     5.000
  23     6     5.000
  24     6     5.000
  25     6     5.000
   1     7     6.700
   2     7     6.700
   3     7     6.700
   4     7     6.700
   5     7     6.700
   6     7     6.700
   7     7     6.700
   8     7     6.700
   9     7     6.700
  10     7     6.700
  11     7     6.700
  12     7     6.700
  13     7     6.700
  14     7     6.700
  15     7     6.700
  16     7     6.700
  17     7     6.700
  18     7     6.700
  19     7     6.700
  20     7     6.700
  21     7     6.700
  22     7     6.700
  23     7     6.700
  24     7     6.700
  25     7     6.700
```

Console Example for RAYGUN

(see Figure 9 for plot)

```
RAYTRACE
NAME OF MODEL
PCT27M6E  <------------------------------ model file name
LIST MODEL COORDINATES? YES=1 Ø
TT CURVE LISTING?,YES=1 Ø                  answer Ø to these options
TT CURVE PLOT?,YES=1 Ø
RAYTRACE PLOT?,YES=1 Ø
       6 LAYER MODEL

PRESENT SHOT POINT COORDINATES ARE:
X=    3.ØØØ
Z=    Ø.ØØØ
LAYER=  1
CELL=  1
CODE? 44  <------------------------------ CODE 44 initiates RAYGUN
DISTANCE SCALE(INCHES)? 18
LEFT EDGE(KM)? 5Ø
RIGHT EDGE(KM)? 75
TIME SCALE(INCHES)? 4.8                    axes parameters
MIN. TIME SCALE(SEC.)? Ø
MAX. TIME SCALE(SEC.)? 1
AUTO-ORIGIN?,YES=1 1
PAUSE : TURN ON PLOTTER
(A)DETECTOR LENGTH LEFT OF S.P.= .3
DETECTOR LENGTH RIGHT OF S.P.= Ø
START SHOT POINT AT X= 5Ø                  distances in km
END SHOT POINT AT X= 75
SHOT POINT STEPPING INCREMENT= Ø.2         angles in degrees
MARK S.P. POSITIONS, YES=1 Ø
GIVE INCLUDED ANGLE OF BEAM 8Ø
GIVE STEPPING ANGLE IN BEAM 1Ø
REFLECTING LAYER= 1
REFLECTING LAYER= 2                        LAYER 0 returns user to RAYTRACE
REFLECTING LAYER= 3
REFLECTING LAYER= Ø                        LAYER 99 returns user to (A)
```

# Appendix II: RAYTRACE Support Programs

# Program MODFORM

## Description of Program

Computer program MODFORM develops the initial two-dimensional velocity-depth model used by RAYTRACE (Appendix I). MODFORM operates at the console in a conversional mode whereby the user is queried for information needed to construct a plane layered, non-dipping, multi-celled model. The following example gives the console I/0 and model listing.

## I/0 Example and Program Listing

```
MODFORM
GIVE NAME OF NEW MODEL
SLOPEMOD0
 GIVE NUMBERS OF CELLS AND LAYERS 4,4
GIVE HEADER CARD FOR THIS MODEL
SIMPLE TEST OF BASIN - SLOPE INTERSECTION
NOTE: COORDINATES ARE IN KM WITH Z POSITIVE BELOW S.L..
GIVE X AND Z COORDINATE OF UPPER L.H.CORNER 0,0
GIVE HORIZONTAL LENGTH OF MODEL 10
GIVE DEPTH TO BOTTOM OF EACH LAYER
Z(I)= 2.333
Z(I)= 3.
Z(I)= 3.5
Z(I)= 4.
CHECK YOUR DEPTHS - ARE THEY CORRECT?(YES=1) 1
GIVE LAYER VELOCITIES AND HALF-SPACE VELOCITY
V(I)= 1.5
V(I)= 3.
V(I)= 2.1
V(I)= 2.6
 H.S.V= 3.
CHECK YOUR VELOCITIES - ARE THEY CORRECT?(YES=1) 1
MODEL IS DONE
STOP
R
```

```
        SLOPEMOD0                          6/18/76  11:47:32        PAGE  1
  1;SIMPLE TEST OF BASIN - SLOPE INTERSECTION
  2;  4  4
  3;     0.000     0.000
  4;     2.500     0.000
  5;     5.000     0.000
  6;     7.500     0.000
  7;    10.000     0.000
  8;     0.000     2.333
  9;     2.500     2.333
 10;     5.000     2.333
 11;     7.500     2.333
 12;    10.000     2.333
 13;     0.000     3.000
 14;     2.500     3.000
 15;     5.000     3.000
 16;     7.500     3.000
 17;    10.000     3.000
 18;     0.000     3.500
 19;     2.500     3.500
 20;     5.000     3.500
 21;     7.500     3.500
 22;    10.000     3.500
 23;     0.000     4.000
 24;     2.500     4.000
 25;     5.000     4.000
 26;     7.500     4.000
 27;    10.000     4.000
 28;     1.500
 29;     1.500
 30;     1.500
 31;     1.500
 32;     3.000
 33;     3.000
 34;     3.000
 35;     3.000
 36;     2.100
 37;     2.100
 38;     2.100
 39;     2.100
 40;     2.600
 41;     2.600
 42;     2.600
 43;     2.600
 44;     3.000
 45;     3.000
 46;     3.000
 47;     3.000
```

```
     MODFORM                       7/24/78  16:28:35      PAGE  1
C       MODFORM
C       PROGRAM MODFORM:  THIS PROGRAM FORMS MULTICELLED MODELS OF
C         NONDIPPING UNIFORM VELOCITY LAYERS
        DIMENSION IHEADER(40), IFILE(6), Z(21), V(21)
        LMAX=20
        CMAX=25
        TYPE"GIVE NAME OF NEW MODEL"
        READ(11,100) IFILE(1)
  100   FORMAT(S10)
        CALL FOPEN(1,IFILE)
  110   ACCEPT" GIVE NUMBERS OF CELLS AND LAYERS ",NC, NL
        IF(NC.LE.CMAX.AND.NL.LE.LMAX) GO TO 120
        TYPE" MAX.NUMBER OF CELLS=25, MAX LAYERS=20"
        GO TO 110
  120   TYPE"GIVE HEADER CARD FOR THIS MODEL"
        READ(11,130) IHEADER
  130   FORMAT(40A2)
        NCP1=NC+1
        NLP1=NL+1
        TYPE"NOTE: COORDINATES ARE IN KM WITH Z POSITIVE BELOW S.L.,
       1 VELOCITY IN KM/SEC"
        ACCEPT"GIVE X AND Z COORDINATE OF UPPER L.H.CORNER ",X0,Z(1)
        ACCEPT"GIVE HORIZONTAL LENGTH OF MODEL ",D
        TYPE"GIVE DEPTH TO BOTTOM OF EACH LAYER "
  135   DO 140 I=2,NLP1
  140   ACCEPT "Z(I)= ",Z(I)
        ACCEPT"CHECK YOUR DEPTHS - ARE THEY CORRECT?(YES=1) ",IANS
        IF(IANS.NE.1) GO TO 135
        TYPE"GIVE LAYER VELOCITIES AND HALF-SPACE VELOCITY"
  145   DO 150 I=1,NL
  150   ACCEPT"V(I)= ", V(I)
        ACCEPT" H.S.V= ",V(NLP1)
        ACCEPT"CHECK YOUR VELOCITIES - ARE THEY CORRECT?(YES=1) ",IANS
        IF(IANS.NE.1) GO TO 145
        WRITE(1,155) IHEADER
  155   FORMAT(1X,40A2)
        WRITE(1,158) NC,NL
  158   FORMAT(1X,2I2)
        DSTEP=D/NC
        DO 165 I=1,NLP1
        ZM=Z(I)
        SUM=0.
        DO 160 M=1,NCP1
        XM=X0+SUM
        WRITE(1,170) XM,ZM
  160   SUM=SUM+DSTEP
  165   CONTINUE
  170   FORMAT(1X,2F8.3)
        DO 190 I=1,NLP1
        VM=V(I)
        DO 180 M=1,NC
  180   WRITE(1,200) VM
  190   CONTINUE
  200   FORMAT(1X,F8.3)
        CALL FCLOS(1)
        TYPE"MODEL IS DONE"
        END
```

# Program MODFIX

## Description of Program

Computer program MODFIX is a conversational program used to modify velocity-depth models for RAYTRACE (Appendix I). Modifications include x,z, coordinates, cell velocities, complete P to S velocity conversions (with provisions to exclude water velocities), addition of layers or cell columns, horizontal shift of x-axis, and reversal of x-axis. The following example, which includes console I/0 and model listing, is a modification to the example model developed earlier by MODFORM.

## I/0 Example and Program Listing

```
MODFIX
GIVE NAME OF OLD MODEL
SLOPEMODØ
GIVE NAME OF NEW MODEL
SLOPEMOD1
THIS IS THE OLD HEADER CARD
SIMPLE TEST OF BASIN - SLOPE INTERSECTION
 CHANGE THIS HEADER IN NEW FILE?,YES=1 Ø
OLD MODEL IS A  4 CELL BY  4 LAYER MODEL
CODE LIST FOR OPERATING PROGRAM
  CODE 99=STOP PROGRAM AND OUTPUT FILE
  CODE  1=CHANGE INDIVIDUAL COORDINATES
  CODE  2=SHIFT OR REVERSE X-AXIS
  CODE  3=ADD A LAYER OR CELL COLUMN
  CODE  4=CHANGE CELL VELOCITIES
  CODE  5=LIST CODES
CODE? 4
SEE WRITE-UP ON HOW TO CHANGE VELOCITIES
INDIVIDUAL CHANGES(1) OR P TO S CHANGES(2)? 1
GIVE LAYER AND CELL NUMBER OF VEL. 2,1
OLD VELOCITY IS:   3.ØØØ
GIVE NEW VELOCITY= 2.1
CONTINUE?,YES=1 1
```

```
GIVE LAYER AND CELL NUMBER OF VEL. 2,2
OLD VELOCITY IS:   3.000
GIVE NEW VELOCITY= 2.1
CONTINUE?,YES=1 1
GIVE LAYER AND CELL NUMBER OF VEL. 3,4
OLD VELOCITY IS:   2.100
GIVE NEW VELOCITY= 3.
CONTINUE?,YES=1 1
GIVE LAYER AND CELL NUMBER OF VEL. 4,4
OLD VELOCITY IS:   2.600
GIVE NEW VELOCITY= 3.
CONTINUE?,YES=1 0
CODE? 1
SEE WRITE-UP ON HOW TO SPECIFY COORDINATES
GIVE LAYER AND CELL NUMBERS 2,1
OLD COORDINATES ARE: X=    0.000    Z=    2.333
GIVE NEW COORDINATES: X,Z 0,3.
CONTINUE?,YES=1 1
GIVE LAYER AND CELL NUMBERS 2,2
OLD COORDINATES ARE: X=    2.500    Z=    2.333
GIVE NEW COORDINATES: X,Z 2.5,3.
CONTINUE?,YES=1 1
GIVE LAYER AND CELL NUMBERS 2,3
OLD COORDINATES ARE: X=    5.000    Z=    2.333
GIVE NEW COORDINATES: X,Z 5,3
CONTINUE?,YES=1 1
GIVE LAYER AND CELL NUMBERS 2,5-4
OLD COORDINATES ARE: X=    7.500    Z=    2.333
GIVE NEW COORDINATES: X,Z 7.5,2.7
CONTINUE?,YES=1 0
CODE? 99
THANK YOU, YOUR NEW MODEL IS DONE
STOP
R
```

```
      SLOPEMOD1                    5/18/78  11:48: 2      PAGE  1
 1;SIMPLE TEST OF BASIN - SLOPE INTERSECTION
 2; 4 4
 3;    0.000    0.000
 4;    2.500    0.000
 5;    5.000    0.000
 6;    7.500    0.000
 7;   10.000    0.000
 8,    0.000    3.000
 9;    2.500    3.000
10;    5.000    3.000
11;    7.500    2.700
12;   10.000    2.333
13;    0.000    3.000
14;    2.500    3.000
15;    5.000    3.000
16;    7.500    3.000
17;   10.000    3.000
18;    0.000    3.500
19;    2.500    3.500
20;    5.000    3.500
21;    7.500    3.500
22;   10.000    3.500
23;    0.000    4.000
24;    2.500    4.000
25;    5.000    4.000
26;    7.500    4.000
27;   10.000    4.000
28;    1.500
29;    1.500
30;    1.500
31;    1.500
32;    2.100
33;    2.100
34;    3.000
35;    3.000
36;    2.100
37;    2.100
38,    2.100
39;    3.000
40;    2.600
41;    2.600
42;    2.600
43,    3.000
44;    3.000
45;    3.000
46;    3.000
47;    3.000
```

```
      MODFIX                          7/24/78  16.20.35     PAGE  1
C     PROGRAM MODFIX.  THIS IS A CONVERSATIONAL PROGRAM THAT IS
C             USED TO CHANGE RAYTRACE MODEL COORDINATES, VELOCITIES
C             AND TO ADD WHOLE LAYERS AND CELL COLUMNS.
C       AUTHOR.  P.R. JONES  12 MAY 77, REVISED 18 MAY 78
      DIMENSION IFILE(7),NFILE(7),IHEADER(40),NHEADER(40),
     1  X(21,26),Z(21,26),V(21,25),XN(26),ZN(26),VN(25),
     2  XR(21,26),ZR(21,26),VR(21,25)
      LMAX=20
      CMAX=25
      TYPE "GIVE NAME OF OLD MODEL"
      READ(11,100) IFILE(1)
      TYPE "GIVE NAME OF NEW MODEL"
      READ(11,100) NFILE(1)
  100 FORMAT(S12)
      CALL FOPEN(1,IFILE)
      CALL FOPEN(2,NFILE)
      READ(1,110) IHEADER
  110 FORMAT(40A2)
      TYPE "THIS IS THE OLD HEADER CARD"
      WRITE(10,120) IHEADER
  120 FORMAT(1X,40A2)
      ACCEPT "CHANGE THIS HEADER IN NEW FILE?,YES=1 ",IANS
      IF(IANS.NE.1) GO TO 130
      TYPE "GIVE NEW HEADER CARD (40A2)"
      READ(11,110) NHEADER
      GO TO 135
  130 DO 132 I=1,40
  132 NHEADER(I)=IHEADER(I)
C  READ IN OLD MODEL COORDINATES AND VELOCITIES
  135 READ(1,140) NC,NL
  140 FORMAT(2I2)
      WRITE(10,145) NC,NL
  145 FORMAT(1H ,'OLD MODEL IS A',I3,' CELL BY',I3,' LAYER MODEL')
      NLP1=NL+1
      NCP1=NC+1
      DO 150 I=1,NLP1
      DO 150 K=1,NCP1
  150 READ(1,160) X(I,K),Z(I,K)
  160 FORMAT(2F8.3)
      DO 170 I=1,NLP1
      DO 170 K=1,NC
  170 READ(1,180) V(I,K)
  180 FORMAT(F8.3)
C
C  THE REMAINDER OF THIS PROGRAM IS USED TO MAKE MODEL CHANGES
C
  200 TYPE "CODE LIST FOR OPERATING PROGRAM"
      TYPE "  CODE 99=STOP PROGRAM AND OUTPUT FILE"
      TYPE "  CODE  1=CHANGE INDIVIDUAL COORDINATES"
      TYPE "  CODE  2=SHIFT OR REVERSE X-AXIS"
      TYPE "  CODE  3=ADD A LAYER OR CELL COLUMN"
      TYPE "  CODE  4=CHANGE CELL VELOCITIES"
      TYPE "  CODE  5=LIST CODES"
  210 ACCEPT "CODE? ",NCODE
      IF(NCODE.EQ.99) GO TO 900
      IF(NCODE.EQ.1) GO TO 300
      IF(NCODE.EQ.2) GO TO 700
      IF(NCODE.EQ.3) GO TO 400
```

```
      IF(NCODE.EQ.4) GO TO 600
      IF(NCODE.EQ.5) GO TO 200
      GO TO 210
C
  300 TYPE "SEE WRITE-UP ON HOW TO SPECIFY COORDINATES"
  305 ACCEPT "GIVE LAYER AND CELL NUMBERS ",IFL,IFC
      WRITE(10,310) X(IFL,IFC),Z(IFL,IFC)
  310 FORMAT(1H ,'OLD COORDINATES ARE: X=',F8.3,3X,'Z=',F8.3)
      ACCEPT "GIVE NEW COORDINATES, X,Z ",X(IFL,IFC),Z(IFL,IFC)
      ACCEPT "CONTINUE?,YES=1 ",IANS
      IF(IANS.EQ.1) GO TO 305
      GO TO 210
C
  400 TYPE "SEE WRITE-UP ON HOW TO ADD LAYERS AND CELLS"
      ACCEPT "IS THIS A NEW LAYER(1) OR NEW CELL(2)? ",IALC
      IF(IALC.EQ.1) NL=NL+1
      IF(IALC.EQ.2) NC=NC+1
      IF(IALC.EQ.1) GO TO 500
      IF(IALC.EQ.2) GO TO 405
      GO TO 210
  405 ACCEPT "GIVE POSITION NUMBER OF NEW CELL COLUMN ",NCN
      ACCEPT "SAME X COORDINATE FOR THE WHOLE COLUMN?,YES=1 ",IANS
      IF(IANS.EQ.1) GO TO 415
      TYPE "GIVE X,Z COORDINATES BY LAYER OF L.H. WALLS"
      NCP1=NCP1+1
      DO 410 I=1,NLP1
  410 ACCEPT "X,Z= ",XN(I),ZN(I)
      GO TO 419
  415 ACCEPT "GIVE X COORDINATE ",XFIX
      TYPE "GIVE Z COORDINATES"
      DO 416 I=1,NLP1
      ACCEPT "Z= ",ZN(I)
  416 XN(I)=XFIX
  419 TYPE "GIVE VELOCITIES TO NEW CELLS AND H.S. FROM TOP TO BOTTOM"
      DO 420 I=1,NL
  420 ACCEPT "V= ",VN(I)
      ACCEPT "H.S. V= ",VN(NLP1)
C     ADJUST THE MODEL FOR THIS NEW CELL COLUMN
      IF(NCN.EQ.NC) GO TO 450
      DO 430 I=1,NLP1
      K=NCP1
      DO 430 J=NCN,NC
      X(I,K)=X(I,K-1)
      Z(I,K)=Z(I,K-1)
      IF(K.EQ.NCP1) GO TO 430
      V(I,K)=V(I,K-1)
  430 K=K-1
      DO 440 I=1,NLP1
      X(I,NCN)=XN(I)
      Z(I,NCN)=ZN(I)
  440 V(I,NCN)=VN(I)
      GO TO 210
  450 DO 460 I=1,NLP1
      X(I,NCP1)=XN(I)
      Z(I,NCP1)=ZN(I)
  460 V(I,NCN)=VN(I)
      GO TO 210
  500 ACCEPT "GIVE NEW LAYER NUMBER ",NLN
```

```
  505 TYPE "GIVE X,Z COORDINATES FROM LEFT TO RIGHT"
      NLP1=NLP1+1
      DO 510 I=1,NCP1
  510 ACCEPT "X,Z= ",XN(I),ZN(I)
      ACCEPT "ARE COORDINATES CORRECT?,YES=1 ",IANS
      IF(IANS.NE.1) GO TO 505
  515 TYPE "GIVE VELOCITIES TO CELLS OF THIS LAYER (L TO R)"
      DO 520 I=1,NC
  520 ACCEPT "V= ",VN(I)
      ACCEPT "ARE VELOCTIES CORRECT? ,YES=1 ",IANS
      IF(IANS.NE.1) GO TO 515
C  ADJUST MODEL FOR THIS NEW LAYER
      NLNP1=NLN+1
      IF(NLN.EQ.NL) GO TO 540
      K=NLP1
      DO 535 I=NLN,NL
      DO 530 J=1,NCP1
      IF(K.EQ.NLNP1) GO TO 532
      X(K,J)=X(K-1,J)
      Z(K,J)=Z(K-1,J)
  532 IF(J.EQ.NCP1) GO TO 530
      V(K,J)=V(K-1,J)
  530 CONTINUE
  535 K=K-1
  540 K=NLN
      IF(NLN.EQ.NL) K=NLNP1
      DO 550 I=1,NCP1
      X(NLNP1,I)=XN(I)
      Z(NLNP1,I)=ZN(I)
      IF(I.EQ.NCP1) GO TO 550
      V(K,I)=VN(I)
  550 CONTINUE
      GO TO 210
C  SECTION FOR CHANGING VELOCITIES
  600 TYPE "SEE WRITE-UP ON HOW TO CHANGE VELOCITIES"
      ACCEPT "INDIVIDUAL CHANGES(1) OR P TO S CHANGES(2)? ",IANSV
      IF(IANSV.EQ.2) GO TO 615
  605 ACCEPT "GIVE LAYER AND CELL NUMBER OF VEL. ",IVL,IVC
      WRITE(10,610) V(IVL,IVC)
  610 FORMAT(1H ,'OLD VELOCITY IS:',F8.3)
      ACCEPT "GIVE NEW VELOCITY= ",V(IVL,IVC)
      ACCEPT "CONTINUE?,YES=1 ",IANS
      IF(IANS.EQ.1) GO TO 605
      GO TO 210
  615 ACCEPT "GIVE CONSTANT C, VNEW = C*VOLD ",VCON
      ACCEPT "WATER VELOCITY DOES NOT CHANGE, GIVE OLD VALUE ",WV
      DO 620 I=1,NLP1
      DO 620 K=1,NC
      IF(WV.EQ.V(I,K)) GO TO 620
      V(I,K)=VCON*V(I,K)
  620 CONTINUE
      GO TO 210
C  SECTION FOR SHIFTING OR REVERSING X-AXIS
  700 ACCEPT "IS THIS AN AXIS SHIFT(1) OR A REVERSAL(2)? ",IAX
      IF(IAX.EQ.1) GO TO 710
      IF(IAX.EQ.2) GO TO 750
      GO TO 210
  710 ACCEPT "GIVE CONSTANT TO BE ADDED TO X-AXIS ",XCON
```

```
      DO 720 I=1,NLP1
      DO 720 K=1,NCP1
  720 X(I,K)=X(I,K)+XCON
      GO TO 210
  750 ACCEPT "SIGN OF X-AXIS AFTER REVERSAL? ",XSIGN
      DO 760 I=1,NLP1
      DO 760 K=1,NCP1
      XR(I,K)=XSIGN*X(I,K)
      ZR(I,K)=Z(I,K)
      IF(K.GT.NC) GO TO 760
      VR(I,K)=V(I,K)
  760 CONTINUE
      NCP2=NC+2
      DO 770 I=1,NLP1
      DO 770 K=1,NCP1
      KR=NCP2-K
      X(I,K)=XR(I,KR)
  770 Z(I,K)=ZR(I,KR)
      DO 780 I=1,NLP1
      DO 780 K=1,NC
      KR=NCP1-K
  780 V(I,K)=VR(I,KR)
      GO TO 210
  900 WRITE(2,910) NHEADER
  910 FORMAT(1X,40A2)
      WRITE(2,920) NC,NL
  920 FORMAT(1X,2I2)
      DO 930 I=1,NLP1
      DO 930 K=1,NCP1
  930 WRITE(2,940) X(I,K),Z(I,K)
  940 FORMAT(1X,2F8.3)
      DO 950 I=1,NLP1
      DO 950 K=1,NC
  950 WRITE(2,960) V(I,K)
  960 FORMAT(1X,F8.3)
      CALL FCLOS(2)
      TYPE "THANK YOU, YOUR NEW MODEL IS DONE"
      END
```